UNIVERSITÀ DEGLI STUDI DI PADOVA

DIPARTIMENTO DI INGEGNERIA INDUSTRIALE

CORSO DI LAUREA MAGISTRALE IN CHEMICAL AND PROCESS ENGINEERING

Tesi di Laurea Magistrale in

Chemical and Process Engineering

Control of a feed-effluent heat exchanger/reactor system: assessment by dynamic simulation

Relatore: prof. Massimiliano Barolo

Laureando: FILIPPO BALDAN

ANNO ACCADEMICO 2023-2024

Summary

Feed-effluent heat exchangers (FEHE) are commonly employed in the chemical industry to preheat the feed to exothermic adiabatic tubular reactor systems by recovering heat from the hot reactor effluent. While this approach enhances thermal efficiency and reduces both capital and operating costs, it introduces complex, non-linear dynamics that can lead to open-loop instability, reactor quenching, or significant temperature increases. This Thesis investigates various FEHE/reactor system designs and control strategies through dynamic simulations, with a particular focus on how feed flow disturbances (which are common in industrial plants due to fluctuations in production demand or raw material availability) affect system performance.

The study begins with an analysis of the base design configuration, highlighting the critical role of controlling the reactor inlet temperature for both steady-state and dynamic performance. It then examines a modified design featuring a bypass around the heat exchanger, introducing a manipulated variable to control the reactor inlet temperature. The impact of the bypass selection on process controllability is assessed, revealing that a larger bypass results in a larger heat exchanger area, which enhances control robustness and allows efficient preheating of the reactor feed even under anomalous high throughputs compared to nominal conditions.

Subsequently, the Thesis explores a conventional design that incorporates a furnace to enable process start-up, addressing the absence of an external heat source in both the base and bypass-only configurations. The performance of this new design and the relevant control strategy, which uses two manipulated variables (i.e., the bypass fraction and furnace duty) is compared to an alternative design and control structure proposed by Luyben (2012, *Ind. Eng. Chem. Res*. **51**, 25, 8566-8574.). The alternative design demonstrates improved control performance and reduced operational costs under low throughput conditions, though it requires higher furnace duty at elevated throughputs.

Table of contents

Introduction

Feed-effluent heat exchangers (FEHE) are widely used in the chemical industry to preheat the feed of high-temperature exothermic adiabatic tubular reactor systems. In this setup, the heat duty required to preheat the reactor feed is recovered directly from the hot reactor effluent, thus increasing the process thermal efficiency and reducing both the plant capital investment and operating costs.

Several papers in the literature address the dynamics and control challenges of FEHE/reactor configurations. For instance, the article provided by Douglas et al. (1962) shows that this systems presents multiple steady-state solutions, which can also be dynamically unstable. Additionally, the positive feedback of energy from the reactor back to the preheater and the complex dynamics of the adiabatic packed tubular reactor, such as the inverse outlet temperature response following a variation in the inlet temperature, contribute to the overall complexity of the FEHE/reactor system. Consequently, when these configurations are perturbed during operation, anomalous and complex dynamics can emerge, resulting in reactor quenching (where the system stabilizes at a new steady-state with low conversion) or significant temperature increases. In some cases, the system may even exhibit oscillating behaviours around an unstable steady-state.

The purpose of this Thesis is to assess and compare various FEHE designs and their associated control strategies through dynamic simulation in Aspen Plus Dynamics V14. Specifically, the focus is on evaluating how disturbances in process feed flow impact these configurations. Understanding if the system can be efficiently operated at different throughputs compared to the design condition is crucial from an industrial perspective, as fluctuations in production demand or raw material availability are common. Additionally, studying these disturbances helps identify ways to optimize process designs and control strategies to improve controllability, ensure efficient operation, and determine the operational limits of a process.

In Chapter 1, the base design configuration for the production of dimethyl ether from methanol, as investigated by Luyben (2012), is introduced. Both steady-state and dynamic analyses are conducted on the adiabatic packed tubular reactor in isolation, highlighting key characteristics of this reactor type. The reactor inlet temperature is shown to play a critical role, influencing both steady-state performance and process controllability. The Chapter also delves into the typical inverse response of the reactor outlet temperature following variations in the inlet temperature, a distinctive behaviour of this type of reactor. Special attention is given to the importance of accurate reactor discretization and modeling in dynamic simulations to capture such inverse responses. Several tests are conducted to properly characterize the catalyst and simulate the reactor, to replicate the process described by Luyben (2012). Once a reliable reactor

model is established, the entire process is dynamically evaluated under varying throughput disturbances. This evaluation reveals critical dynamic behaviour of the FEHE/reactor system and exposes limitations from a process control perspective. In particular, the absence of a manipulated variable to control the crucial reactor inlet temperature poses significant challenges for maintaining optimal operation and stability, underscoring the need for improved designs and control strategies.

In Chapter 2, the base design configuration is modified by introducing a bypass stream around the heat exchanger. Two configurations are developed: one with a 20 % bypass and the other with a 40 % bypass. The bypass stream enables the development of a control loop with a dual split-ranged controller manipulating the flow through and around the FEHE to control the reactor inlet temperature, addressing the control limitations identified in the base design. Both configurations are studied at steady-state to assess the impact of bypass selection on heat exchanger design and its implications on process controllability. Additionally, these designs are simulated dynamically to evaluate and compare the performance of the relevant temperature control loops.

In Chapter 3, more realistic designs are explored, incorporating a furnace into the previous design configuration with heat exchange bypass. The furnace is crucial for the process start-up, because the autothermal FEHE/reactor system alone cannot initiate the reaction without an external heat source. Without the furnace, the system would not achieve the necessary conditions for the reaction to occur and sustain operation. The Chapter first introduces the conventional process design integrating both bypass and furnace. The associated control structure is discussed, and its performance is evaluated under various process feed flows. Specifically, this design is shown to operate inefficiently especially at low throughputs, as it consumes unnecessary furnace fuel despite the lower heat demand.

To address these inefficiencies, a new alternative design and control strategy, suggested by Luyben (2012), is presented. This new approach aims to reduce furnace fuel consumption and improve process controllability. Finally, the performance of the new control structure is assessed and then compared with that of the conventional design under varying operating conditions.

Chapter 1

Process analyzed

This Chapter presents the industrial process under study and the base design case is configured, detailing all relevant features of the equipment used throughout the Thesis. Subsequently, the reactor dynamics is examined and the impact of the reactor discretization on its dynamics is analyzed. Finally, all control loops are introduced, and the process is studied dynamically.

1.1 Base case design

The process considered in this Thesis is the synthesis of dimethyl ether (DME) by methanol dehydration over an acid zeolite catalyst, as reported in Turton et al. (2020). This reaction is described by:

$$2CH_3OH \rightleftarrows CH_3OCH_3 + H_2O. \tag{1.1}$$

This reversible reaction is performed in vapor-phase using a feed molar flow rate of 295.2 kmol/h, with a molar composition of 95 % methanol and 5 % water.
The reaction is exothermic, as indicated by the standard heat of reaction, $\triangle H_R^\circ$, which is:

$$\triangle H_R^\circ = \sum_i \nu_i \cdot \triangle H_{F,i}^\circ = -\,24.040\ \frac{\text{kJ}}{\text{mol}}, \tag{1.2}$$

where ν_i represents the stoichiometric coefficient of component i, and the standard enthalpies of formation, $\triangle H_{F,i}^\circ$, of the species i are sourced from Poling et al. (2001, Table A.20-34).
From a thermodynamic standpoint, the reaction is favoured by low temperatures, as it is exothermic and reversible. Consequently, the equilibrium conversion is higher at lower temperatures. Additionally, pressure has no effect on the equilibrium conversion since the reaction is equimolar. However, at low temperatures, the reaction kinetic is slow, and achieving the maximum possible conversion, which for a reversible reaction is the equilibrium conversion, would require an excessively large reactor volume.
Therefore, the reactor inlet temperature is selected considering a compromise between reaction kinetics and thermodynamics to reach the desired conversion within a reasonable reactor volume.

The reaction kinetics for both the direct and reverse reactions are provided by Luyben (2012):

$$R_d = p^2_{CH_3OH} \cdot 3.23 \cdot 10^{-4} \cdot \exp\left(\frac{-E_d}{R_G \cdot T}\right), \tag{1.3}$$

$$R_r = p_{CH_3OCH_3} \cdot p_{H_2O} \cdot 2.888 \cdot 10^{-3} \cdot \exp\left(\frac{-E_r}{R_G \cdot T}\right), \tag{1.4}$$

where R_d and R_r are the direct and the reverse reaction rates in [mol·m^{-3}·s^{-1}], respectively, p_i is the partial pressure of component i in [Pa], R_G is the universal gas constant in [J·mol^{-1}·K^{-1}], and T is the temperature in [K]. The direct activation energy is E_d = 80300 J/mol, and the reverse activation energy is E_r = 101860 J/mol.

The reaction is performed in an adiabatic tubular packed bed reactor and all the relevant data are provided by Luyben (2012). The reactor has a length (L) and diameter (d) of 12 m and 1.2 m, respectively. The bed voidage (ε) of 0.28 and the catalyst solid density (ρ_{cat}) of 1700 kg/m^3. The catalyst particles size distribution is uniform, with spherical particles having a diameter (d_p) of 0.01 m. This particle diameter is selected in order to achieve a reactor outlet pressure of 12 atm as considered by Luyben (2012), assuming a reactor inlet pressure of 12.5 atm. The reactor pressure drops are evaluated with the Ergun equation.

To determine the optimum reactor inlet temperature, the reactor is modelled as an adiabatic homogenous plug-flow reactor, thus neglecting the catalyst presence at this stage. The material and energy balances are defined by the following ordinary differential equations (ODEs):

$$\frac{\mathrm{d}\dot{n}_i}{\mathrm{d}V_R} = \nu_i \cdot (R_d - R_r), \tag{1.5}$$

$$\frac{\mathrm{d}T}{\mathrm{d}V_R} = \frac{-\dot{Q}_R}{\sum_i \dot{n}_i \cdot c_{P,i}}, \tag{1.6}$$

where $\dot{n}_i$ is the molar flow rate of the component i in [mol/s], ν_i is the stoichiometric coefficient of component i, V_R is the reactor volume coordinate in [m^3], $c_{P,i}$ is the molar heat capacity at constant pressure of the specie i expressed in [J·mol^{-1}·K^{-1}], sourced from Poling et al. (2001, Table A.35-46). Additionally, the volumetric heat transfer rate of reaction, $\dot{Q}_R$, is expressed in [W/m^3] and it is calculated by:

$$\dot{Q}_R = \sum_i \nu_i \cdot \left(\triangle H^{\circ}_{F,i} + \int_{T_0}^{T} c_{P,i}\,\mathrm{d}T\right) \cdot (R_d - R_r), \tag{1.7}$$

where T_0 = 298 K is the reference temperature to which the standard enthalpies of formation for each specie i are referred.

Finally, the reactor volume coordinate V_R, used in equations (1.5) and (1.6), is expressed using:

$$V_R = \varepsilon \cdot \frac{\pi}{4} \cdot d^2 \cdot x, \tag{1.8}$$

with the reactor axial coordinate x, ranging from 0 m at the reactor inlet to 12 m at the outlet. These balances are implemented in Matlab® and solved for different reactor inlet temperature, using the function `ode89`. In order to solve the aforementioned ODEs, the initial reactor conditions are provided, specifically the inlet molar flow rates of the three species i and different reactor inlet temperatures. Subsequently, for each inlet temperature, the methanol conversion at the reactor outlet is calculated, and the results are presented in Figure 1.1.

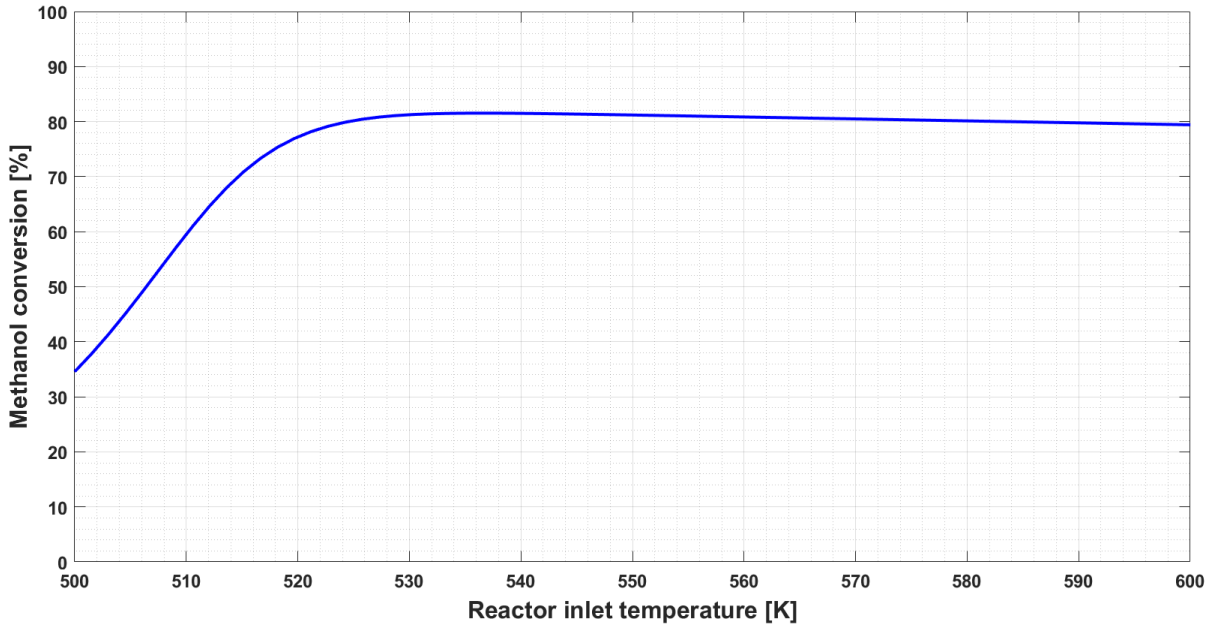

Figure 1.1. *Methanol conversion profile against inlet temperature of the adiabatic packed tubular reactor under examination.*

As shown in Figure 1.1, the optimal reactor inlet temperature for the examined reactor ranges between 535 K and 545 K, achieving the maximum methanol conversion. Specifically, a temperature of 541 K is selected, as indicated by Luyben (2012), where the methanol conversion reaches 81.5 %. This inlet temperature enables achieving approximately 81.5 % methanol conversion even with increased feed molar flow rate.

The same reactor is then studied using various vapor feed molar flow rates in order to assess its performance under different throughput conditions compared to the design conditions, and the results of this study are presented in Figure 1.2. In Figure 1.2(a), the methanol conversion along the reactor length is illustrated for different vapor feed molar flow rates: + 50 % and + 20 % of the nominal value of 295.2 kmol/h are represented by a solid red line with asterisk markers and a dotted red line, respectively. Similarly, - 50 % and - 20 % variations of the nominal value are

depicted by the solid blue and dash-dot blue lines, respectively, with the nominal value shown as the dashed black line. Figure 1.2(b) presents the corresponding reactor temperature profiles along its length.

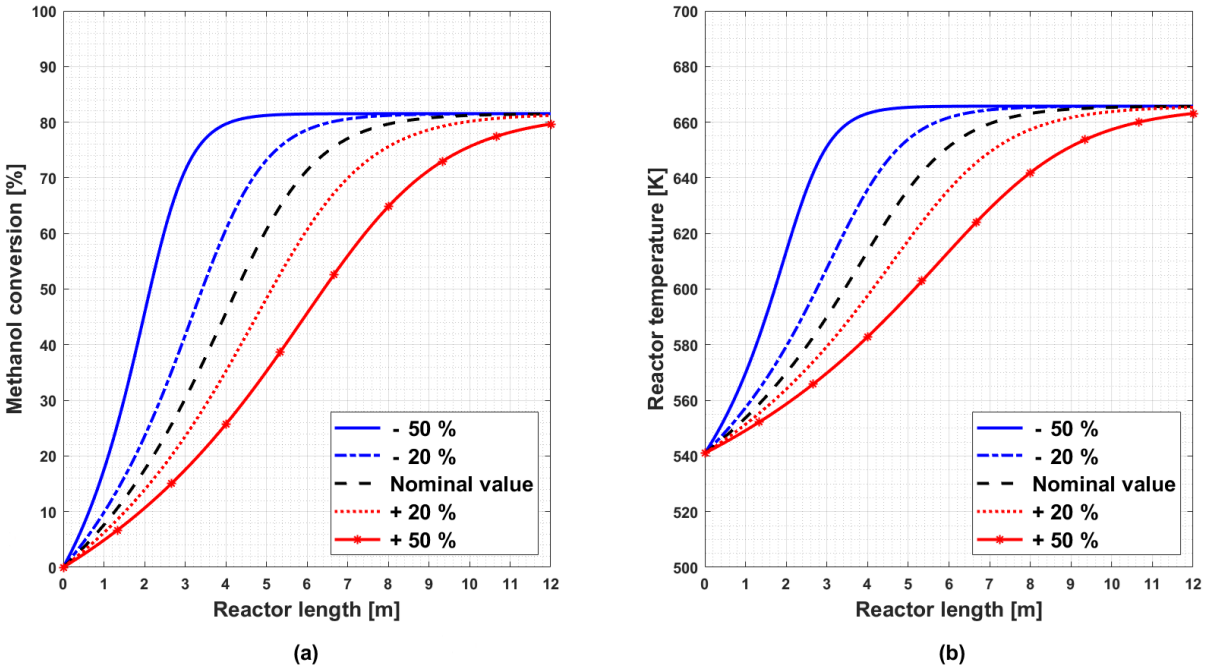

Figure 1.2. (a) *Methanol conversion profile along the reactor axial coordinate at different feed flow rates and* (b) *reactor temperature along the reactor axial coordinate at different feed flow rates.*

This analysis provides foundation for upcoming chapters, which will explore disturbances in the feed flow rate during dynamic simulations. From Figure 1.2, it is evident that the reactor design is sufficiently sized to reach its intended conversion across a wide range of feed molar flow rates, with minimal variation in reactor outlet temperature.

Additionally, Figure 1.2(b) reveals another feature of the adiabatic tubular reactor performing an exothermal reaction: the reactor temperature profile increases monotonically along its length. Therefore, the reactor inlet temperature fixes the temperature rise within the reactor, thereby setting the reactor outlet temperature, as discussed by Luyben (2007, p. 252). This aspect will be revisited when studying the reactor dynamics.

Based on the data retrieved about the reactor from Luyben (2012) and the reactor inlet temperature from the previous analysis, the process presented in the same article is developed and implemented in Aspen Plus V14, using the UNIQUAC activity coefficient model for the thermodynamic property calculation of this multi-component system.

Specifically, the process feed consists of a liquid molar flow rate of 295.2 kmol/h, with a molar composition of 95 % of methanol and 5 % of water, entering the process at a temperature of 298 K, and a pressure of 20 atm. Subsequently, it is vaporized using vaporizer E - 101, operating at 14 atm.

The vaporizer is modelled in Aspen Plus using the `Flash2` block with vapor fraction of one, ensuring that no liquid streams leave the flash tank. The reasons behind selecting the flash model are discussed in §1.3 when the dynamics of this process are studied.

The heating fluid used in the vaporizer is medium pressure steam at 9 bar, whose saturation temperature at this pressure is 448 K and the mass specific enthalpy of condensation is - 2030.5 kJ/kg, both sourced from the NIST Chemistry WebBook (2024). This heating utility provides a sufficient minimum temperature difference, considering that the saturation temperature of the process fluid at the vaporizer pressure of 14 atm is approximately 425 K.

The saturated vapor exiting the vaporizer is then preheated in E - 102 heat exchanger to the temperature of 541 K before entering the adiabatic tubular reactor R - 101, which is modelled as a plug-flow reactor with the `RPlug` block in Aspen Plus. At the reactor exit, the hot reactor effluent at a temperature of approximately 663 K is sent back to E - 102 in order to recover the heat provided by the exothermal reaction before exiting the process.

Regarding E - 102, the overall heat transfer coefficient U, as provided by Luyben (2012), is assumed to be 170 $W \cdot m^{-2} \cdot K^{-1}$, consistent with this gas/gas application. The resulting required heat exchange area (A) is 27.5 m^2 and the heat exchanger is configured with one shell pass and two tube passes (1-2 configuration, not shown in Figure 1.3 for convenience). The required heat duty ($\dot{Q}$) to preheat the cold vapor flow to the desired reactor inlet temperature is 0.5433 MW.

Finally, Figure 1.3 illustrates the process flow diagram of this base design configuration, featuring all the described equipment. The corresponding stream table, Table A.1, and equipment table, Table A.2, are provided in Appendix A.

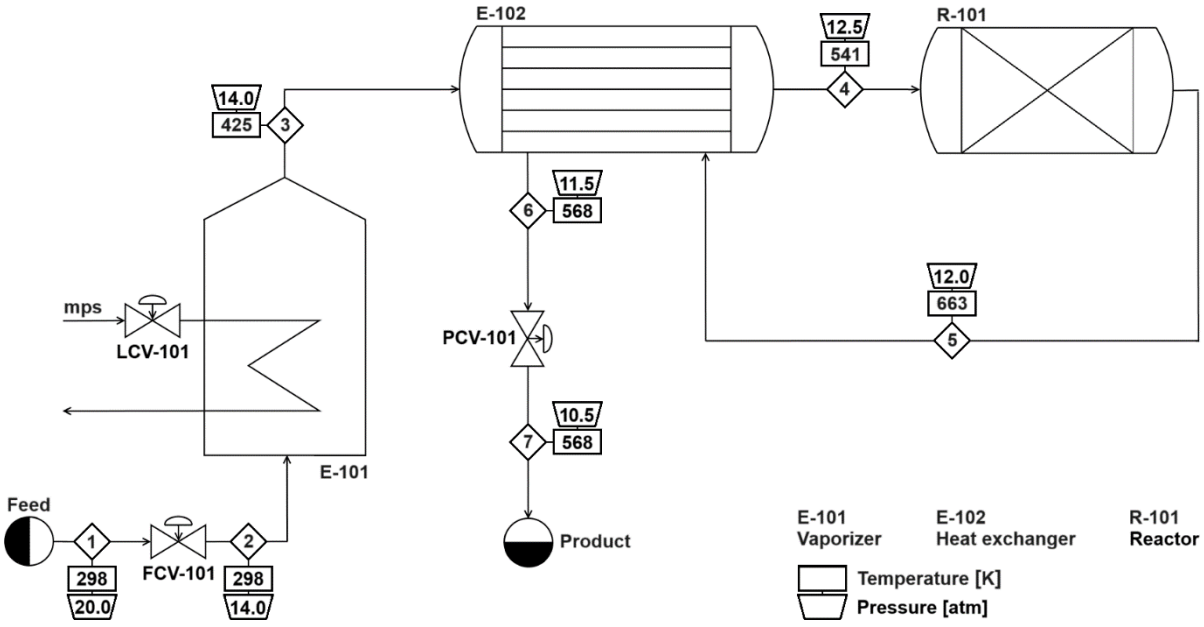

Figure 1.3. *Process flow diagram of the base design configuration, illustrating all equipment schematics and the temperatures and pressures of all streams.*

The process flow diagram shown in Figure 1.3 includes three control valves: FCV - 101 on the

process feed line, LCV - 101 on the medium pressure steam stream line, and PCV - 101 on the heat exchanger hot side outlet stream line. The operation of these valves and relevant information about them are discussed in detail in §1.3.

1.2 Reactor dynamics

In this section, the reactor dynamics are studied independently from the process described in §1.1, reproducing the results presented by Luyben (2012). To initiate this study, a steady-state simulation is developed in Aspen Plus using the same reactor configuration of the base design. In Figure 1.4, the flowsheet implemented in Aspen Plus is presented, along with all the temperature and pressures of all streams.

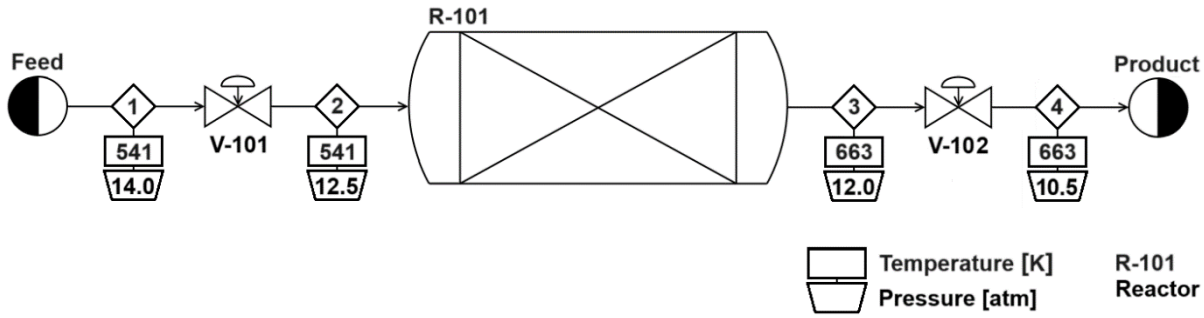

Figure 1.4. *Process flow diagram of the reactor in isolation, illustrating all the temperatures and pressures of all streams.*

In Table 1.1, the molar flow rates and molar fractions of methanol (x_{CH_3OH}), water (x_{H_2O}), and dimethyl ether ($x_{CH_3OCH_3}$) are presented for all the streams depicted in Figure 1.4.

Table 1.1. *Molar flow rates and compositions of all the stream.*

Stream number	***Molar flow rate*** **[kmol/h]**	x_{CH_3OH} **[%]**	x_{H_2O} **[%]**	$x_{CH_3OCH_3}$ **[%]**
1	295.2	95.0	5.0	0.0
2	295.2	95.0	5.0	0.0
3	295.2	17.6	43.7	38.7
4	295.2	17.6	43.7	38.7

The two valves, V - 101 and V - 102, are necessary for implementing the process in Aspen Plus Dynamics V14, to include a pressure drop/flow relationship for both the feed and product streams, which is required for pressure-driven dynamic simulations.

In a pressure-driven simulation, the flow rates are related to the pressure drops, and although it is more complex than a flow-driven simulation, it is preferred as it simulates the process more realistically. Thus, in all the dynamic simulations discussed in this Thesis, pressure-driven flows are considered.

Before exporting the steady-state simulation from Aspen Plus to Aspen Plus Dynamics, it is necessary to provide additional information related to the size and the dynamic behaviour of all the equipment in the flowsheet, in this case only the reactor.

Among the various parameters related to the reactor operation, the `heat transfer at equal temperatures` option is selected, assuming fast heat transfer between the catalyst and process fluid, resulting in both being always at the same temperature. This option enables accounting for the heat transfer between catalyst and process fluid, necessitating the information on the bed voidage, the catalyst solid density, which have been already provided, as well as the heat capacity of the catalyst, which is not mentioned by Luyben (2012).

Additionally, to accurately simulate the tubular reactor, selecting an appropriate number of discretization points of the reactor, referred to as lumps, is crucial. The tubular reactor dynamic model is described by a system of partial differential and algebraic equations (PDAEs), which is modelled in Aspen Plus Dynamics using the Method of lines approach, as reported by Aspen Technology (2022b). Specifically, using a partial differential equation discretization scheme, the PDAE system is transformed into ordinary differential and algebraic equations (DAEs), which are subsequently integrated dynamically using the in-built solvers. The selected discretization scheme is the first-order backward finite difference method, the default option provided in Aspen Plus.

Therefore, the number of discretization points affects the accuracy of the simulation, and if not adequately selected, mismatches are introduced in Aspen Plus Dynamics after exporting the Aspen Plus simulation, due to the different solution strategies used for the tubular reactor model between these two software.

In order to determine an appropriate number of lumps and the value of the catalyst heat capacity, the reactor is simulated with Aspen Plus Dynamics, selecting different values for these parameters and trying to replicate the results presented by Luyben (2012). Specifically, the goal was to reproduce the dynamic behaviour of the reactor and its outlet temperature response following a step increase in reactor inlet temperature from 541 K to 551 K after 0.5 h. Ultimately, by using 100 lumps and a catalyst heat capacity ($c_{P,cat}$) of 1280 $J \cdot kg^{-1} \cdot K^{-1}$, consistent with the findings of Sierra et al. (2013), a response reasonably similar to that of Luyben (2012) is achieved. The results are depicted in Figure 1.5.

In Figure 1.5(a), the step change in reactor inlet temperature at time 0.5 h is depicted, while Figure 1.5(b) illustrates the corresponding dynamic response of the reactor outlet temperature. Two scenarios are compared: one where heat transfer between the process gas and the catalyst is considered, represented by the solid blue line, and one where it is neglected, represented by the dashed red line.

When heat transfer is considered, a counterintuitive response is observed. Specifically, after the step increase in reactor inlet temperature, the reactor outlet temperature initially decreases, reaching a minimum value of about 652 K at 1.4 h. Thereafter, it begins to increase, eventually

attaining a new steady-state value of about 671 K, which matches the steady-state condition observed in the case where heat transfer is neglected. This new steady-state value corresponds to the expected outcome from a steady-state simulation of the reactor, with the reactor inlet temperature set to 551 K instead of the nominal 541 K.

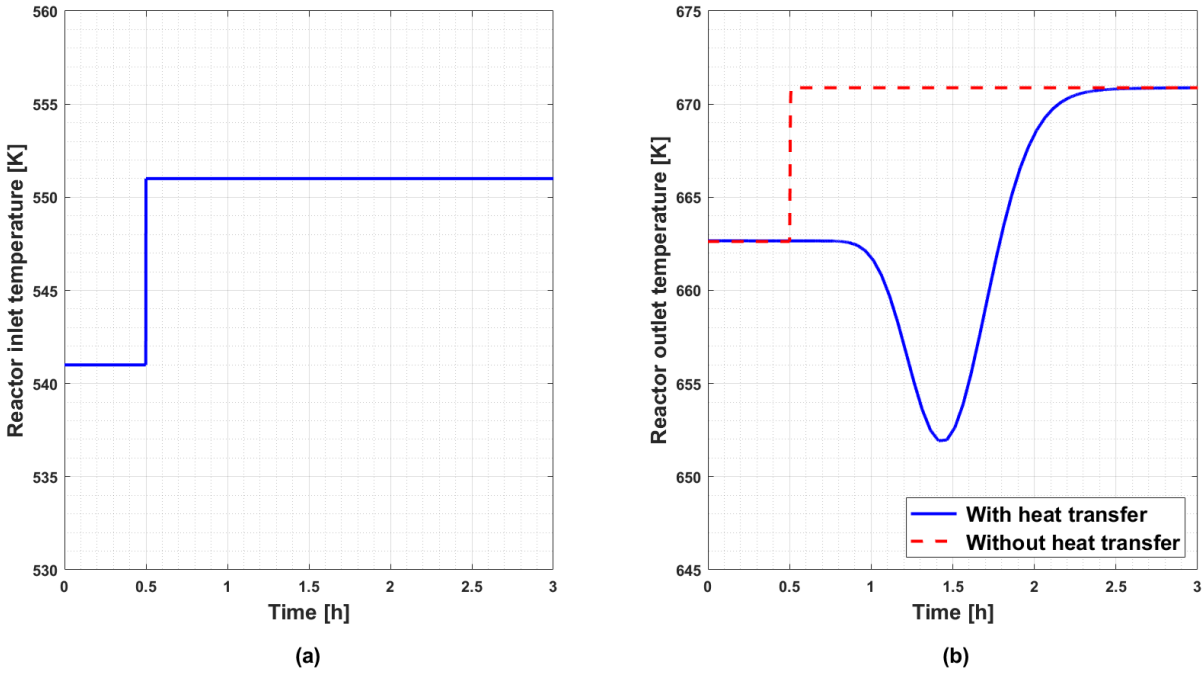

Figure 1.5. (a) *Step increase of reactor inlet temperature at the time of 0.5 h and* (b) *reactor outlet temperature over time for the case where heat transfer between process gas and catalyst is considered compared to the case where it is neglected.*

This severe inverse response of the reactor when considering heat transfer between the process gas and the catalyst is attributed to the thermal capacitance of the catalyst, which has a significantly larger mass and heat capacity compared the gaseous process fluid, the high per pass conversion, and the absence of axial dispersion as the tubular reactor is modelled with the `RPlug` block of Aspen Plus, which assumes only perfect radial mixing. This phenomenon is explained in detail by Luyben et al. (1999, pp. 99-104) and Luyben (2007, pp. 319-323).

Due to the thermal inertia of the catalyst, following the inlet temperature step increase, it takes some time for the temperature at the front end of the reactor to begin rising. As this temperature increases, methanol conversion in this section starts to increase due to the enhanced rate of reaction. However, the methanol concentration in the subsequent sections of the reactor is reduced, leading to a decrease of rate of reaction at these axial coordinates. Consequently, a transient temperature decrease is observed along the reactor because less heat is produced from the exothermic reaction. Ultimately, the higher reactor inlet temperature results in a new steady-state with higher temperatures along the entire reactor length compared to the previous steady-state conditions, reproducing the expected temperature rise of the adiabatic tubular reactor with an inlet temperature of 551 K.

1.2.1 Number of lumps

During the study of the reactor dynamics, it is observed that the number of lumps critically impacts the dynamic behaviour of the reactor. Therefore, the number of lumps effect on the reactor dynamics is assessed in detail in this section.

In particular, the reactor outlet temperature response is studied following the same step change in reactor inlet temperature as considered in §1.2, using the same reactor characteristics and catalyst properties but varying the number of reactor discretization points. The reactor outlet temperature responses are then collected and compared. Figure 1.6(a) and Figure 1.6(b) compares the minimum reactor outlet temperature achieved during the inverse response and the time at which it occurs for different numbers of lumps, respectively. As expected, a finer discretization of the tubular reactor results in more accurate representation of its dynamic behaviour. This increased accuracy is particularly evident on the magnitude of the entire inverse response and the minimum temperature reached which is represented in Figure 1.6(a). For instance, with ten lumps, the minimum temperature drops slightly below 660 K, compared to the initial steady-state value of approximately 663 K, whereas with eight hundred lumps, the temperature reaches slightly less than 650 K. Accordingly, the magnitude of the temperature variations under dynamic simulation is strongly influenced by the discretization of the reactor.

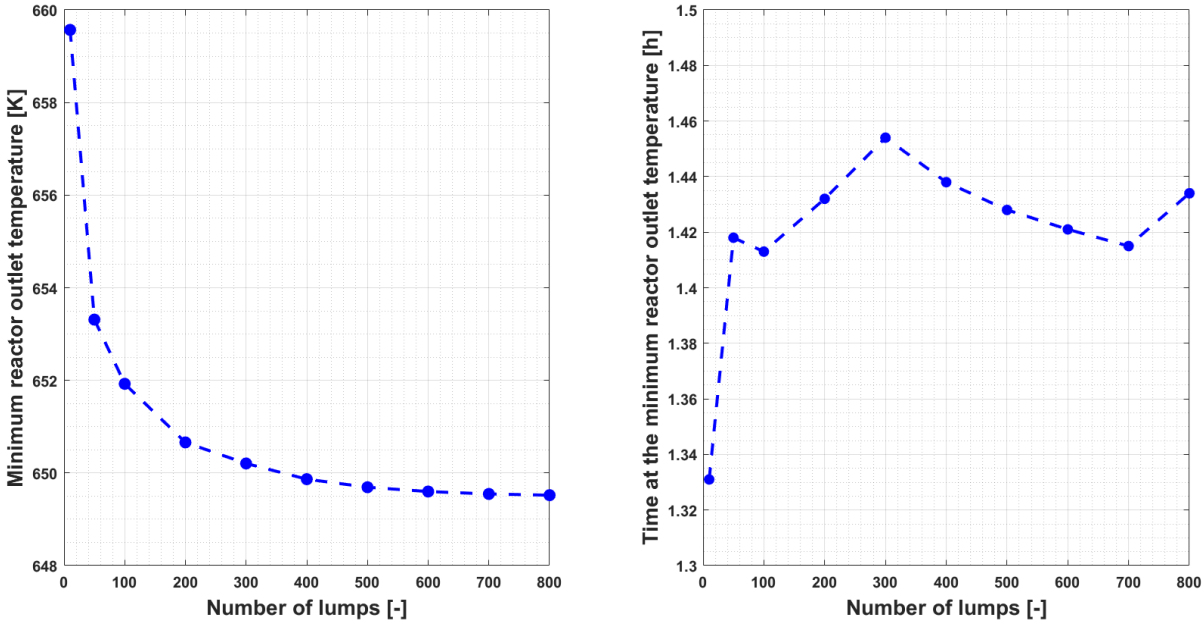

Figure 1.6. (a) *Minimum temperature reached at the reactor outlet temperature and* (b) *the time of its occurrence after a step increase of 10 K of the reactor inlet temperature at time 0.5 h, considering different number of discretization points (lumps) of the reactor.*

However, when considering the duration of the dynamic response of the reactor and the time at which the minimum reactor outlet temperature occurs, these factors are not as significantly influenced by the number of lumps. With fifty lumps, the reactor dynamic behaviour is already

adequately represented.

While finer discretization of the reactor yields greater accuracy, it also increases the computational effort, resulting in slower dynamic simulations that may not run, especially when the reactor is part of a more complex process. Considering this trade-off between accuracy and computational effort and following the suggestion provided by Aspen Technology (2022a) to use five lumps for every 10 K change in temperature or 10 % change in composition, the final selection of 50 lumps is made. This choice provides satisfactory results with reasonable computational effort, enabling the successful execution of the dynamic simulations for further studies in this Thesis.

The same plot with 100 lumps, represented in Figure 1.7, is recreated with 50 lumps and compared to the case with 100 lumps in Figure 1.5. Comparing the 50 lumps case to the 100 lumps case, the reactor outlet temperature decreases by about 1.5 K less with 50 lumps. Additionally, the reactor dynamics appears slightly slower with 50 lumps. Nonetheless, the reactor dynamic behaviour is still adequately represented.

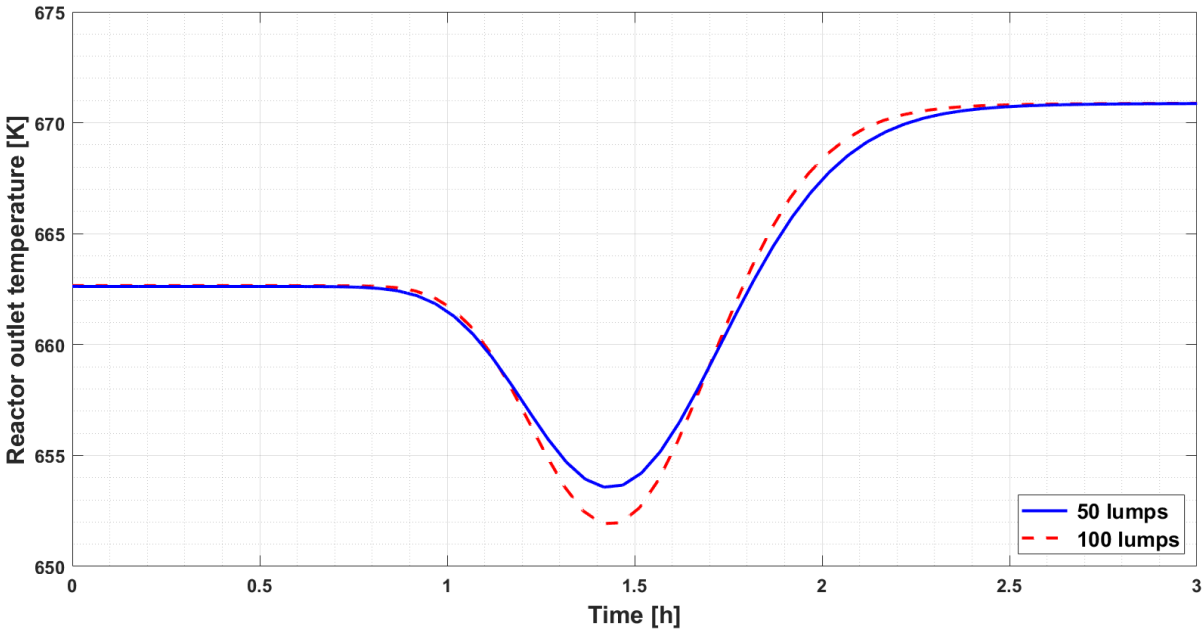

Figure 1.7. *Reactor outlet temperature over time, following a step increase of 10 K of the reactor inlet temperature at time 0.5 h, for the cases where 50 and 100 lumps are considered.*

In conclusion, the reactor dynamics has been thoroughly studied and is now properly modelled with 50 lumps. Therefore, this configuration will remain unchanged in the subsequent study.

1.3 Base case dynamic simulation

Following the study of the reactor dynamics and maintaining the same information on reactor modelling and catalyst properties, the Aspen Plus simulation of the base design case is prepared

to be exported into the Aspen Plus Dynamics environment, where the process control schemes are implemented, and the process is simulated dynamically.
Table 1.2 summarizes all the reactor design and modelling parameters, along with the catalyst properties, which are presented and discussed in sections §1.1 and §1.2.

Table 1.2. *Summary of all reactor R - 101 design parameters and catalyst properties.*

Number of lumps	L [m]	d [m]	ε [-]	ρ_{cat} [kg/m^3]	d_p [m]	$c_{P,cat}$ [J·kg^{-1}·K^{-1}]
50	12	1.2	0.28	1700	0.01	1280

Regarding the vaporizer, additional information on the vessel geometry and the heating utility is required. The `Flash2` unit is used to simulate a flash tank with a vapor fraction of 1. This choice allows for proper modelling of the vessel geometry and consideration of a liquid level within the unit, which will be further controlled with a liquid level controller.
The vaporizer is sized to provide 5 min of liquid holdup when half full. Considering the design vapor volumetric flow rate exiting the vaporizer, the corresponding volume of vapor in 5 min of operation is calculated. This volume, representing half of the tank volume, is then doubled to obtain the total vessel volume. Assuming a vertical cylindrical vessel with a flat head type and an aspect ratio of three, the vessel diameter (d_v) and the height (h_v) are calculated. The nominal steady-state volume of liquid within the tank is then set at half the overall tank volume. Finally, all features of the vaporizer design are summarized in Table 1.3.

Table 1.3. *Summary of all vaporizer E - 101 design parameters.*

Vessel type	***Vessel orientation***	***Head type***	d_v [m]	h_v [m]
Cylindrical	Horizontal	Flat	1.02	3.05

For the heating utility, since condensing steam is used, the `Condensing` heat transfer option is selected. With this method, the heating medium temperature remains constant, and the vaporizer heat duty is evaluated as the lesser of the heat duty due to temperature differential between the liquid in the tank and the medium pressure steam, and the duty calculated assuming complete condensation of the steam, as provided by Aspen Technology (2022a).
Regarding the heat exchanger, the dynamic modelling of this unit requires the volume specifications at the inlet and outlet of both the hot and cold sides. To evaluate these values, the procedure suggested by Luyben (2007, pp. 391-395) is followed. The heat exchanger area (A) is used to approximate the number of tubes (N_t), using standard values for the tube length (L_t), tube thickness (s_t), and tube external diameter ($d_{t,ext}$). All these parameters are utilized to calculate the volume inside the tubes (V_t), which is subsequently equally allocated between the

tube inlet and outlet. Consequently, the section volume (V_{sec}) obtained for both the tube inlet and outlet is also assumed for the shell volume at the inlet and outlet. These volumes are essential to approximate the dynamics of the heat exchanger, specifically to evaluate the residence time of the process gas on both sides of the equipment.

Additionally, a default value for the heat exchanger heat capacity of 500 $J \cdot kg^{-1} \cdot K^{-1}$ and a mass density of 7700 kg/m^3 are considered, consistent with steel as the material of construction. This density is used to calculate the tube mass, which is assumed to approximate the heat exchanger mass (m), thus neglecting the shell mass. This mass is equally distributed between the inlet and outlet of the shell and tube sides, and the obtained mass is referred to as section mass (m_{sec}). Each section mass and the heat exchanger heat capacity are used to model the equipment heat transfer during the dynamic simulation. Table 1.4 details all preheater main characteristics.

Table 1.4. *Summary of all heat exchanger E - 102 design parameters.*

Configuration	$\dot{Q}$ [MW]	U [$W \cdot m^{-2} \cdot K^{-1}$]	A [m^2]	L_t [m]	s_t [m]	$d_{t,ext}$ [m]	N_t [-]	V_t [m^3]	V_{sec} [m^3]	m [kg]	m_{sec} [kg]
1-2	0.5433	170	27.5	10	0.002	0.025	35	0.12	0.06	389	97

Finally, the Aspen Plus file with all this additional information is exported into Aspen Plus Dynamics, where the dynamic simulation is run. This Aspen Plus Dynamics file exhibits slight discrepancies in the flow rates of all streams compared to the previous steady-state simulation. This issue arises because the valves are not appropriately sized for the application. Additionally, the vaporizer liquid level is observed to be at zero, indicating the absence of liquid in the tank. To address the liquid level issue, a solution was implemented by exporting a new steady-state file from Aspen Plus where the process feed is set with a molar flow rate that is 1.0001 times greater than the previous value, specifically at 295.2 kmol/h. Furthermore, the vapor fraction in the flash unit is set to 0.9999 instead of 1.

These slightly modified values will be adjusted during the dynamic simulation. Specifically, the valve on the liquid stream line exiting the flash is closed. Thereafter, the process is simulated, and the process feed flow rate is adjusted to the correct value of 295.2 kmol/h using the feed flow rate controller, which will be discussed subsequently in this Chapter. In conclusion, by pressing the `Initialization` button, the correct steady-state values of all the variables and the correct liquid level are saved in the simulation.

For the flow rates mismatches due to the inadequate valve sizing, the valve `Resize` function in Aspen Plus Dynamics is used to recalculate the valve flow coefficients (K_v). This function is implemented following the guidelines provided by the International Society of Automation (2007) and requires selecting the correct valve fail-position, the valve characteristic, the valve nominal conditions, and the `Rigorous` model for each valve.

In this application, the valve characteristics considered for all valves are either equal-percentage

or linear. The equal-percentage characteristic is implemented in Aspen Plus Dynamics as:

$$f = \frac{l^2}{\sqrt{2.0 - l^4}}, \tag{1.9}$$

where f is the inherent flow characteristic, which is dimensionless and ranges from 0 to 1, and l is the stem position, which is also dimensionless and ranges from 0 to 1. The linear characteristic is implemented as follows:

$$f = l. \tag{1.10}$$

Considering, valve LCV - 101 on the steam line presented in Figure 1.8, Aspen Plus and Aspen Plus Dynamics do not allow for the presence of this stream in the simulation. However, in Aspen Plus Dynamics, it is possible to manipulate the flow rate of the heating utility directly. This can be considered a limitation of this study, as a simplified level control loop will be introduced. However, this simplification is not of significant concern for the focus of this study, which is primarily on the feed-effluent heat exchanger/reactor system. In a real application, valve LCV - 101 would be chosen as fail-closed, preventing the provision of additional heat to the system and stopping the liquid evaporation in the tank.

The main features of valves FCV - 101 on the process feed line and PCV - 101 on the final product stream line, also illustrated in Figure 1.8, are considered in Table 1.5. This Table shows the nominal conditions, including the nominal volumetric flow rate (q), the nominal pressure drop ($\triangle P_v$), and stem position, and all the main features of each valve.

Table 1.5. *Summary of all valves FCV - 101 and PCV - 101 design parameters.*

Valve	***q*** **[m^3/h]**	**$\triangle P_v$ [atm]**	***Valve opening*** **[%OP]**	**K_v [$m^3 \cdot h^{-1} \cdot bar^{-0.5}$]**	***Valve action***	***Valve characteristic***
FCV - 101	11.6	6	50	23.5	Air-to-open	Equal-percentage
PCV - 101	1195.0	1	50	225.3	Air-to-close	Linear

Considering valve FCV - 101, the fail position is set to fail-close to avoid introducing additional material into the process in case of failure. Equal-percentage valve characteristic is chosen, because it allows for the introduction of process feed molar flow rates up to 1.5 times the nominal value of 295.2 kmol/h, which will be required in the simulations of the next chapters. Additionally, choosing a linear characteristic the valve would not provide such high flow rates, and it would require increasing the inlet feed pressure up to 26 atm, resulting in a designed valve pressure drop of 12 atm, which is twice the actual value, in order to introduce the same high flow rates.

Regarding valve PCV - 101, the fail position is set to fail-open in order to allow all material in

the system to leave, thereby avoiding hazardous over pressurization. Linear valve characteristic is selected because the valve performs comparably well with the equal-percentage characteristic but avoids the use of an unnecessarily larger valve as would be the case with the latter.

Finally, all the valves are configured with default first-order dynamics, featuring a time constant of 0.1 s and a valve gain of 1 %OP/%CO.

With the dynamic simulation now prepared, the control loops for this base design case are implemented. Specifically, the system includes an inlet process feed flow rate controller, a tank liquid level controller, and a heat exchanger hot side outlet pressure controller.

In Figure 1.8, the base design configuration with all these control loops is represented. The relevant stream table, Table A.1, and equipment table, Table A.2, are provided in Appendix A.

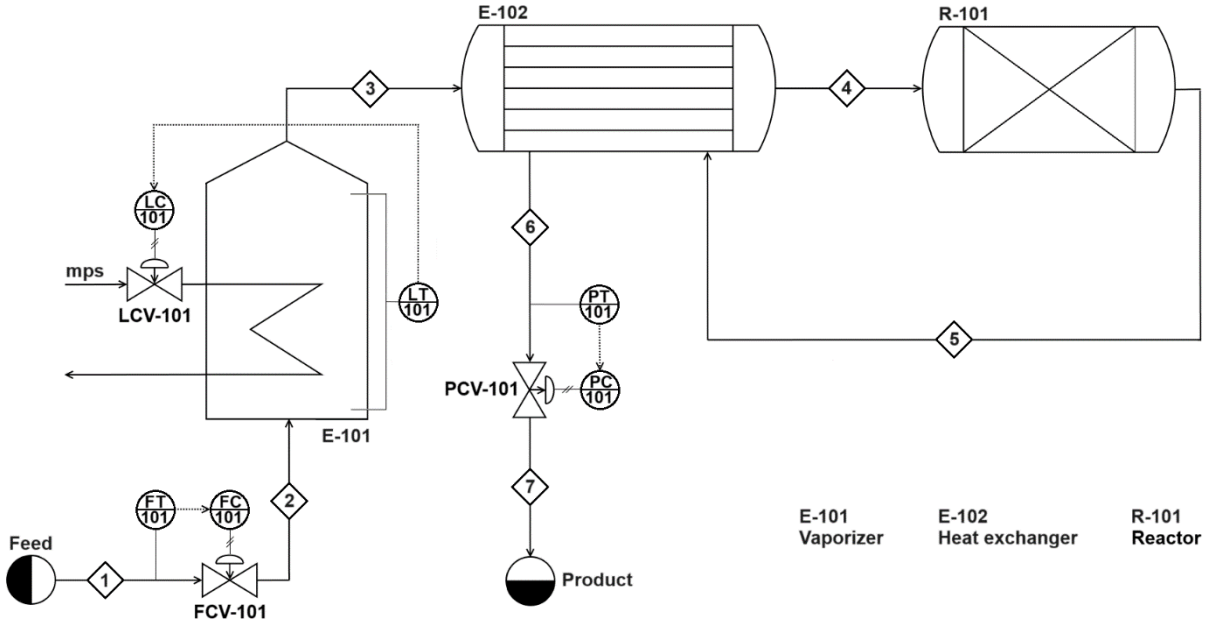

Figure 1.8. *Process flow diagram of the base design configuration and all the control loops.*

Firstly, the control loop with the fastest dynamics, namely the process feed control loop, is implemented. This loop utilizes the measurement of process feed molar flow rate via a sensor-transmitter unit, FT - 101, which has negligible dynamics.

The feed flow rate controller, FC - 101, uses this measurement to manipulate the opening of valve FCV - 101. The controller action is set to reverse, considering that the valve is air-to-open. For example, if the sensor measures a molar flow lower than the set point of 295.2 kmol/h, the controller increases its output, resulting in a greater valve opening to raise the molar flow rate accordingly.

The selected sensor transmitter range is 0 - 590 kmol/h, which enables the controller output to be at 50 %CO at nominal steady-state conditions and is sufficiently large for the purposes of this application. The tuning of the proportional-integral (PI) controller is configured with a controller gain (K_C) of 0.5 %CO/%TO and an integral time constant (τ_I) of 0.3 min, as suggested

by Luyben (2002, pp. 26-27), with proven satisfactory performance after implementation.
Secondly, with the feed controller in automatic, the heat exchanger hot side outlet pressure control loop is studied. This loop utilizes a sensor-transmitter unit, PT - 101, also with negligible dynamics, with a range of 6 - 17 atm. This range is selected to ensure the controller output to be at 50 %CO at nominal steady-state conditions and sufficiently large for this application. The pressure controller, PC - 101, exploits this measurement to manipulate the opening of valve PCV - 101. The controller action is set to reverse, as the valve is air-to-close. For example, if the sensor measures a pressure higher than the set point of 11.5 atm, the controller reduces its output, resulting in a greater valve opening to reduce the heat exchanger hot side outlet pressure accordingly.
This controller is implemented with a PI action, and its parameters are found by first performing a relay feedback test (ATV) to find the ultimate controller gain and period, which are approximately 13.0 %CO/%TO and 0.3 min. Then, the Tyreus-Luyben controller tuning rules are applied, and after slight adjustments, the controller parameters are finalized with a gain of 4 %CO/%TO and an integral time constant of 0.3 min.
Finally, the level control scheme is implemented with the other two controllers already in automatic mode. This scheme utilizes a sensor-transmitter unit, LT - 101, whose dynamic behaviour is neglected, with a range of 0 - 3.05 m, in order to cover the entire vaporizer height. The level controller, LC - 101, uses this measurement to directly manipulate the mass flow rate of the medium pressure steam. Therefore, the controller output range is set to 0 - 3.55 kg/s, directly referring to the manipulated variable, and ensuring that at nominal steady-state, the output of the controller, which is 1.78 kg/s, is centred within this range.
The controller action is set to direct, so that, for example, if the sensor measures a level higher than the set point of 1.53 m, the controller increases the heating utility mass flow rate. Additionally, this controller is implemented with a PI action, and its parameters are evaluated by first performing an ATV test to find the ultimate controller gain and period, approximately 16.6 %CO/%TO and 1.9 min. Then, the Tyreus-Luyben controller tuning rules are applied, and after slight adjustments, the controller parameters are finally determined, with a controller gain of 4 %CO/%TO and an integral time constant of 5 min.

Table 1.6. *Tuning parameters of all the controllers in the base case configuration.*

Controller	***Span***	K_C **[%CO/%TO]**	τ_I **[min]**	***Action***
FC - 101	590 kmol/h	0.5	0.3	Reverse
PC - 101	11 atm	4	0.3	Reverse
LC - 101	3.05 m	4	5	Direct

In Table 1.6 all the relevant features of the three controllers are summarized.
With all the control loops integrated into Aspen Plus Dynamics, the base design case is studied

dynamically, focusing specifically on the reactor inlet and outlet temperatures, both of which are critical in the heat exchanger/reactor system. The inlet temperature is particularly important, as for an adiabatic tubular reactor, it directly determines the steady-state temperature rise within the reactor, thereby fixing the steady-state value of the reactor outlet temperature.

The outlet temperature is also significant because it reveals the inverse responses of the packed tubular reactor following changes in the inlet temperature, as well as the potential dynamic lags of the reactor in response to these changes.

To conduct this study, various process feed flow rates are introduced as disturbances to the process via FC - 101 by changing the set point of this controller. In particular, step variations in the set point of this controller are introduced at time 0.5 h, corresponding to ± 10 % and ± 50 % of its nominal value of 295.2 kmol/h. These disturbances are intended to reveal different dynamic behaviours and assess the potential instability of the system.

In Figure 1.9, the aforementioned positive step increases of the feed flow rate are considered. In Figure 1.9(a), the case with a 10 % step increase of the process feed flow rate at time 0.5 h is presented. In Figure 1.9(b), the same approach is used to present the case with a 50 % step increase.

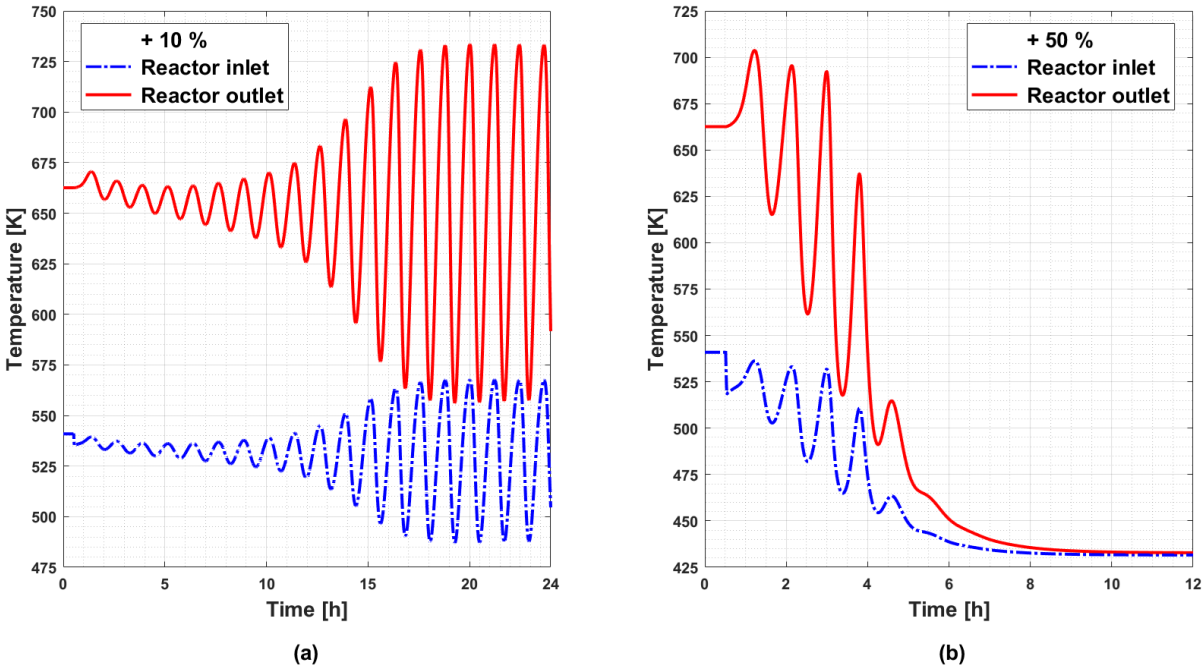

Figure 1.9. *Base case dynamic behaviour, considering the inlet and outlet reactor temperatures following a step increase of* (a) *10 % and* (b) *50 % of the process feed molar flow rate at time 0.5 h.*

The 10 % step increase in the process feed flow rate produces an oscillating response in the reactor inlet and outlet temperatures, with an approximately constant period but an increasing amplitude. This amplitude increase stops for both temperatures at about 17 h after the perturbation of the system.

As reported by Luyben et al. (1999, pp. 176-181), this FEHE/reactor system exhibits multiple steady-state conditions. However, under the increased process feed flow rates being examined, the system demonstrates a steady-state condition which is dynamically unstable. Consequentely, the severe inverse reactor response analyzed in §1.2, coupled with the positive feedback of energy from the reactor back to the preheater, induces oscillatory behaviour around the unstable steady-state.

A similar behaviour is observed also with higher step increases of the process feed molar flow. However, at a 50 % step increase, as represented in Figure 1.9(b), the dynamic behaviour changes. With this larger disturbance, the reactor inlet and outlet temperatures, after few initial oscillations, begin to decline. After about 6 h, the system achieves a new steady-state at lower temperatures.

In this scenario, the increased molar flow rate shifts the system operating region into a low-temperature steady-state condition which is dynamically stable. This behaviour, known as "quenching," represents a situation where the reaction is nearly stopped. Therefore, after the initial oscillations due to the inverse reactor response and the positive feedback of energy, less heat is gradually generated by the reaction and thus recovered in the preheater, until the system stabilizes at a low-temperature condition close to the temperature of the vapor cold stream exiting the vaporizer E - 101.

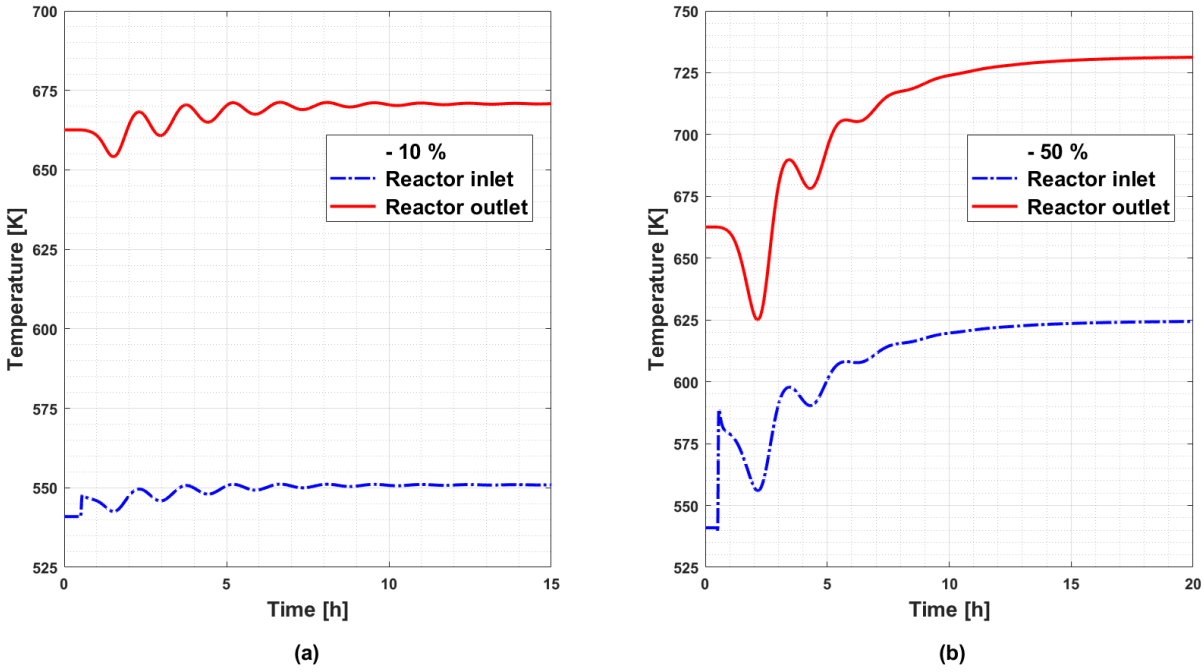

Figure 1.10. *Base case dynamic behaviour, considering the inlet and outlet reactor temperatures following a step decrease of* (a) *10 % and* (b) *50 % of the process feed molar flow rate at time 0.5 h.*

In Figure 1.10(a), a 10 % step decrease in the feed flow is considered, while in Figure 1.10(b), a 50 % step decrease is examined.

Both the - 10 % and - 50 % step changes in the process feed flow rate, as well as intermediate step changes, produce oscillating responses in the reactor inlet and outlet temperatures. These oscillations are dampened within approximately 7 h for both the step changes, ultimately settling at new steady-state values with higher temperatures compared to the nominal steady-state values. These two case studies, along with observations from intermediate step decreases, show that lower process feed flow rates result in higher final temperatures in the new steady-state condition.

This phenomenon is explained as follows: the perturbed system initially results in an increased preheating achieved by the vapor stream flowing into the heat exchanger and entering the reactor. Consequentely the outlet temperature decreases, due to the reactor inverse response, which also reduces the reactor inlet temperature. This generates a series of oscillations that are ultimately dampened as the system shifts towards the high-temperature steady-state, which is dynamically stable, as shown in Figure 1.10.

Finally, these results confirm the strong non-linearities and critical dynamic problems of the heat exchanger/reactor system, suggesting the need for a careful and thorough analysis of the design configurations and strategies to control the reactor inlet and, consequently, the outlet temperatures, thereby promoting stable and optimal system operation, under different throughput conditions.

Chapter 2

Control with bypass

Following the issues discussed in §1.3, this Chapter introduces two design configurations and a control strategy to control the reactor inlet temperature: the design case with 20 % bypass and the design case with 40 % bypass. For both configurations, all control loops are implemented. Finally, the two case studies are dynamically simulated to evaluate the performance of the control schemes.

2.1 Design case with 20 % bypass

In §1.3, the dynamic behaviour of the base design configuration is observed in response to step changes in the feed molar flow rate, observing oscillatory behaviour, as well as quenching or significant increase in the reactor inlet and outlet temperatures. Consequently, these issues, critical for both safety and process performance, highlight the necessity to develop a control system capable of stabilizing the process dynamics and mitigating the effects of throughput variations.

As observed in §1.3 and reported by Luyben (2012), the reactor inlet temperature is a crucial variable considering both the steady-state performance and the dynamic controllability of the process. From a steady-state perspective, this temperature dictates the temperature rise along the adiabatic tubular reactor and the methanol conversion. Therefore, it is important to control this temperature, as it ensures the desired conversion and determines the outlet reactor temperature.

From a dynamic standpoint, variations in the reactor inlet temperature cause inverse response in the reactor outlet temperature. These variations are then recycled back through the heat exchanger, leading to oscillations in both temperatures. For this reason, and due to the inherent time delays in reactor dynamics, controlling the outlet temperature can result in inappropriate and challenging controller actions. In contrast, controlling the reactor inlet temperature can mitigate these oscillatory dynamics.

Considering the base design configuration presented in Figure 1.8, there are no available variables to manipulate in order to control the reactor inlet temperature. Therefore, this Chapter introduces a new process design, enabling the implementation of the aforementioned control loop.

2.1.1 Steady-state design and Aspen Plus simulation

In this section, a new process design is developed, starting from the base case configuration presented in Figure 1.3. Specifically, the vapor stream exiting the vaporizer is split into two streams: the main stream, which subsequently flows into the heat exchanger, and the bypass stream, which flows around the heat exchanger before mixing with the main stream. The resulting mixed stream then enters the reactor. The reactor and vaporizer are implemented as described in §1.2, while modifications to heat exchanger E - 102 are required due to the introduction of the bypass stream.

The design bypass fraction, *b*, defined as the ratio between the bypass flow rate and the process feed molar flow, is fixed at 20 %, as indicated by Luyben (2012). Due to the presence of the bypass stream, the flow rate of the cold stream through preheater E - 102 is reduced. Consequently, the heat exchanger must raise the temperature of this stream to about 568 K, compared to the 541 K of the base design configuration. Although the cold vapor flow through the heat exchanger and its outlet temperature are modified, the heat exchanger heat transfer rate ($\dot{Q}$) remains at 0.5433 MW, as the overall heat duty to preheat the outlet vaporizer flow rate to the desired reactor inlet temperature is unchanged. Additionally, assuming the same overall heat transfer coefficient (U) of 170 $W \cdot m^{-2} \cdot K^{-1}$ and a 1-2 heat exchanger configuration, the heat exchange area (A) is increased to 34.0 m^2, from the previous value of 27.5 m^2 (+ 24 %), to accommodate for the decreased log-mean temperature difference (LMTD).

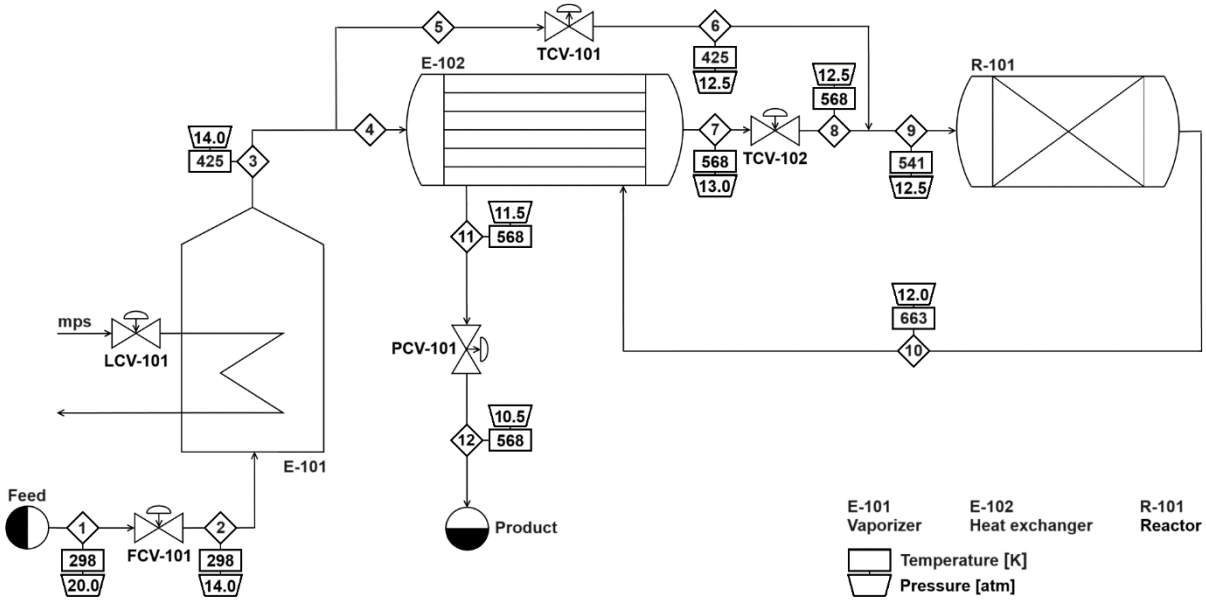

Figure 2.1. *Process flow diagram of the design case with 20 %, illustrating all equipment schematics and the temperatures and pressures of all streams.*

This 20 % bypass design configuration is depicted in Figure 2.1, with the relevant stream table, Table B.1, and equipment table, Table B.2, provided in Appendix B. Two additional control valves, TCV - 101 and TCV - 102, are included on the bypass line and after the heat exchanger

cold side outlet, respectively, whose features are discussed in detail in §2.1.2. Indeed, this configuration introduces one manipulated variable, namely the bypass fraction, which enables the implementation of the reactor inlet temperature control loop. However, as a consequence of the lower temperature differential compared to the base design case, the heat exchange area must be increased. Consequently, this new configuration requires greater capital investments.
The selection of the bypass stream aligns with the heuristic provided by Luyben (2011), which recommends that the stream to be bypassed should be the one whose temperature needs to be controlled. This strategy ensures that the hot reactor effluent flows entirely into the heat exchanger, thereby maximizing the utilization of the heat generated by the exothermic reaction. Meanwhile, the cold vapor flow rate through the heat exchanger is adjusted to control the reactor inlet temperature. Moreover, the dynamics of mixing between the cold stream passing through the heat exchanger and the bypassed stream occur almost instantaneously. Consequently, precise temperature control can be achieved downstream of the mixing point, as indicated by Luyben (2011).
Before focusing on the new temperature control loop and conducting dynamic studies of this bypass design, the configuration is first evaluated from a steady-state perspective following Soave and Barolo (2021), with necessary adaptations specific to this FEHE system under examination. In this system, the cold and hot heat exchanger flows occur along the same stream line, so variations in the former directly affect the latter. This study is crucial for understanding how selecting the design 20 % bypass fraction, which defines the operating region of heat exchanger under nominal conditions, impacts the controllability of the heat exchanger with bypass system under different throughputs. To recreate the conditions of the proposed approach, the heat exchanger presented in Figure 2.1 is simulated at steady-state to determine how the heat transfer rate changes with respect to the considered process feed molar flow rate. The analysis is conducted using Matlab®, employing the `fsolve` function to solve a system of non-linear algebraic equations. Specifically, this system comprises three equations: the cold side energy balance, the hot side energy balance, and the heat exchanger design equation.
The energy balance equation of the heat exchanger cold side at steady-state is expressed as:

$$\dot{Q} = \dot{n}_{cold} \cdot \int_{T_{C,in}}^{T_{C,out}} c_{P,cold}\, \mathrm{d}T = (1 - b) \cdot \dot{n}_{tot} \cdot \int_{T_{C,in}}^{T_{C,out}} c_{P,cold}\, \mathrm{d}T, \tag{2.1}$$

where the cold vapor molar flow rate, $\dot{n}_{cold}$, is given in [mol/s], and the cold side inlet and outlet temperatures, $T_{C,in}$ and $T_{C,out}$, are in [K]. The bypass fraction is fixed at 20 %. The molar heat capacity at constant pressure of the cold vapor stream, $c_{P,cold}$, is expressed in [J·mol^{-1}·K^{-1}]. This heat capacity is approximated as the sum of the heat capacities of the individual components, weighted by their molar fractions (x_i) which are the same of the process feed, namely of 0.95 for methanol, and 0.05 for water.

Additionally, $\dot{n}_{tot}$ is the total vapor molar flow rate exiting the vaporizer, expressed in [mol/s]. This flow is equal to the hot vapor molar flow, $\dot{n}_{hot}$, exiting the reactor. This equivalence holds because the reaction is equimolar, meaning that the molar flow rate entering the reactor remains constant along the reactor length, despite changes in composition.
The hot side energy balance at steady-state is defined as:

$$\dot{Q} = \dot{n}_{hot} \cdot \int_{T_{H,out}}^{T_{H,in}} c_{P,hot}\, \mathrm{d}T = \dot{n}_{tot} \cdot \int_{T_{H,out}}^{T_{H,in}} c_{P,hot}\, \mathrm{d}T, \tag{2.2}$$

where $\dot{n}_{hot}$ is in [mol/s], and the hot side inlet and outlet temperatures are $T_{H,in}$ and $T_{H,out}$, respectively, both in [K]. The molar heat capacity at constant pressure of the hot vapor stream $c_{P,hot}$ is expressed in [J·mol^{-1}·K^{-1}]. This heat capacity is approximated as the sum of the heat capacities of the individual components, weighted by their molar fractions. In this case, the molar fractions are approximately 0.176 for the methanol, 0.437 for the water, and 0.387 for the dimethyl ether, in accordance with the design methanol conversion of 81.5 %.
The heat exchanger design equation is presented as follows:

$$\dot{Q} = F_{T1\text{-}2} \cdot U \cdot A \cdot \frac{(T_{H,in} - T_{C,out}) - (T_{H,out} - T_{C,in})}{\ln \dfrac{T_{H,in} - T_{C,out}}{T_{H,out} - T_{C,in}}}, \tag{2.3}$$

where $F_{T1\text{-}2}$ is the temperature correction factor for the 1-2 heat exchanger configuration, accounting for the non-ideal counter-current, as provided by Kern (1997, pp. 144-177):

$$F_{T1\text{-}2} = \frac{\sqrt{R^2+1} \cdot \ln \dfrac{1 - S}{1 - R \cdot S}}{(R - 1) \cdot \ln \dfrac{2 - S \cdot \left(R + 1 - \sqrt{R^2+1}\right)}{2 - \mathrm{S} \cdot \left(R + 1 + \sqrt{R^2+1}\right)}}. \tag{2.4}$$

The two dimensionless parameters, R and S, in equation (2.4) are defined as follows:

$$R = \frac{T_{H,in} - T_{H,out}}{T_{C,out} - T_{C,in}}, \tag{2.5}$$

$$S = \frac{T_{C,out} - T_{C,in}}{T_{H,in} - T_{C,in}}. \tag{2.6}$$

Finally, the system composed of the three equations (2.1), (2.2), and (2.3), is solved using different values of $\dot{n}_{tot}$, to find the three unknowns $T_{C,in}$, $T_{H,out}$, and $\dot{Q}$. The overall heat transfer

coefficient is assumed to be 170 $W \cdot m^{-2} \cdot K^{-1}$ for each process feed molar flow considered, and the heat exchange area is fixed at 34.0 m^2.

As different feed molar flows are considered in this analysis, the vaporizer ($\dot{n}_{tot}$) is assumed to always equal the respective feed flow. This assumption holds as long as the vaporizer utility is properly regulated for each process feed flow, ensuring steady-state operation of the vaporizer. Subsequently, the dimensionless cold molar flow rate is expressed as follows:

$$N_{cold} = \frac{\dot{n}_{cold} \cdot \bar{c}_{P,cold}}{U \cdot A}, \tag{2.7}$$

where $\bar{c}_{P,cold}$ is the average value of $c_{P,cold}$ between the cold side inlet and outlet of E - 102.

The dimensionless heat duty is defined as the ratio between the maximum heat duty and the actual heat duty as follows:

$$Q_d = \frac{\dot{Q}}{\dot{Q}_{max}} = \frac{\dot{Q}}{U \cdot A \cdot (T_{H,in} - T_{C,in})}, \tag{2.8}$$

Finally, the results of the study are presented in Figure 2.2.

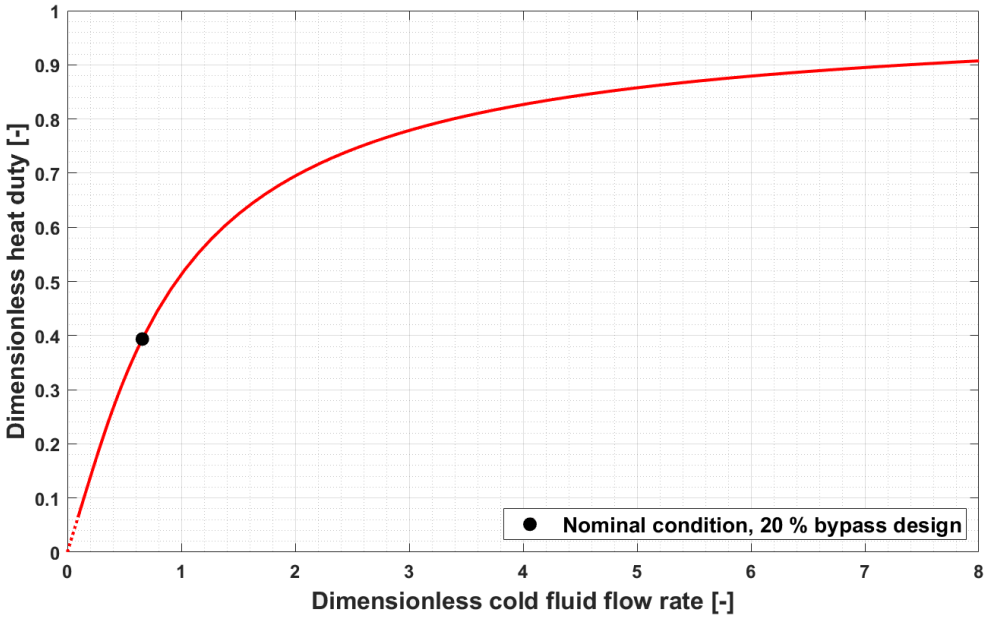

Figure 2.2. *Dimensionless heat duty as a function of the dimensionless cold fluid flow obtained by simulating at steady-state the heat exchanger E - 102 of the design configuration with 20 % bypass fraction, under different process feed molar flow.*

In Figure 2.2, the dimensionless heat duty (Q_d) is presented as a function of the dimensionless cold fluid flow rate (N_{cold}). The nominal operating region of heat exchanger E - 102, determined by the selected 20 % design bypass fraction, is indicated by a black marker. Within this region, the heat exchanger operates such that changes in the manipulated variable, specifically the cold

fluid flow rate through E - 102, lead to nearly linear and significant changes in the heat duty. Therefore, the selected bypass fraction ensures that the steady-state gain between the manipulated variable and the preheater heat duty, which is connected to the reactor inlet temperature to be controlled, is almost constant and relatively high, improving the system controllability. Finally, at low values of N_{cold}, specifically below 0.1, the curve is shown as dotted due to the several numerical issues that are encountered by the solver in this region.

This study provides only a qualitative description of the heat exchanger E - 102 steady-state operation. The molar composition and inlet temperature of the hot side stream are considered at their design values, even though the system is simulated at steady-state with different feed flows from the nominal value of 295.2 kmol/h. It is important to note that this approximation is valid only if the reactor inlet temperature remains at the desired value of 541 K. Indeed, this temperature is crucial as it fixes the methanol conversion and the temperature rise in the reactor R - 101. Thus, it is essential to ensure that the composition and the temperature of the hot reactor effluent entering the heat exchanger E - 102 remain close to their nominal design value even under different throughputs, as illustrated in Figure 1.2.

To achieve the desired reactor inlet temperature of 541 K from a steady-state simulation of this FEHE system, the bypass fraction would need to be adjusted according to the considered process feed flow. However, in this study, the bypass fraction is maintained at its design value of 20 %. Without proper adjustment of this bypass fraction relative to the process feed flow, it is not possible to maintain the desired reactor inlet temperature. As a result, for each feed flow considered the temperature and composition of the hot reactor temperature are different from the design values, leading to a deviation in the dimensionless heat duty profile with respect to the dimensionless cold fluid flow from the profile shown in Figure 2.2.

In conclusion, the description of the heat exchanger steady-state operation under different throughputs provided in Figure 2.2 is only qualitative. However, it remains sufficiently accurate within the dimensionless cold fluid flow region, approximately between 0.2 and 1.2, which is the region of primary interest for the dynamic studies in §2.1.2.

2.1.1.1 Steady-state evaluation of the bypass fraction across different throughputs

In this section, a steady-state analysis is conducted to determine how the bypass fraction should be adjusted relative to the considered process feed flow, and consequently the reactor feed flow, to ensure the desired reactor inlet temperature of 541 K, whose critical importance has been thoroughly assessed in the previous sections. Additionally, this analysis allows for an estimation, from a steady-state perspective, of the maximum feed flow at which the heat exchanger E - 102 can effectively preheat the reactor feed by recovering the necessary heat duty from the hot reactor effluent to achieve the desired reactor inlet temperature. Consequently, based on this analysis, during the dynamic studies to be presented in §2.1.2, which will explore this design configuration following disturbances in the feed flow, it is possible to approximately

predict the maximum feed flow rate at which the adopted reactor inlet temperature control strategy might be able to restore the desired temperature of 541 K. However, it is important to note that the dynamic behaviour of the system following such disturbances will likely affect the final outcome in controlling the reactor inlet temperature, potentially resulting in deviations from the steady-state predictions provided in this section.

To determine the appropriate bypass fraction, b, needed to maintain the desired reactor inlet temperature as a function of the throughput considered, the following approach is used. There are four unknowns: $T_{C,in}$, $T_{H,out}$, and $\dot{Q}$ and b, which must be determined for each feed flow rate considered. To find these variables, the same system of equations used in the previous section is employed, consisting of the cold side energy balance, the hot side energy balance, and the heat exchanger design equation. However, an additional equation must be included, representing the energy balance at the mixing point, defined as follows:

$$\dot{n}_{mix} \cdot \triangle H_{mix} = \dot{n}_{cold} \cdot \triangle H_{cold} + \dot{n}_{by} \cdot \triangle H_{by}, \tag{2.9}$$

where $\dot{n}_{mix}$ and $\dot{n}_{by}$ are the molar flow rates of the mixed stream and the bypass stream, respectively, in [mol/s]. $\triangle H_{mix}$, $\triangle H_{cold}$, and $\triangle H_{by}$, are the molar enthalpies of the mixed stream, the heat exchanger cold side outlet stream, and the bypass stream, respectively.

This balance can be rearranged by noting that $\dot{n}_{mix}$ is equal to $\dot{n}_{tot}$. Furthermore, $\dot{n}_{cold}$ and $\dot{n}_{by}$ can be expressed in terms of the bypass fraction and represents the total vapor molar flow rate exiting the vaporizer as follows: $\dot{n}_{cold} = (1 - b) \cdot \dot{n}_{tot}$ and $\dot{n}_{by} = b \cdot \dot{n}_{tot}$.

Finally, as all the three streams have the same molar composition of the process feed, the energy balance at the mixing point is redefined as:

$$0 = \sum_i x_i \cdot \left(\int_{T_{C,out}}^{T_{mix}} c_{P,i} \, \mathrm{d}T - b \cdot \int_{T_{C,in}}^{T_{C,out}} c_{P,i} \, \mathrm{d}T \right), \tag{2.10}$$

where all the enthalpies of equation (2.9) are rearranged considering the contribution of each specie i and assuming for simplicity to operate with an ideal mixture. The molar fractions x_i are those of the process feed, and T_{mix} is the temperature of the mixed stream entering the reactor.

Finally, after solving the aforementioned system of equations for different feed flows, the results of this steady-state analysis are illustrated in Figure 2.3. Specifically, the plot shows the bypass fraction as a function of the process feed flow rate. This illustrates, from a steady-state perspective, how the bypass fraction should be set according to the considered process feed molar flow to ensure that the desired T_{mix} = 541 K is maintained. Starting from the design flow rate of 295.2 kmol/h, for feed flow rates lower than this value, the bypass fraction must be set higher than the design value of 20 %. For instance, for molar flow rates below 100 kmol/h, the bypass fraction should be adjusted to approximately 37%.

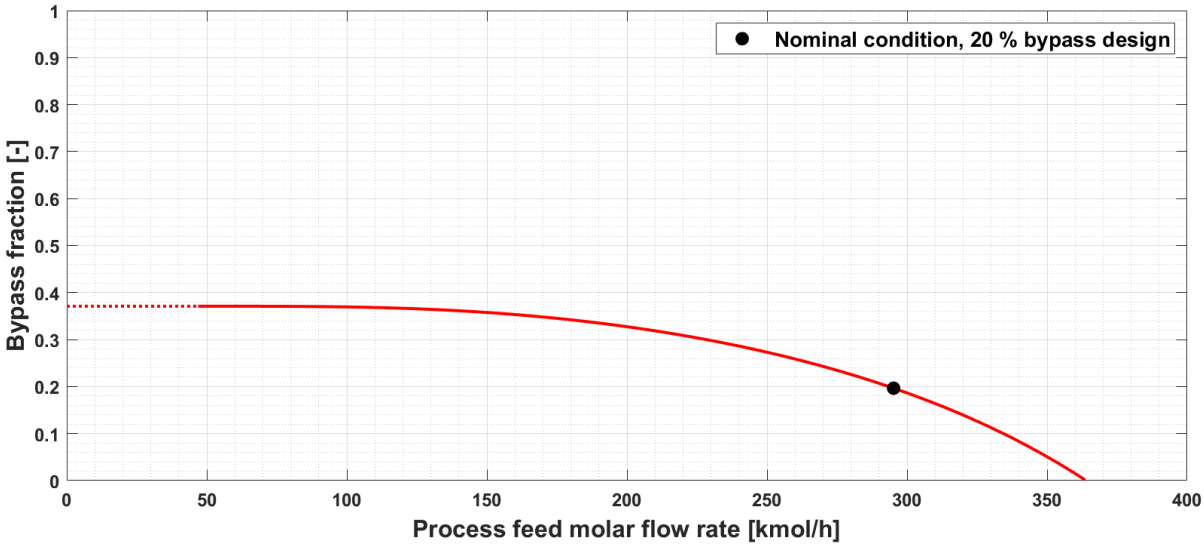

Figure 2.3. *Bypass fraction required to ensure from a steady-state standpoint the desired reactor inlet temperature of 541 K across different process feed molar flows in the design configuration with a 20 % bypass.*

Conversely, at flow rates higher the nominal value of 295.2 kmol/h, the bypass fraction must be reduced from the design value of 20 %, as a larger amount of vapor needs to be preheated. Finally, at a molar flow rate approximately of 23 % higher than the design value, the bypass fraction must be set to zero. This is the maximum reactor feed flow that the heat exchanger can preheat in order to achieve the desired reactor inlet temperature.
Now that the steady-state performance of this design configuration has been assessed in detail, the temperature control loop and the system dynamics are presented in the next section (§2.1.2).

2.1.2 Aspen Plus Dynamics simulation

In this section, the Aspen Plus simulation of the 20 % bypass design configuration is prepared in order to be exported into Aspen Plus Dynamics, allowing for a dynamic study of the system. The vaporizer and the reactor maintain the same characteristics implemented in §1.3. However, the heat exchanger model is updated to account for the increased heat exchange surface. Specifically, using the same procedure detailed in §1.3, Table 2.1 illustrates all the main features describing the heat exchanger E - 102.

Table 2.1. *Summary of all heat exchanger E - 102 design parameters.*

Configuration	$\dot{Q}$ [MW]	U [W·m^{-2}·K^{-1}]	A [m^2]	L_t [m]	s_t [m]	$d_{t,ext}$ [m]	N_t [-]	V_t [m^3]	V_{sec} [m^3]	m [kg]	m_{sec} [kg]
1-2	0.5433	170	34.0	10	0.002	0.025	44	0.15	0.08	488	122

Aspen Plus Dynamics is then opened, and similar issues to those encountered in the base design configuration are managed using the procedures described in §1.3.

The valves shown in Figure 2.1 are adequately sized, with the same features of the base design case assigned to valves FCV - 101, LCV - 101, and PCV - 101 and presented in §1.3. In this configuration, two additional valves are introduced: valve TCV - 101 on the bypass stream line and TCV - 102 at the E - 102 cold side outlet stream line. Specifically, Table 2.2 shows the nominal conditions and all the main characteristics of each of these two valves.

Table 2.2. *Summary of all valves TCV - 101 and TCV - 102 design parameters.*

Valve	q [m^3/h]	ΔP_v [atm]	*Valve opening* [%OP]	K_v [$m^3 \cdot h^{-1} \cdot bar^{-0.5}$]	*Valve action*	*Valve characteristic*
TCV - 101	146.5	1.5	50	29.3	Air-to-close	Linear
TCV - 102	815.5	0.5	50	164.5	Air-to-open	Linear

The higher pressure drop of TCV - 101 is set in order to ensure that the bypass line provides the same pressure drops of the line with the heat exchanger and TCV - 102.
For both valves, the linear characteristic is chosen as the valves perform comparably well with the equal percentage characteristic without unnecessarily requiring larger valve. Additionally, the valves TCV - 101 and TCV - 102 are complementary dual-split range valves, as described by Kuphaldt (2019), used in pairs to manipulate the bypass fraction, thereby controlling the fluid flow towards both the bypass and the heat exchanger line simultaneously. Consequently, these two valves are selected with opposite actions. Specifically, this selection follows the heuristics that in case of failure, cold fluid must enter the reactor to stop the reaction. This is achieved only if all the fluid passes through the bypass line, thus avoiding the heat exchanger line. Therefore, valve TCV - 101 is set to air-to-close, thus with a reverse action, while valve TCV - 102 is air-to-open, so with a direct action. Furthermore, the complementary split-range action is described in Table 2.3, which presents the relationship between the output of the temperature controller to be discussed later, and the two valve openings.

Table 2.3. *Relationship between the temperature controller output and the valve opening of TCV - 101 and TCV - 102.*

Controller output [%CO]	*TCV - 101 opening*	*TCV - 102 opening*
0	Fully closed	Fully open
25	25 % open	75 % open
50	50 % open	50 % open
75	75 % open	25 % open
100	Fully open	Fully closed

This configuration ensures that each valve complements the position of the other valve, and within the controller output range, the two valves are never fully open nor fully closed simultaneously.

Finally, all the valves are modelled again with default first-order dynamics as in §1.3.
Figure 2.4 illustrates the process flow diagram including all control loops for the design with a 20 % nominal bypass fraction. This diagram is also applicable to the configuration with a 40 % nominal bypass fraction, which will be discussed subsequently. For the 20 % bypass design, the relevant stream table, Table B.1, and equipment table, Table B.2, are provided in Appendix B.

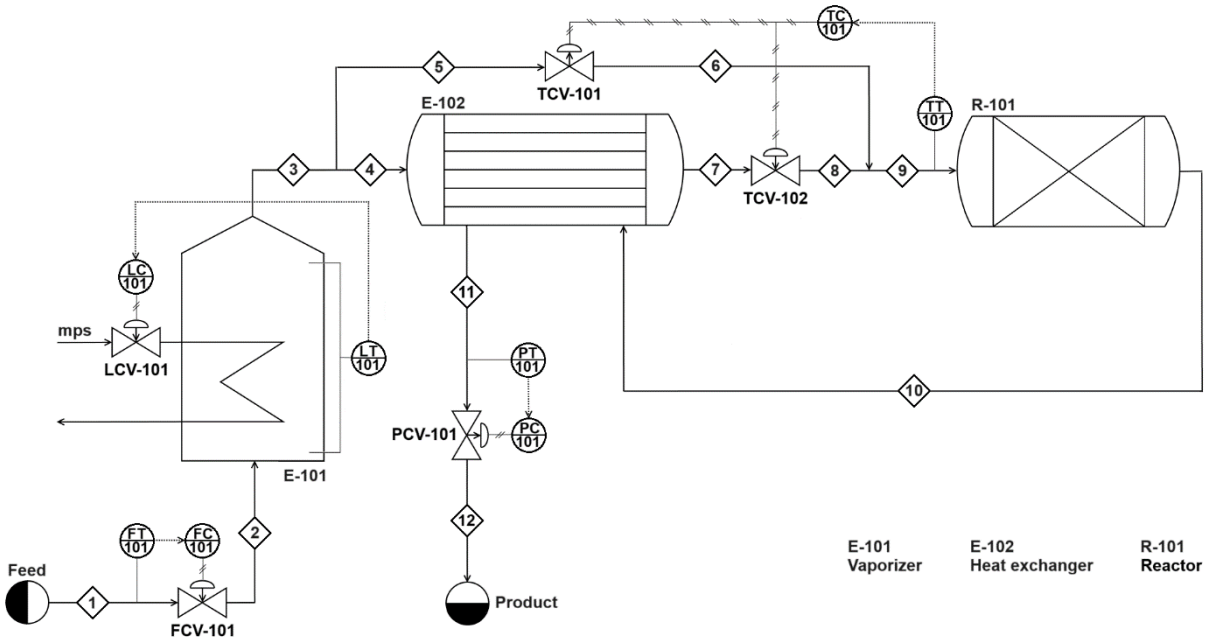

Figure 2.4. *Process flow diagram with all the control loops and equipment schematics used in both the 20 % and 40 % bypass design configurations.*

Specifically, this system presents, as in the base design case, an inlet process feed flow rate controller, a tank liquid level controller, and a heat exchanger hot side outlet pressure controller, which are implemented with the same features described in §1.3, as their performance is comparably effective to those in the base design configuration. However, this configuration introduces the reactor inlet temperature loop.
With all the other controller set to automatic mode, the reactor inlet temperature controller is implemented. This control loop utilizes the measurement of the reactor inlet temperature via a sensor-transmitter unit, TT - 101, whose dynamics is approximated introducing a 1 min deadtime into the control loop, as suggested by Luyben (2012).
The reactor inlet temperature controller, TC - 101, uses the measurement from TT - 101 to manipulate the opening of valves TCV - 101 and TCV - 102. The controller action is set to reverse, considering the action of the two valves. For example, if the sensor measures a temperature lower than the set point of 541 K, the controller increases its output, resulting in valve TCV - 101 closing and the TCV - 102 opening correspondingly, thereby increasing the flow rate through the heat exchanger line. The higher preheating of this stream ultimately raises the reactor inlet temperature after being mixed with the reduced bypass flow rate.
The selected sensor-transmitter range is 273 - 809 K, which enables the controller output to be

at 50 %CO at nominal steady-state conditions and is sufficiently large for this application. The controller is implemented with a PI action, and its parameters are determined by first performing an ATV test to find the ultimate controller gain and period, which are approximately of 23.9 %CO/%TO and 2.6 min. Then, the Tyreus-Luyben tuning rules are applied, resulting in a controller gain of 7.5 %CO/%TO and an integral time constant of 5.8 min. After testing with step changes in the process feed flow, these controller parameters are adjusted to 2 %CO/%TO and 1.8 min. This reduced integral time constant enhances the controller performance during step changes at higher throughput. However, the controller gain is reduced from the initial value to avoid too aggressive controller actions at low throughput conditions. Finally, in Table 2.4 the main features of controller TC - 101 are summarized.

Table 2.4. *Tuning parameters of controller TC - 101.*

Controller	***Span***	K_C **[%CO/%TO]**	τ_I **[min]**	***Action***
TC - 101	536 K	2	1.8	Reverse

With all the control loops implemented into Aspen Plus Dynamics, the 20 % bypass design configuration is studied dynamically.

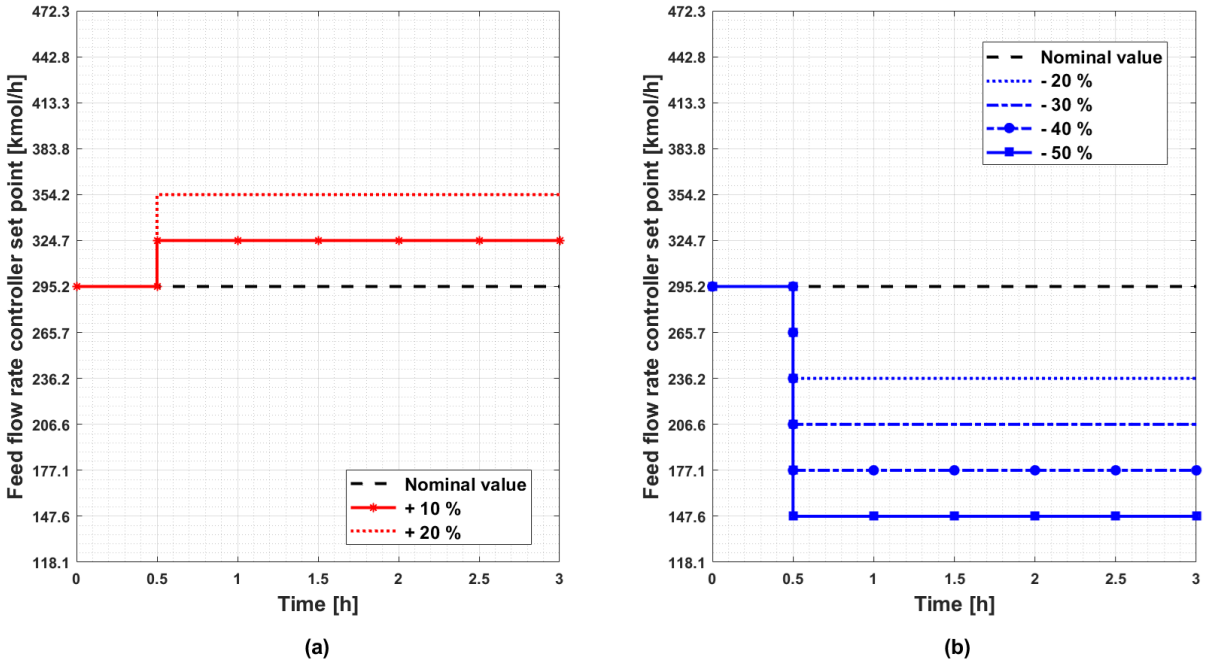

Figure 2.5. *Disturbances analyzed during the dynamic simulations introduced at time 0.5 h.* (a) *Positive step changes in the set point of the feed molar flow rate controller with respect to the nominal value and* (b) *negative step changes.*

The performance of the temperature controller is assessed at different throughputs. These conditions are introduced as step changes in the set point of controller FC - 101. Figure 2.5 depicts all the disturbances considered, with positive increment shown in (a) and negative step

changes represented in (b).

Firstly, the + 10 % disturbance is analyzed, and Figure 2.6 illustrates the results of the dynamic simulation. In Figure 2.6(a), the controlled variable of TC - 101, the reactor inlet temperature is represented.

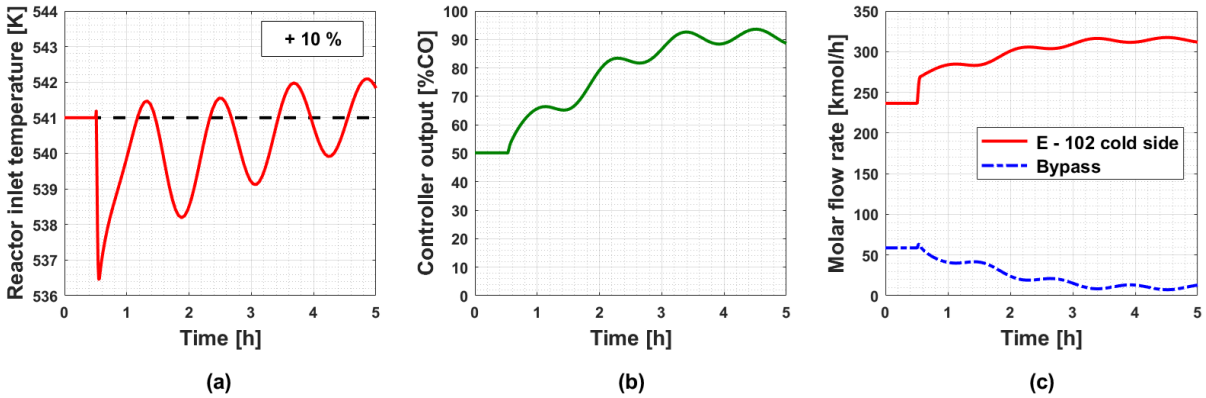

Figure 2.6. (a) *Reactor inlet temperature following a + 10 % feed flow rate disturbance at 0.5 h.* (b) *Controller TC - 101 output and* (c) *molar flow rates for both the bypass stream and the cold side of E - 102.*

Upon the introduction of the disturbance, the temperature rapidly decreases, reaching a minimum of 536.5 K after approximately 5 min. This initial decrease is attributed to the delayed response of the controller in adjusting the opening of the two valves TCV - 101 and TCV - 102 to reduce the bypass fraction. Given the higher flow compared to the nominal value, it is necessary to increase the flow rate through the preheater, as a higher heat duty is required to maintain the reactor inlet temperature at 541 K. This rapid decrease is also related to the dynamics of the system. As the process feed flow rate increases, the cold side flow rate of the heat exchanger increases first, followed by the hot side flow rate. Consequently, due to the time required for the disturbance to propagate through the streams, the cold side flow rate is insufficiently preheated during this brief interval because the hot side flow rate has not increased yet.

Subsequently, as the controller TC - 101 increases its output, as observed in Figure 2.6(b), the bypass fraction is diminished, resulting in a reduction in the bypass stream and a rise in the heat exchanger cold side flow rate, as illustrated in Figure 2.6(c). Consequently, from the aforementioned minimum temperature, the reactor inlet temperature begins to rise. However, the reactor dynamic behaviour produces inverse responses in the outlet temperature relative to the inlet temperature variations, as discussed in §1.3, which propagate into the heat exchanger. As a result, the controller action struggles to dampen the oscillating reactor inlet temperature variations, and at 5 h the temperature is still oscillating around the nominal value with an amplitude which is reduced to about 1 K. Finally, the reactor inlet temperature is restored to the nominal value in approximately 10 h after the disturbance was introduced (not shown).

The final steady-state value reached by the bypass fraction is 5 %, instead of the approximated

value of about 10 % calculated with Matlab® and presented in Figure 2.3. However, this discrepancy is justified by the combined effect of the approximations applied in the previous study, specifically on the outlet reactor temperature and molar composition, the properties calculation, the solver model used, other than the overall system dynamics. Therefore, the study presented in the previous section, §2.1.1.1, provides only a qualitative description of the system, albeit offering relevant information on the system behaviour during dynamic simulations.

Following the analysis of the + 10 % feed flow disturbance, which the control scheme manages to reject despite some difficulties, a + 20 % disturbance is considered to determine if this configuration is sufficiently oversized to manage a larger disturbance. Additionally, as discussed in §2.1.1.1, the steady-state analysis indicates that a + 23 % feed flow rate is the threshold at which the reactor inlet temperature can still achieve the desired value of 541 K. Therefore, the + 20 % disturbance is close to this threshold value.

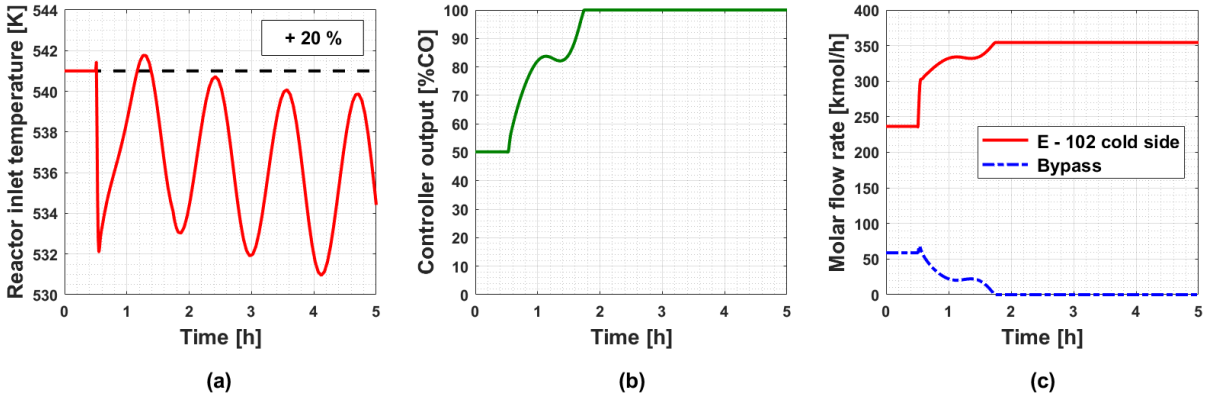

Figure 2.7. (a) *Reactor inlet temperature following a + 20 % feed flow rate disturbance at 0.5 h.* (b) *Controller TC - 101 output and* (c) *molar flow rates for both the bypass stream and the cold side of E - 102.*

In Figure 2.7(a), the reactor inlet temperature response following the + 20 % set point step change of FC - 101 at time 0.5 h is presented. Figure 2.7(b) depicts the corresponding controller output response, and Figure 2.7(c) shows the bypass and E - 102 cold side flow rates.

In this case study, the controller TC - 101 fails to mitigate the reactor inlet temperature variations following the system perturbation. Similar to the previous case, the temperature initially undershoots and then begins to oscillate. However, in this instance, the oscillations are not dampened; instead, their amplitude increases hazardously over time. Ultimately, the amplitude stabilizes, with oscillations maintained between maximum and minimum temperatures of approximately 560 K and 480 K, respectively.

As it is observed in both Figure 2.7(b) and Figure 2.7(c), the controller responds to this large perturbation by increasing its output, which saturates after 1 h from the onset of the disturbance. As a result, the bypass fraction drops to zero, and all the vapor flow from the vaporizer is directed to the heat exchanger due to the higher heat duty required to preheat this larger flow. Nevertheless, in this case, the heat exchanger is not adequately sized, resulting in an insufficient

exchange area to recover all the heat required by the cold stream. Consequently, the reactor inlet temperature is not brought back to the desired set point. Obviously, the problem for this large increase of the throughput is not in the control system, but in the equipment design.

Now that the system response to step increases in feed flow rate has been analyzed, evaluating its capability to reject such disturbances up to its limits, the performance of controller TC - 101 is next assessed in the context of negative step variations in the feed flow rate.

Firstly, the TC -101 performance under a - 20 % disturbance is evaluated. Figure 2.8 illustrates the system response to this negative perturbation, as with the other case studies.

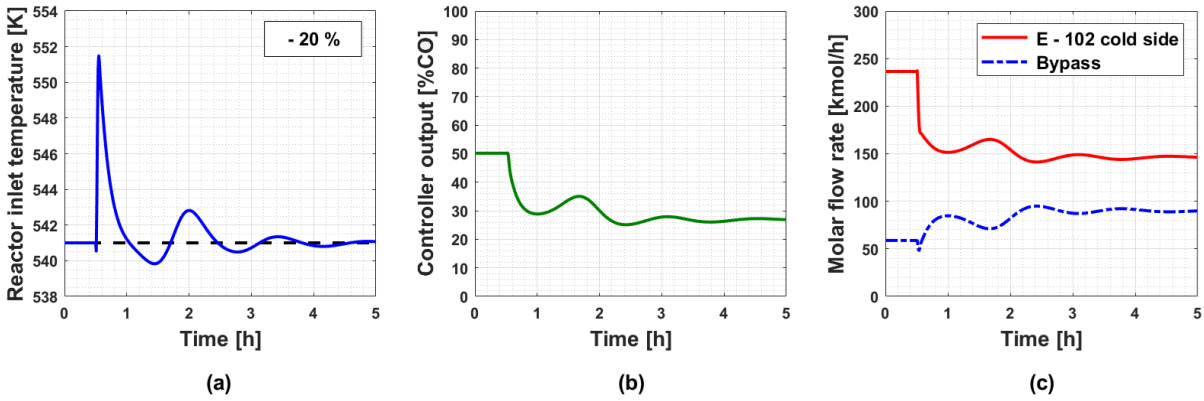

Figure 2.8. (a) *Reactor inlet temperature following a - 20 % feed flow rate disturbance at 0.5 h.* (b) *Controller TC - 101 output and* (c) *molar flow rates for both the bypass stream and the cold side of E - 102.*

As shown in Figure 2.8(a), the reactor inlet temperature initially overshoots reaching approximately 552 K. Then, the controller TC - 101 restores it to the set point after a few oscillations, stabilizing around 3 h after the disturbance is introduced. As in previous scenarios the overshoot, even if with opposite direction, is due to the delayed action of the TC - 101 to regulate the bypass fraction, resulting in an initial overheating of the reactor feed, which requires a lower heat duty than the nominal design conditions due to the reduced flow entering the process. This overheating is also related to the delayed, though rapid, reduction of the hot side heat exchanger flow compared to the reactor inlet stream line.

Regarding the controller output, as illustrated in Figure 2.8(b), it is decreased to rise the bypass fraction, as it is expected considering the discussion in §2.1.1.1. Therefore, the E - 102 cold side flow rate is reduced, and the bypass flow is increased, as shown in Figure 2.8(c).

Subsequently, the system is studied under more severe step reductions in feed flows. The controller performs reasonably well under these conditions, although the profiles exhibit more critical overshoots and oscillations compared to the - 20 % scenario. Figure 2.9 illustrates the results corresponding to the most severe case analyzed: a 50 % step reduction in feed flow.

As illustrated in Figure 2.9, controller TC - 101 restores the reactor inlet temperature after the initial critical positive overshoot of 27 K and subsequent oscillations, stabilizing about 3 h after the disturbance is introduced. In this scenario, fewer oscillations are observed compared to the

- 20 % case. These oscillations are not due to the controller tuning but are explained by considering the open-loop dynamics of this system under these disturbances. Indeed, in both cases, the reactor inlet temperature initially oscillates before settling to the higher temperature steady-state, as discussed in §1.3, with more oscillations observed in the lower feed flow step decrease open-loop scenario.

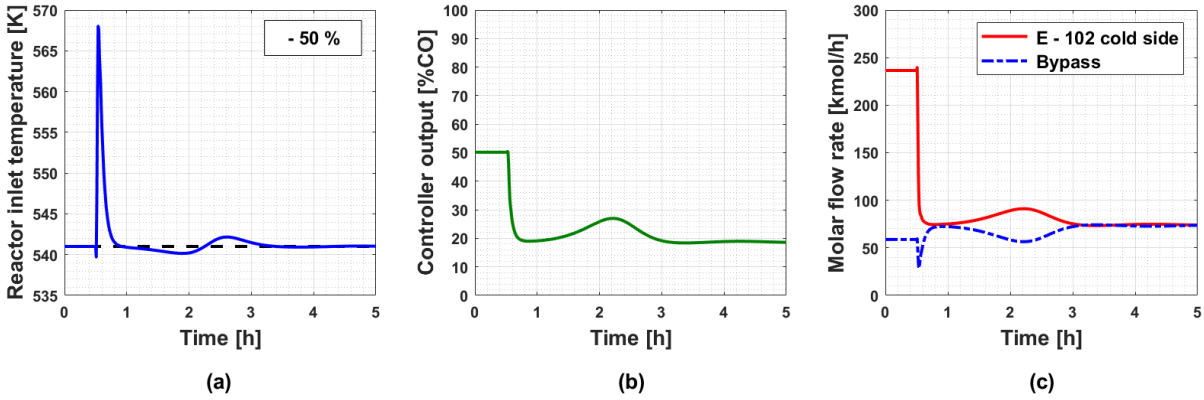

Figure 2.9. (a) *Reactor inlet temperature following a - 50 % feed flow rate disturbance at 0.5 h.* (b) *Controller TC - 101 output and* (c) *molar flow rates for both the bypass stream and the cold side of E - 102.*

In conclusion, the design configuration with 20 % bypass is studied, and the reactor inlet temperature control loop is introduced. The analysis of the dynamic simulations of this configuration reveals improvements in controlling the reactor inlet temperature, particularly under low throughput conditions. In these cases, the flow rate through the heat exchanger is regulated and reduced to avoid unnecessarily overheating of the reactor feed.

However, the temperature control loop of this configuration is unable to restore the reactor inlet temperature to the nominal set point when the feed flow step increase exceeds 10 % of the nominal value. The + 10 % scenario is controlled, albeit with some difficulty. Larger positive changes are not adequately handled, leading to fixed-amplitude limit cycles in the reactor inlet temperature, similar to what is observed in §1.3 discussing the base design case dynamics. Indeed, the 20 % bypass design results in a heat exchanger with a larger heat exchange area compared to the base case configuration but still insufficiently sized to preheat the reactor feed under high throughput conditions.

The next section will explore a new design configuration aimed at improving the ability of the system to manage these critical scenarios.

2.2 Design case with 40 % bypass

Following the analysis of the 20 % bypass design presented in §2.1, this section considers a new design aimed at overcoming the limitations of the previous configuration, particularly in restoring the reactor inlet temperature after step increases in the feed flow controller set point.

2.2.1 Steady-state design and Aspen Plus simulation

The design presented in this section is configured with an increased nominal bypass fraction of 40 % compared to the previous of 20 %, as proposed by Luyben (2012). The new design configuration is illustrated in Figure 2.10, with the relevant stream table, Table C.1, and equipment table, Table C.2, provided in Appendix C.

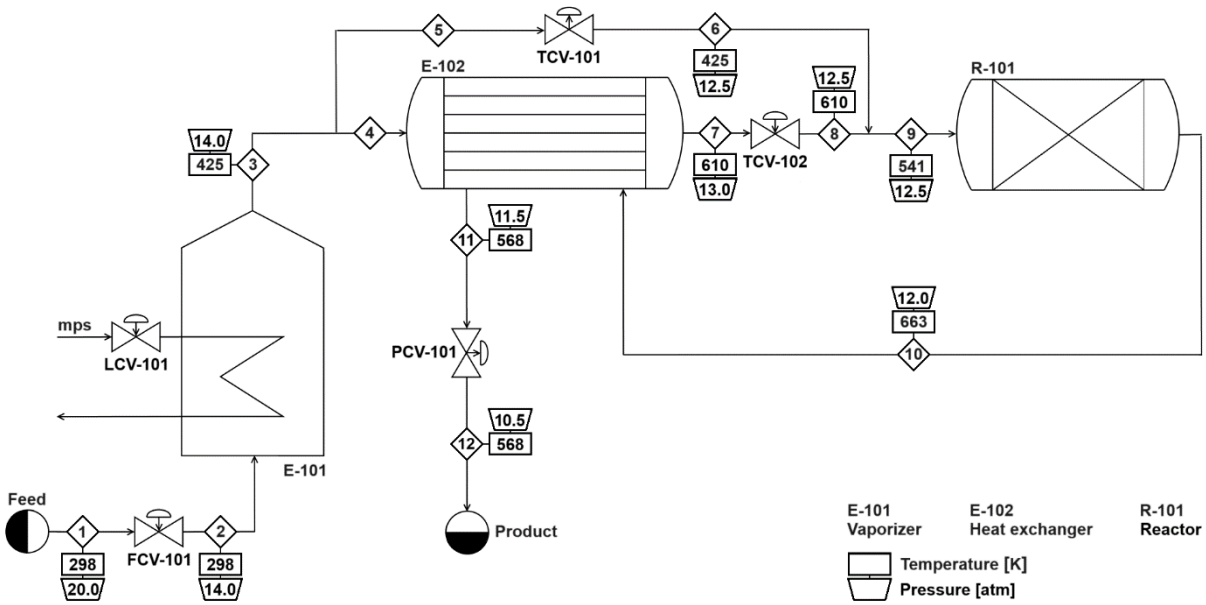

Figure 2.10. *Process flow diagram of the design case with 40 %, illustrating all equipment schematics and the temperatures and pressures of all streams.*

While the reactor and vaporizer remain unchanged from the previous designs, the preheater is modified due to the new bypass fraction, which changes the heat exchanger E - 102 design and operating conditions. Specifically, the nominal heat exchanger heat transfer rate and overall heat transfer coefficient are maintained from the previous designs. The heat duty is unchanged since the same vapor stream exiting the vaporizer needs to be preheated to the same reactor inlet temperature as in the previous cases. However, the higher nominal bypass fraction results in a reduced cold side flow rate compared to the 20 % bypass design. Consequently, to achieve the desired reactor inlet temperature of 541 K, the heat exchanger must raise this reduced flow to about 610 K before it mixes with the colder, increased bypass flow. This higher cold side outlet temperature leads to a decrease in the log-mean temperature difference (LMTD) from 117 K in the 20 % bypass design to approximately 90 K in this new design. The heat exchanger E - 102 is configured with two shell passes and four tube passes (2-4 configuration, not shown in Figure 2.10 for convenience), as a 1-2 configuration would have provided inefficient heat transfer, with a correction factor below 0.8. The correction factor for this preheater design is about 0.9, which is an improvement over the 0.8 correction factor calculated in the 20 % bypass design, which utilized a preheater with a 1-2 configuration. Despite this higher correction factor, the exchange area (A) must be increased to 39.4 m^2 due to the reduced LMTD.

Before delving into the dynamic simulation of this 40 % bypass design, a steady-state evaluation is conducted, using the same methodology applied to the 20 % bypass configuration in §2.1.1 and proposed by Soave and Barolo (2021), with adaptations specific to this FEHE system under examination. The objective of this analysis is to determine, from a steady-state perspective, the operating region of heat exchanger E - 102 under nominal conditions, defined by the selected 40 % bypass fraction. The results of this analysis will be compared to those from the previous 20 % bypass design to assess whether the new design bypass fraction selected enhances the controllability of the relative heat exchanger with bypass system under different process feed flows.

The same systems of equations used in §2.1.1 with the only exception being the heat exchanger design equation (2.3). In this equation, the temperature correction factor $F_{T1\text{-}2}$ is replaced with $F_{T2\text{-}4}$, reflecting the new 2-4 preheater configuration, provided by Kern (1997, pp. 144-177):

$$F_{T2\text{-}4} = \frac{\frac{\sqrt{R^2+1}}{2\cdot(R-1)}\cdot \ln\frac{1-S}{1-R\cdot S}}{\ln\frac{2-S\cdot\left(R+1-\sqrt{R^2+1}\right)+2\cdot\sqrt{(1-S)\cdot(1-R\cdot S)}}{2-S\cdot\left(R+1+\sqrt{R^2+1}\right)+2\cdot\sqrt{(1-S)\cdot(1-R\cdot S)}}}. \tag{2.11}$$

Finally, the results of the two studies are presented and compared in Figure 2.11.

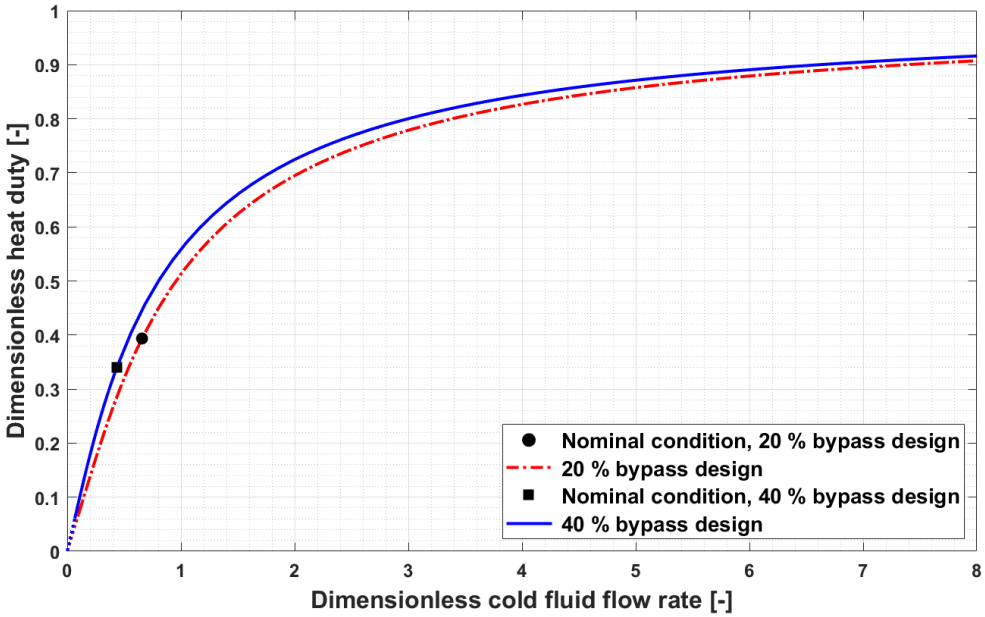

Figure 2.11. *Dimensionless heat duty as a function of the dimensionless cold fluid flow obtained by simulating at steady-state the preheater E - 102 of the two design configurations with 40 % and 20 % bypass fraction, under different process feed flow.*

In Figure 2.11, the dimensionless heat duty (Q_d) is plotted against the dimensionless cold fluid flow (N_{cold}) for both designs with 20 % and 40 % nominal bypass fractions, represented by the

dash-dot red line and solid blue line, respectively. In the case of the 40 % bypass design, the black square marker, which indicates the design condition, is positioned at lower N_{cold} and Q_d values compared to the black circle marker representing the design condition of the 20 % bypass configuration. This shift occurs because in the 40 % bypass design, the nominal N_{cold} is reduced due to the lower cold fluid flow through the preheater and the increased heat exchange area, while the nominal Q_d is also lower due to the larger exchange area.
As it was obtained for the 20 % bypass design, also for the 40 % bypass design, the nominal operating region of the relative heat exchanger E - 102, determined by the selected 40 % nominal bypass fraction, remains optimal for control purposes. In this region the heat exchanger operates such that changes in the manipulated variable, specifically the cold fluid flow through E - 102, lead to nearly linear and significant changes in the heat duty. Therefore, the 40 % bypass fraction selection ensures that the steady-state gain between the manipulated variable and the preheater heat duty, which is connected to the reactor inlet temperature to be controlled, is again almost constant and is even slightly increased compared to the 20 % bypass designs. This leads to a further, though slight, improvement in system controllability.
At lower N_{cold} values, specifically below 0.1, the two lines are shown as dotted due to several numerical issues encountered by the solver in this region. Furthermore, as discussed in §2.1.1 for the 20 % bypass design, the results obtained in this steady-state analysis are only qualitative due to the approximations made in the model description. Despite these limitations, the model remains reliable in the region of interest for subsequent dynamic simulations, where the process feed flow rates are varied between - 50 % and + 50 % of the nominal value of 295.2 kmol/h.

2.2.1.1 Steady-state evaluation of the bypass fraction across different throughputs

In this section, the 40 % bypass design is studied from a steady-state perspective to determine how the bypass fraction should be adjusted relative to the process feed flow to maintain the desired reactor inlet temperature of 541 K. The results of this study, obtained using the same methodology described in §2.1.1.1, are compared with the results for the 20 % bypass design and illustrated in Figure 2.12. In the figure, the solid blue line represents the results relative to 40 % bypass design, while the dash-dot red line represents the 20 % bypass design. The respective design conditions are indicated by the black square and circle markers.
As expected, the larger heat exchange area of the preheater in the 40 % bypass design enables greater heat recovery from the reactor effluent, which is crucial under high throughput conditions to effectively preheat the increased cold vapor flow. Specifically, Figure 2.12 demonstrates that, with appropriate adjustment of the bypass fraction, the 40 % bypass design can maintain the desired reactor inlet temperature even with a feed molar flow up to approximately 55 % above the nominal value of 295.2 kmol/h, compared to about 23 % for the 20 % bypass design. Conversely, at lower process feed molar flow from the nominal value, the bypass fraction should be increased, reaching about 51 % for feed flow rates below 100 kmol/h.

This is higher than the approximately 37 % value obtained for the 20 % bypass design. The larger bypass fraction at lower throughputs prevents excessive overheating that would result from the larger heat exchanger in the 40 % bypass design compared to the 20 % bypass design.

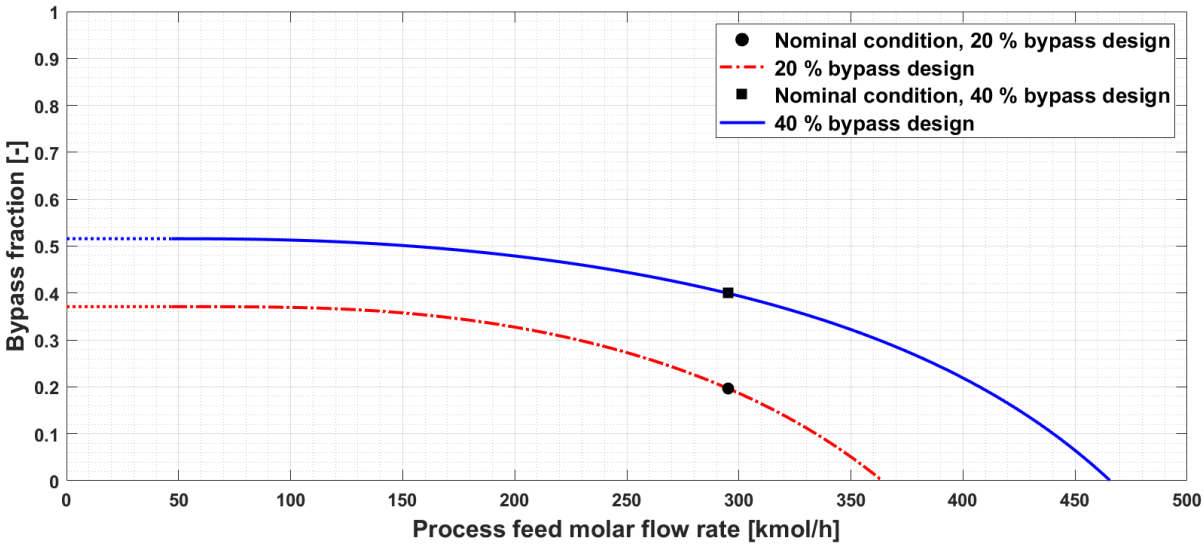

Figure 2.12. *Bypass fraction required to ensure from a steady-state standpoint the desired reactor inlet temperature of 541 K across different process feed molar flows in the design configuration with 20 % and 40 % nominal bypass fraction.*

However, as observed in the dynamic simulation of the 20 % bypass design, the overall system dynamics in response to throughput disturbances can impact the final control of the reactor inlet temperature, potentially causing deviations from the steady-state predictions provided here.

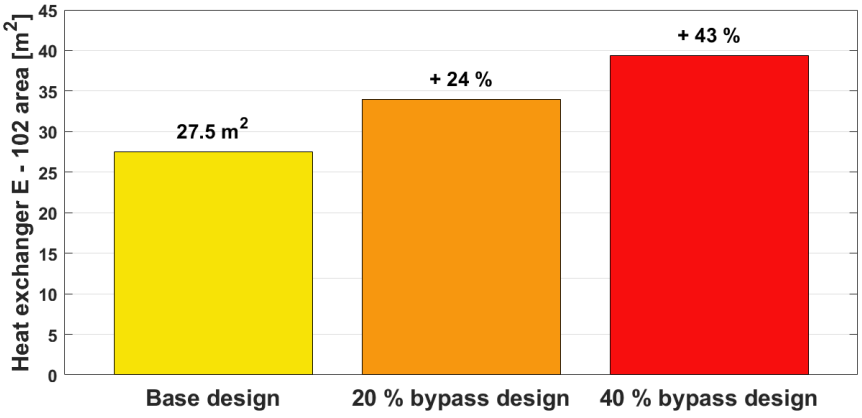

Figure 2.13. *Comparison of the heat exchanger E - 102 exchange areas for the base design, the 20 % bypass design, and the 40 % bypass design. The figure also shows the percentage increase in the exchange area relative to the base design.*

Figure 2.13 presents a bar chart comparing the heat exchanger E - 102 exchange areas for the base design, as well as the 20 % and 40 % bypass designs. Additionally, it illustrates the percentage increase in exchange area for the 20 % and 40 % bypass designs relative to the base case. As discussed in the Chapter, a higher nominal bypass fraction requires a larger heat exchange area due to the reduced LMTD. Consequently, the capital cost of the heat exchanger,

which is directly proportional to the exchange area, is higher for the 40 % bypass design. However, this increased cost can lead to much greater revenues, as the 40 % bypass design allows for operation at substantially higher feed flows compared to the other designs.
This analysis concludes the assessment of the steady-state performance of the 40 % bypass design configuration. In section §2.2.2, the dynamic simulation is prepared, and the system dynamics and temperature control loop performance of this new configuration are studied.

2.2.2 Aspen Plus Dynamics simulation

In this section, the Aspen Plus simulation is prepared to be exported into Aspen Plus Dynamics. The vaporizer and the reactor maintain the same features implemented in §1.3, while the updated specifications of E - 102, reflecting the new design, are detailed in Table 2.5.

Table 2.5. *Summary of all heat exchanger E - 102 design parameters.*

Configuration	$\dot{Q}$ [MW]	U [W·m^{-2}·K^{-1}]	A [m^2]	L_t [m]	s_t [m]	$d_{t,ext}$ [m]	N_t [-]	V_t [m^3]	V_{sec} [m^3]	m [kg]	m_{sec} [kg]
2-4	0.5433	170	39.4	10	0.002	0.025	50	0.17	0.09	556	139

Subsequently, the vaporizer liquid level is adjusted as in §1.3, and the valves are sized.
Specifically, valves FCV - 101, LCV - 101, and PCV - 101 retain the same characteristics as in the base design. In contrast, valves TCV - 101 and TCV - 102 are updated to accommodate the new operating conditions associated with the 40 % bypass configuration. Table 2.6 summarizes the nominal conditions and key characteristics of these two valves.

Table 2.6. *Summary of all valves TCV - 101 and TCV - 102 design parameters.*

Valve	q [m^3/h]	ΔP_v [atm]	*Valve opening* [%OP]	K_v [m^3·h^{-1}·bar$^{-0.5}$]	*Valve action*	*Valve characteristic*
TCV - 101	294.0	1.5	50	58.5	Air-to-close	Linear
TCV - 102	610.0	0.5	50	179.0	Air-to-open	Linear

The only changes from the previous design involve adjustments to the nominal volumetric flow rates and the valve flow coefficients (K_v). Specifically, valve TCV -101 now has a higher valve flow coefficient, driven by the increased bypass stream and the corresponding rise in volumetric flow. Although the molar flow rate through TCV-102 is lower, a higher flow coefficient is still required due to the increased volumetric flow rate, which results from the higher temperature of 610 K at the heat exchanger cold side outlet compared to the previous case.
The process flow diagram including all control loops for this 40 % bypass design is shown in Figure 2.4. The relevant stream table, Table C.1, and equipment table, Table C.2, are provided in Appendix C. Specifically, this system presents the same control loops of the previous design;

however, the reactor inlet temperature controller parameters are updated. With all the other controller set to automatic mode, the controller TC - 101 is implemented, and its parameters are initially determined using an ATV test, yielding an ultimate controller gain and period of approximately 5.6 %CO/%TO and 2.0 min, respectively. Applying the Tyreus-Luyben tuning rules, the resulting controller gain and integral time constant are set to 1.7 %CO/%TO and 4.5 min. After testing with positive and negative step changes in the process feed flow rate, these controller parameters are further adjusted to 2.2 %CO/%TO and 1.0 min, making the controller more aggressive to limit the overshoots magnitude observed in section §2.1.2 and to reduce the oscillatory temperature dynamics. Finally, Table 2.7 summarizes the main features of TC - 101.

Table 2.7. *Tuning parameters of controller TC - 101.*

Controller	***Span***	$\mathbf{K_C}$ **[%CO/%TO]**	$\boldsymbol{\tau_I}$ **[min]**	***Action***
TC - 101	536 K	2.2	1.0	Reverse

With all the controllers tuned, the process is dynamically simulated and perturbed using step changes in the set point of FC - 101. Figure 2.14 summarizes all the disturbances analyzed.

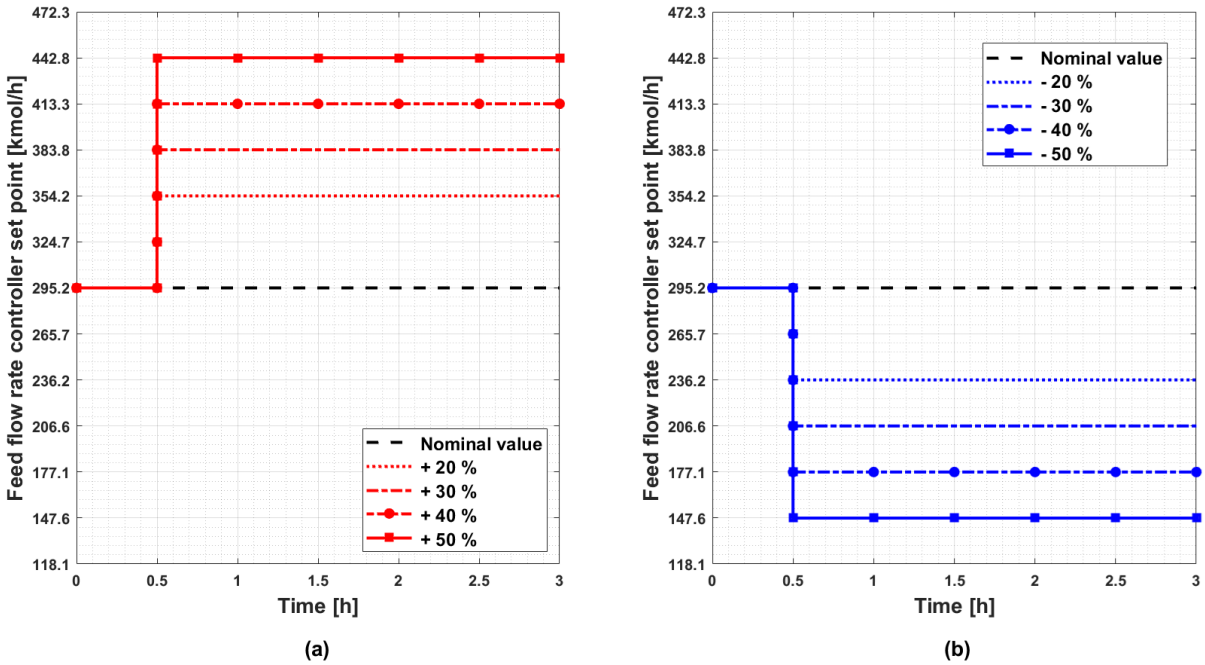

Figure 2.14. *Disturbances analyzed during the dynamic simulations introduced at time 0.5 h.* (a) *Positive step changes in the set point of the feed molar flow rate controller with respect to the nominal value and* (b) *negative step changes.*

Firstly, the most critical disturbance analyzed in section §2.1.2, the + 20 % step change, is considered and presented in Figure 2.15. Specifically, Figure 2.15(a) displays the controlled temperature, Figure 2.15(b) shows the controller output, and Figure 2.15(c) illustrates the molar flow rate in both the bypass line and the cold side of the preheater E - 102.

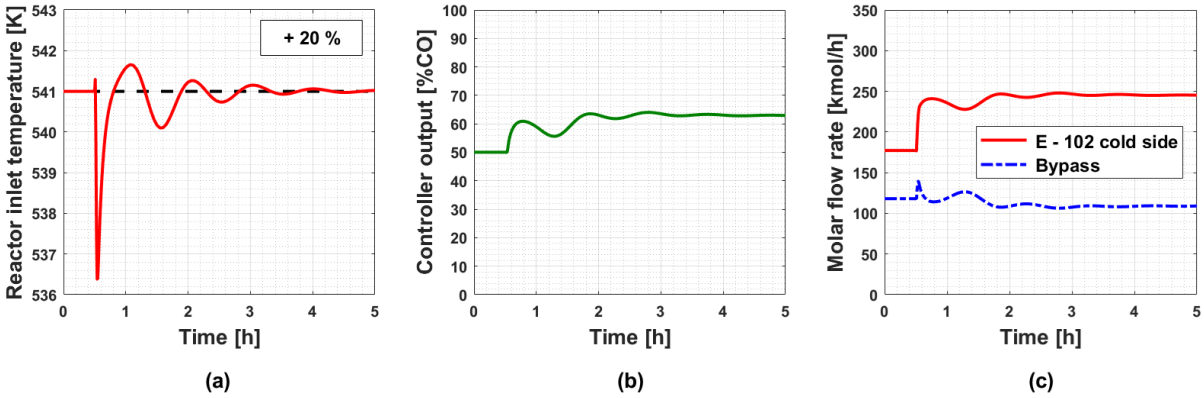

Figure 2.15. (a) *Reactor inlet temperature following a + 20 % feed flow rate disturbance at 0.5 h.* (b) *Controller TC - 101 output and* (c) *molar flow rates for both the bypass stream and the cold side of E - 102.*

As illustrated in Figure 2.15(a), the temperature controller in the 40 % bypass design effectively mitigates the impact of the introduced disturbance. Specifically, the initial temperature undershoot is less than 5 K, and the temperature returns to the set point within 2 h, with only minimal oscillations around the set point thereafter.

In this case, at the new steady-state achieved through the simultaneous regulation of flow rates via valves TCV - 101 and TCV - 102, the final bypass fraction stabilizes at about 31 %, closely aligning with the 31.5 % predicted by the simplified steady-state analysis in section §2.2.1.1. This increased precision, compared to the 20 % bypass configuration, is due to the greater flexibility of the 40 % bypass system in adapting to varying throughput conditions. This flexibility is made possible by the larger heat exchange area of the preheater, which ultimately reinforces the validity of the assumptions made in the analysis.

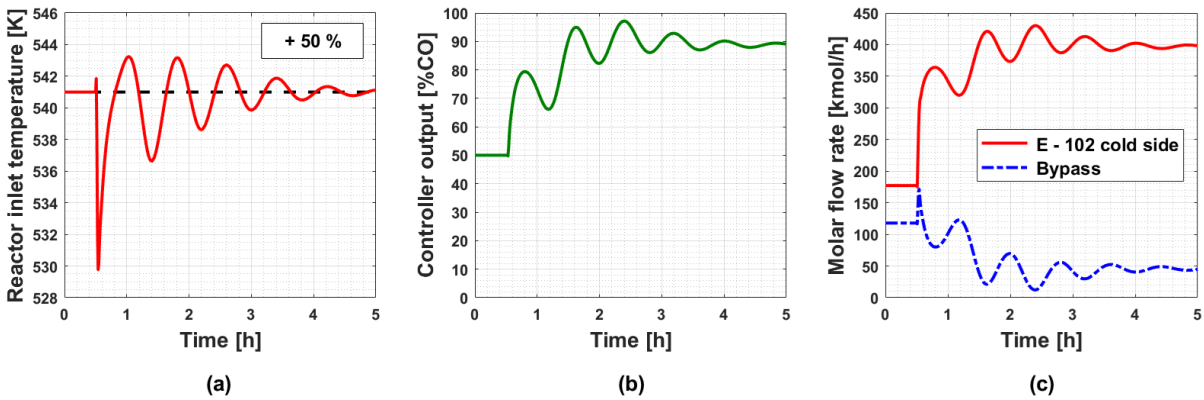

Figure 2.16. (a) *Reactor inlet temperature following a + 50 % feed flow rate disturbance at 0.5 h.* (b) *Controller TC - 101 output and* (c) *molar flow rates for both the bypass stream and the cold side of E - 102.*

Subsequently, following the 20 % step increase in the set point of FC - 101, more severe disturbances are analyzed. In Figure 2.16, the most critical of these, a 50 % step increase, is presented here due to the effective response observed in the intermediate cases.

Despite the significant step increase, the controller TCV - 101 successfully restores the reactor

inlet temperature to its set point within approximately 3 h, limiting the initial undershoot to around 11 K, as shown in Figure 2.16(a).

Also in this case, the final steady-state bypass fraction of 10 % closely matches the predicted value of 9.1 % of the analysis in section §2.2.1.1. Furthermore, since the bypass fraction remains above zero, the system could likely handle even higher flow rates, though these are not studied due to their excessive nature and limited relevance to the study. While the ability to manage a 50 % step increase may not be crucial when compared to more realistic, lower disturbances, it nonetheless highlights the flexibility of the system and the robust performance of the controller, even under extreme and anomalous conditions.

Subsequently, the performance of controller TC - 101 is evaluated in response to step decreases in the set point of controller FC - 101. Figure 2.17 illustrates the results of the dynamic simulations for a 20 % step decrease in the set point, following the same approach used for the other cases.

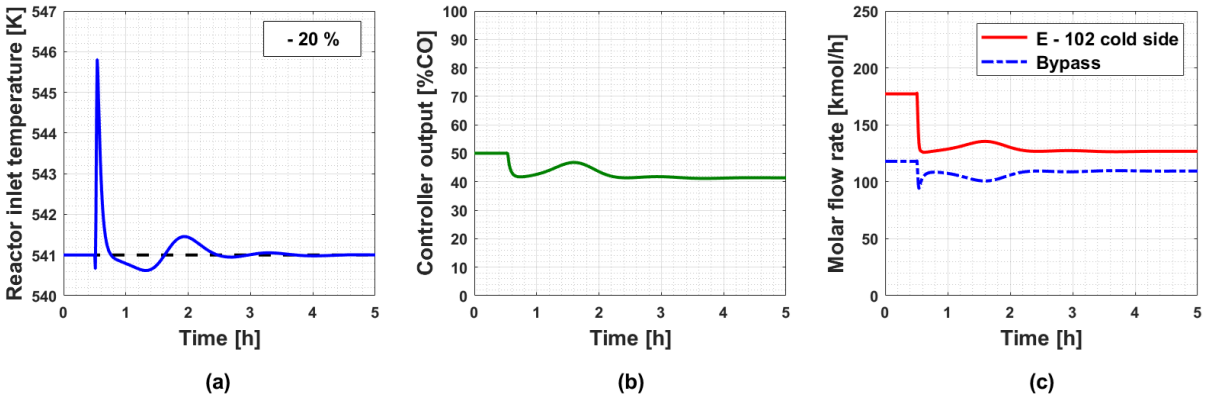

Figure 2.17. (a) *Reactor inlet temperature following a - 20 % feed flow rate disturbance at 0.5 h.* (b) *Controller TC - 101 output and* (c) *molar flow rates for both the bypass stream and the cold side of E - 102.*

The effects of the - 20 % disturbance on the reactor inlet temperature are effectively mitigated by the controller, with performance surpassing that of the 20 % bypass design. As shown in Figure 2.17(a), the overshoot is limited to only about 5 K, and the temperature is restored to the set point within approximately 1.5 h. This is a significant improvement compared to the 11 K overshoot and 3 h recovery time observed in the 20 % bypass design.

Also in this case the final steady-state value of the bypass fraction of 46 % closely matches the predicted value of 45.5 %, obtained in the model presented in the analysis in section §2.2.1.1. This adjustment is necessary due to the reduced process feed, requiring an increase in the bypass fraction from the nominal 40 % to decrease the flow through the preheater. This modification accommodates the lower heat duty requirement of the reactor feed, ensuring the desired temperature of 541 K is achieved.

Finally, the 50 % step decrease in the set point of the feed controller FC - 101 is considered and the results are illustrated in Figure 2.18.

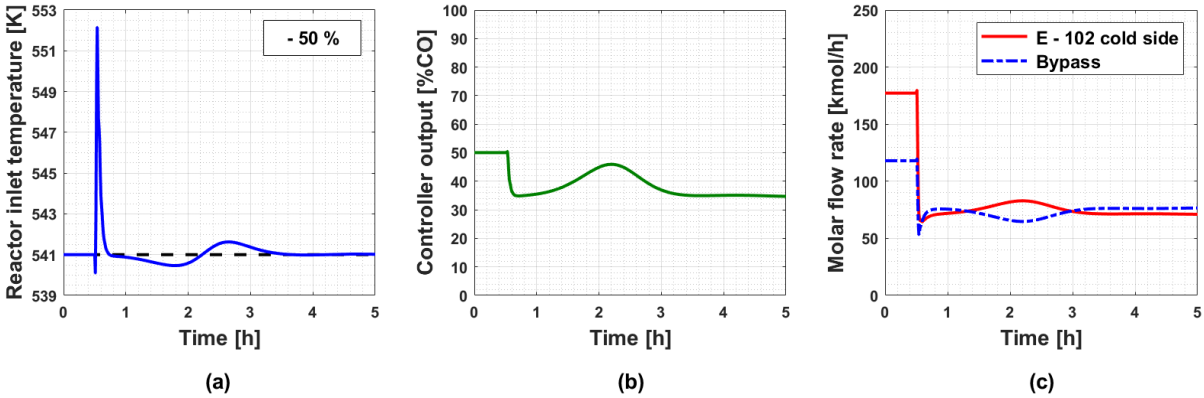

Figure 2.18. (a) *Reactor inlet temperature following a - 50 % feed flow rate disturbance at 0.5 h.* (b) *Controller TC - 101 output and* (c) *molar flow rates for both the bypass stream and the cold side of E - 102.*

In this scenario, the controller TC - 101 successfully manages the disturbance, containing the initial overshoot and effectively damping the subsequent oscillations, ultimately restoring the temperature to set point in 3 h after the introduction of the disturbance. Despite the severity of the disturbance, the initial overshoot is reduced to just 11 K, a significant improvement compared to the 27 K overshoot observed in the 20 % bypass configuration.

In this case the bypass fraction reaches the final steady-state value of 52 %, further validating the steady-state analysis in section §2.2.1.1, where the predicted value was 50.2 %.

In conclusion, the 40 % bypass configuration has been thoroughly studied, and the performance of the temperature controller has been assessed under various disturbances in the process feed flow rate. The controller has demonstrated satisfactory performance, effectively restoring the temperature to the set point across all the anomalous conditions analyzed. This improved performance, particularly at high throughputs, is attributed to slight modifications in the heat exchanger E - 102 design. Specifically, the higher 40 % nominal bypass selected, compared to the 20 % bypass in the previous design, has resulted in an increased heat exchange area. This allows for efficient preheating of the reactor feed, even with feed flow rates exceeding 50 % of the nominal value, enabling the temperature controller to restore the reactor inlet temperature to its set point. In contrast, the 20 % bypass design could not achieve this even with a 20 % increase in feed flow.

However, a limitation of this design is its inability to support process start-up. In this configuration, the only heat supplied to the vapor flow exiting the vaporizer, necessary to achieve the required reactor inlet temperature and reach nominal operating conditions, is recovered from the reactor effluent through the preheater. During start-up, when the reaction has not yet started and no heat is being generated, an external heat source, such as a furnace, is required to bring the reactor feed to the nominal condition.

The next chapter will introduce a new design that includes a furnace, addressing the limitations of the current configuration while still providing effective reactor inlet temperature control.

Chapter 3

Control with both bypass and furnace

This Chapter discusses a new configuration that incorporates a furnace into the design with bypass, which is essential for the start-up phase and in case of quenching. The process control using both the bypass and furnace is then presented, and its performance is assessed. Finally, a new process design and control structure proposed by Luyben (2012) is introduced, and its performance is compared to that of the previous configuration.

3.1 Standard design configuration

In §2.2, the process design with a 40 % bypass and the corresponding reactor inlet temperature control scheme yielded satisfactory results. The temperature controller was tested under various step changes in the set point of the process feed flow controller, which produced nearly corresponding step changes in the molar flow rate of the process feed. The controller effectively managed the effects of these disturbances on the reactor inlet temperature, ensuring good process operation even under these anomalous conditions.

However, the configurations discussed in the previous chapters present significant limitations from a real industrial perspective, particularly concerning the process start-up. In fact, without an external heat source, it is impossible to achieve the desired reactor inlet temperature necessary for reactor operation. Specifically, the reactor feed is preheated by the reactor effluent, but if the exothermic reaction within the reactor is not occurring, no heat can be generated and transferred to the reactor feed.

To address this issue, the introduction of a furnace into the process is necessary. Additionally, the furnace introduces a new manipulated variable: the fuel flow rate burned in the furnace. The new design, incorporating a furnace and referred to as the ‘‘standard’’ configuration in this Thesis due to its common application in industrial FEHE/reactor systems, is presented in §3.1.1. A new control scheme, featuring an additional temperature controller that utilizes this new manipulated variable, is then described in §3.1.2.

3.1.1 Steady-state design and Aspen Plus simulation

Given the good results achieved with the 40 % bypass configuration, the new design incorporating a furnace is developed starting from this configuration. In particular, the furnace

is introduced after the mixing point between the heat exchanger cold side stream and the bypass stream, and before the reactor, as shown in Figure 3.1. The relevant stream table, Table D.1, and equipment table, Table D.2, are provided in Appendix D.

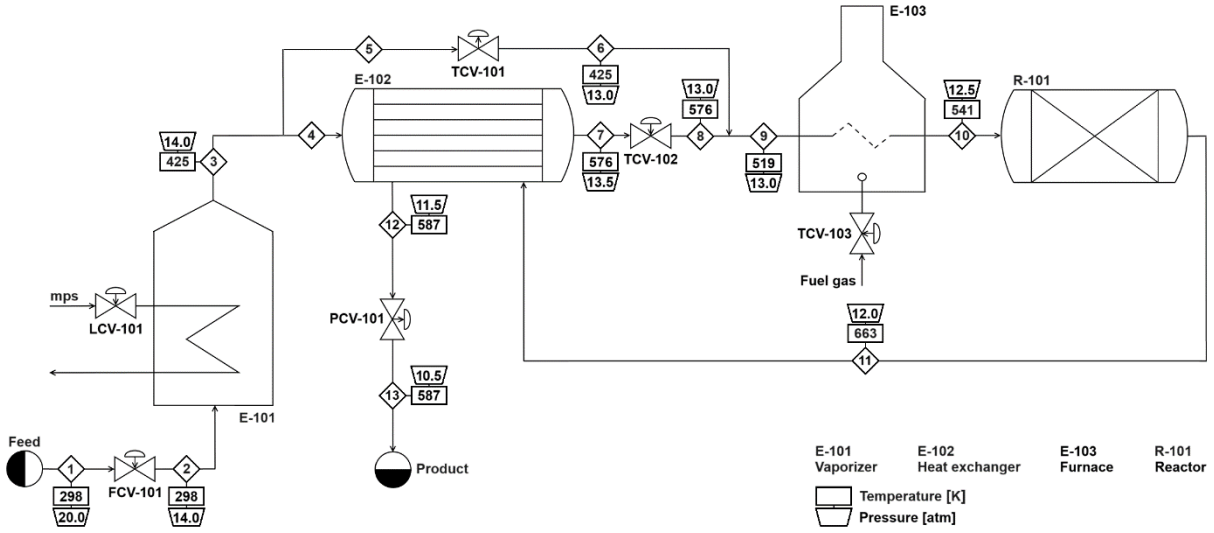

Figure 3.1. *Process flow diagram of the standard design configuration, illustrating all equipment schematics and the temperatures and pressures of all streams.*

The feed conditions, as well as the vaporizer E - 101 and the reactor R - 101 design and operating conditions, are maintained from the previous designs. The thermal duty required to preheat the reactor feed from the vaporizer outlet temperature of 425 K to the reactor inlet temperature of 541 K remains unchanged at 0.5433 MW. However, in this new design, furnace E - 103 is designed to provide 20 % of this thermal duty, equivalent to 0.1087 MW, while the remaining 0.4346 MW is recovered by preheater E - 102 from the reactor effluent. This allocation is consistent with the selection proposed by Luyben (2012), which is based on a trade-off between dynamic controllability, capital investment, and operating costs. On the one hand, the introduction of the furnace increases the overall capital investment of the plant and raises operating costs, as the furnace thermal duty is supplied by burning fuel. On the other hand, a larger furnace can improve the system dynamics, and it reduces the time needed to heat the reactor feed, thereby accelerating the initiation of the reaction during start-up.

Regarding heat exchanger E - 102, the overall heat transfer coefficient is maintained at 170 $W \cdot m^{-2} \cdot K^{-1}$. However, the reduced heat duty results in a decrease in the heat exchange area from of 39.4 m^2 (in the previous 40 % bypass configuration without a furnace) to 25.1 m^2, thereby lowering the heat exchanger capital costs. The heat exchanger E - 102 is designed with a 1-2 configuration, though this detail is omitted in Figure 3.1 for convenience.

In operation, the cold stream through the preheater is heated from 425 K to 576 K. This preheated stream is then mixed with the bypass stream, resulting in a combined stream temperature of 519 K. The mixed stream subsequently enters the furnace, where it is further heated to reach the desired reactor inlet temperature of 541 K. Due to the reduced heat recovery

by preheater E - 102 from the reactor effluent, the outlet temperature of this stream is now of 587 K, compared to 568 K in the previous designs.
To model the furnace, aside from its heat duty, the only additional information required concerns the features of the fuel being consumed. Specifically, a default heating utility value of 600 kJ/kg provided by Aspen Plus is used, resulting in a utility mass flow of about 0.18 kg/s.
To maintain the reactor inlet pressure at 12.5 atm, the pressure drop through the preheater is reduced from 1 atm of the previous design (with bypass and without furnace) to 0.5 atm. This adjustments accounts for the introduction of the furnace into the reactor feed line, which contributes an additional pressure drop of 0.5 atm.
In conclusion, with the steady-state simulation now completed, the next section will focus on the dynamic simulation and the new control structure of this design configuration.

3.1.2 Aspen Plus Dynamics simulation

Before exporting the Aspen Plus simulation into Aspen Plus Dynamics, all necessary information related to the dynamic behaviour of the different equipment is provided. Specifically, the vaporizer E - 101 and the reactor R - 101 are modelled as in §1.3, while the preheater E - 102 is updated to account for the changes implemented in §3.1.1. The specifications for the preheater are detailed in Table 3.1.

Table 3.1. *Summary of all heat exchanger E - 102 design parameters.*

Configuration	$\dot{Q}$ [MW]	U [W·m^{-2}·K^{-1}]	A [m^2]	L_t [m]	s_t [m]	$d_{t,ext}$ [m]	N_t [-]	V_t [m^3]	V_{sec} [m^3]	m [kg]	m_{sec} [kg]
1-2	0.4346	170	25.1	10	0.002	0.025	50	0.11	0.06	356	89

Regarding furnace E - 103, its dynamics can only be approximated by Aspen Plus Dynamics. Consequentely, the `instantaneous` option is selected in Aspen Plus, thus neglecting the furnace dynamics in this instance. However, when discussing the new control loop which utilizes the manipulated variable introduced by the furnace, the dynamics of this equipment will be approximated introducing a deadtime in the control loop. Additionally, for the furnace heat transfer option, `constant duty` is selected, as it is the most appropriate choice for this situation allowing to manipulate the furnace heat duty.
With all the equipment design and dynamics properly modelled, Aspen Plus Dynamics is started, and the vaporizer liquid level issue and the flow rates mismatches are solved as in the other simulations. The valves depicted in Figure 3.1 are sized, with FCV - 101 and LCV - 101 valves maintaining the same specifications as in the base design. However, differently from all the previous design configurations, valve PCV - 101 on the final product stream line requires to be resized due to changes in the volumetric flow rate through it. Specifically, the reduced heat duty exchanged from the reactor effluent to the cold side stream in heat exchanger E - 102

results in a hotter hot side outlet stream, with a temperature of 587 K instead of 567 K. This higher temperature leads to a lower density of the vapor stream, ultimately increasing its nominal volumetric flow.

Regarding valves TCV - 101 and TCV - 102, these also requires resizing compared to the previous design without furnace. Specifically, the nominal pressure drop of valve TCV - 101 is reduced from 1.5 atm to 1 atm, aligning with the combined nominal pressure drop through the preheater E - 102 cold side and the valve TCV - 102. Indeed, the design pressure drop through the preheater cold side is decreased from 1 atm to 0.5 atm, as mentioned in §3.1.1, due to the introduction of the furnace in the reactor feed line, while the nominal pressure drop through TCV - 101 remains at 0.5 atm. Additionally, the design volumetric flow through TCV - 102 is decreased due to the lower cold side outlet temperature of E - 102 compared to the previous design without furnace.

The valve TCV - 103 on the furnace fuel stream is required to manipulate the fuel flow rate and ultimately the furnace heat duty. However, this valve is not implemented in the simulation because the `Heater` block used to model the furnace in Aspen Plus does not include a utility stream line. As a result, in Aspen Plus Dynamics, it is not possible to manipulate the fuel flow rate. Instead, the software allows direct regulation of the heat duty, which will be explained in the context of the reactor inlet temperature control strategy for this new design.

In a real application, valve TCV - 103 would be selected as fail-closed. This configuration ensures that, in case of a failure, the valve will close automatically, stopping the furnace operation. Consequently, this will limit the preheating of the reactor feed and contribute to the shutdown of the reactor operation.

The main features of the updated valves PCV - 101, TCV - 101, and TCV - 102 are detailed in Table 3.2.

Table 3.2. *Summary of all valves PCV - 101, TCV - 101, and TCV - 102 design parameters.*

Valve	q [m^3/h]	ΔP_v [atm]	*Valve opening* [%OP]	K_v [$m^3 \cdot h^{-1} \cdot bar^{-0.5}$]	*Valve action*	*Valve characteristic*
PCV - 101	1236.6	1	50	229.3	Air-to-close	Linear
TCV - 101	293.9	1	50	69.6	Air-to-close	Linear
TCV - 102	620.6	0.5	50	170.3	Air-to-open	Linear

Finally, in this simulation all valves are configured with the default first-order dynamics, as described in §1.3.

With all valves correctly implemented, the control scheme proposed for this design is shown in Figure 3.2, and the relevant stream table, Table D.1, and equipment table, Table D.2, are provided in Appendix D. The control scheme includes the same flow controller FC - 101, level controller LC - 101, and pressure controller PC - 101 of the previous designs. However, unlike

the control strategy shown in §2.1.2, this design utilizes two temperature controllers: the furnace inlet temperature controller TC - 101 and the reactor inlet temperature controller TC - 102.

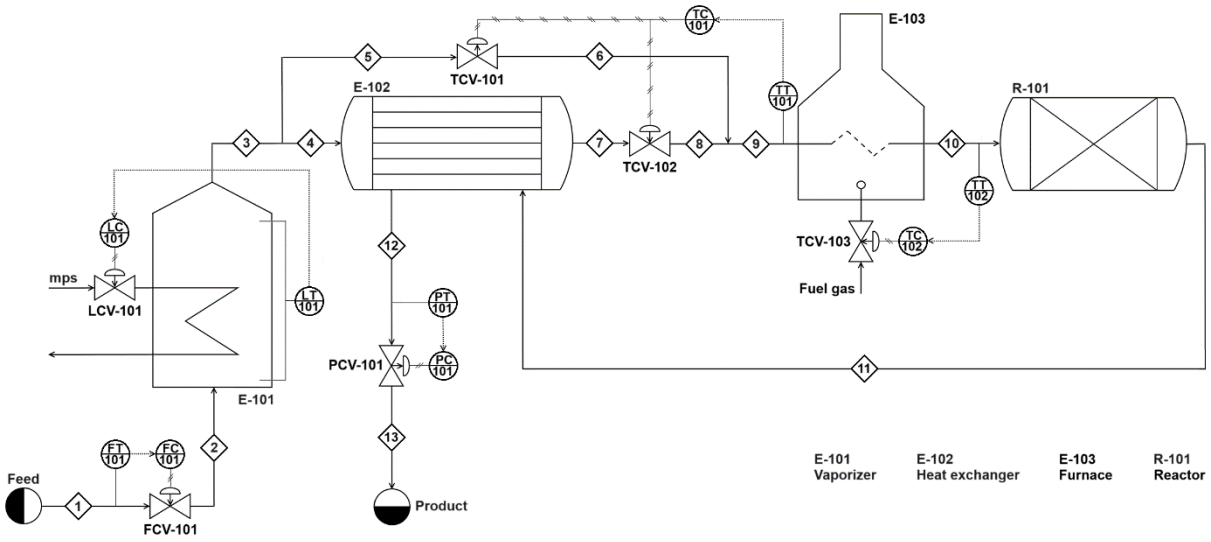

Figure 3.2. *Process flow diagram of the standard design configuration and all the control loops, illustrating all equipment schematics.*

With all other controllers set to automatic mode, the two temperature controllers are then tuned. The first control loop to be implemented is the one with faster dynamics: the furnace inlet temperature control loop. This loop is designed to control the furnace inlet temperature by adjusting the valve openings of both TCV - 101 and TCV - 102 valves, thereby regulating the flows through and around the preheater E - 102. This temperature control loop is similar to the one used for controlling the reactor inlet temperature in §2.1.2, as it employs the same complementary dual split-range control method outlined in Table 2.3.

To approximate the dynamics of the temperature sensor-transmitter TT - 101, a 1 min deadtime is introduced into the control loop. The furnace inlet temperature controller, TC - 101, uses the measurement from TT - 101 to adjust the opening of the two valves, TCV - 101 and TCV - 102. The controller is configured with a reverse action, considering the action of these two valves. For instance, if the sensor detects a temperature below the set point of 519 K, the controller increases its output, which results in valve TCV - 101 closing and TCV - 102 opening, thereby increasing the flow through the preheater line and enhancing the heat transfer rate. As a result, the greater heat exchange elevates the temperature of the mixed stream, which corresponds to the furnace inlet temperature.

The sensor-transmitter is selected with a range of 273 - 765 K, ensuring that the controller output is at 50 %CO under nominal steady-state conditions, and providing a sufficient span for the purposes of this study. The controller is implemented with a PI action. Its parameters are initially calculated using the ATV test, yielding an ultimate controller gain of 3.7 %CO/%TO and an ultimate period of 1.9 min. These values are then used to derive the controller gain and integral time constant according to the Tyreus-Luyben tuning rules, resulting in an integral time

constant of 4.1 min and a controller gain of 1.2 %CO/%TO. The controller tuning is further optimized, resulting in a gain of 2.2 %CO/%TO and an integral time constant of 1 min.
Once the TC - 101 controller is set to automatic mode, the reactor inlet temperature control loop is implemented. This loop employs the measurements from the sensor-transmitter TT - 102 to regulate the fuel flow through valve TCV - 103, thereby adjusting the furnace heat duty to control the reactor inlet temperature. However, as previously mentioned, in the simulation, the manipulated variable is the furnace heat duty rather than the TCV - 103 valve opening.
As discussed in §3.1.1, the furnace dynamics is only approximately simulated by Aspen Plus Dynamics. Thus, to better approximate both the furnace and the sensor-transmitter TT - 102 dynamics, a 2 min deadtime is introduced into the control loop following the approach used by Luyben (2012). This approximation represents a limitation of the study, alongside the direct manipulation of the furnace heat duty instead of the fuel flow rate.
The sensor-transmitter range for this loop is 273 - 809 K, ensuring that the controller output is 50 %CO under nominal steady-state condition, which corresponds to the design furnace duty of 0.1087 MW, and providing an adequately large span for the application. The controller action is configured as reverse, considering the action of valve TCV - 103. For example, if the sensor measures a reactor inlet temperature lower than the set point of 541 K, the controller increase its output, increasing the valve opening. This, in turn, raises the fuel flow to the furnace, thereby enhancing the heat transfer rate within the furnace. Consequentely, the increased preheating of the reactor feed elevates its temperature, restoring it to the nominal set point.
The controller is implemented with a PI action, and its tuning parameters are determined following an ATV test, which identifies the ultimate controller period and gain as 5.6 min and 15.5 %CO/%TO. The Tyreus-Luyben tuning rules are then applied, yielding a controller gain of 4.9 %CO/%TO and an integral time constant of 12.4 min. During performance testing of this controller, significant interactions with the controller TC - 101 are observed. Specifically, it is found that TC - 101, following the implementation of TC - 102, has an overly aggressive action. Thus, TC - 101 is slightly detuned, with a reduced controller gain of 2 %CO/%TO and an increased integral time constant of 1.5 min. Finally, the tuning of TC - 102 is optimized, resulting in a controller gain of 1.8 %CO/% TO and an integral time constant of 1.6 min.
Finally, in Table 3.3 the main features of the two temperature controllers are summarized.

Table 3.3. *Tuning parameters of controllers TC - 101 and TC - 102.*

Controller	***Span***	$\mathbf{K_C}$ **[%CO/%TO]**	$\boldsymbol{\tau_I}$ **[min]**	***Action***
TC - 101	492 K	2	1.5	Reverse
TC - 102	536 K	1.8	1.6	Reverse

With all the controllers implemented, the standard design configuration is studied dynamically.

Specifically, the same disturbances presented in Table 2.12 are analyzed, including positive and negative step variations in the set point of the feed flow controller FC - 101.
Firstly the + 20 % step change scenario is analyzed, and the performance of the two temperature controllers, TC - 101 and TC - 102, in response to this disturbance is illustrated in Figure 3.3.

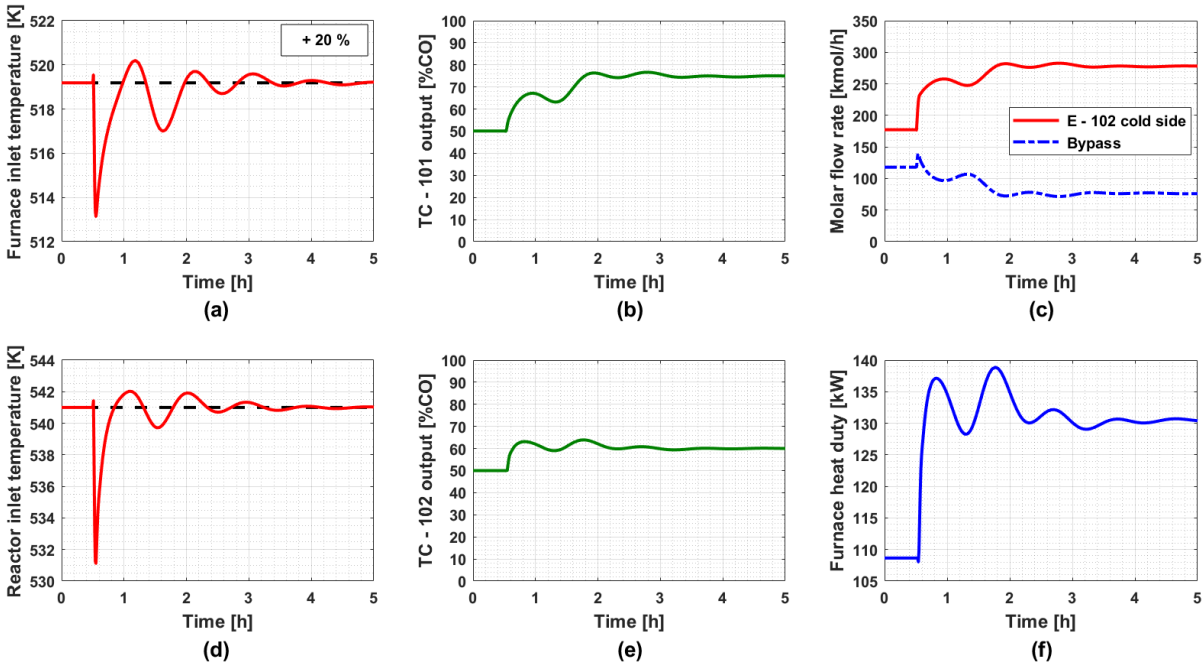

Figure 3.3. *Scenario with a + 20 % feed flow rate disturbance at 0.5 h:* (a) *furnace inlet temperature,* (b) *controller TC - 101 output,* (c) *molar flow rates for both the bypass stream and the cold side of E - 102,* (d) *reactor inlet temperature,* (e) *controller TC - 102 output, and* (f) *furnace heat duty.*

In this case study, the controller TC - 101 restores the furnace inlet temperature in approximately 2 h following the introduction of the perturbance, while the controller TC - 102 similarly regulates the reactor inlet temperature.

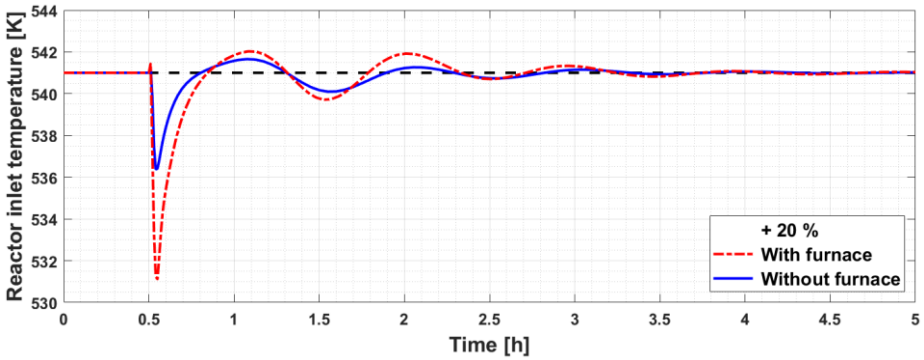

Figure 3.4. *Reactor inlet temperature following a + 20 % feed flow rate disturbance at 0.5 h in the 40 % bypass configuration with and without furnace.*

Specifically, as shown in Figure 3.4, the dynamic behaviour of the reactor inlet temperature in this design is comparable to that observed with the 40 % bypass design presented in §2.2.2.

However, the initial undershoot is more pronounced in this new design, with the temperature dropping to 531 K, compared to about 536 K in the previous configuration without furnace. This poorer response is attributed to the combined delayed actions of TC - 101 in reducing the bypass fraction and TC - 102 in increasing the furnace duty, as the higher flow rate necessitates a greater preheating to achieve the optimal reactor inlet temperature of 541 K.

Finally, as depicted in Figures 3.3(c) and 3.3(f), at the final steady-state, the bypass fraction is reduced to approximately 21.5 %, and the furnace heat duty is increased by about 22 kW, representing a 20 % increase over the nominal duty. However, this new steady-state condition is not the most effective solution. The bypass fraction could have been further reduced, allowing for better recovery of the available heat from the hot reactor effluent, while the furnace heat duty could have been increased by less than the additional 22 kW.

Subsequently, more severe perturbations than the + 20 % disturbance are studied. Specifically, the + 30 % disturbance, which is not detailed in this thesis, yielded satisfactory results similar to those of the + 20 % scenario. Given the similarities between the + 40 % and + 50 % disturbances, it is decided to present only the latter, as was done for the previous designs, as it is the most severe of these anomalous conditions. This scenario is illustrated in Figure 3.5.

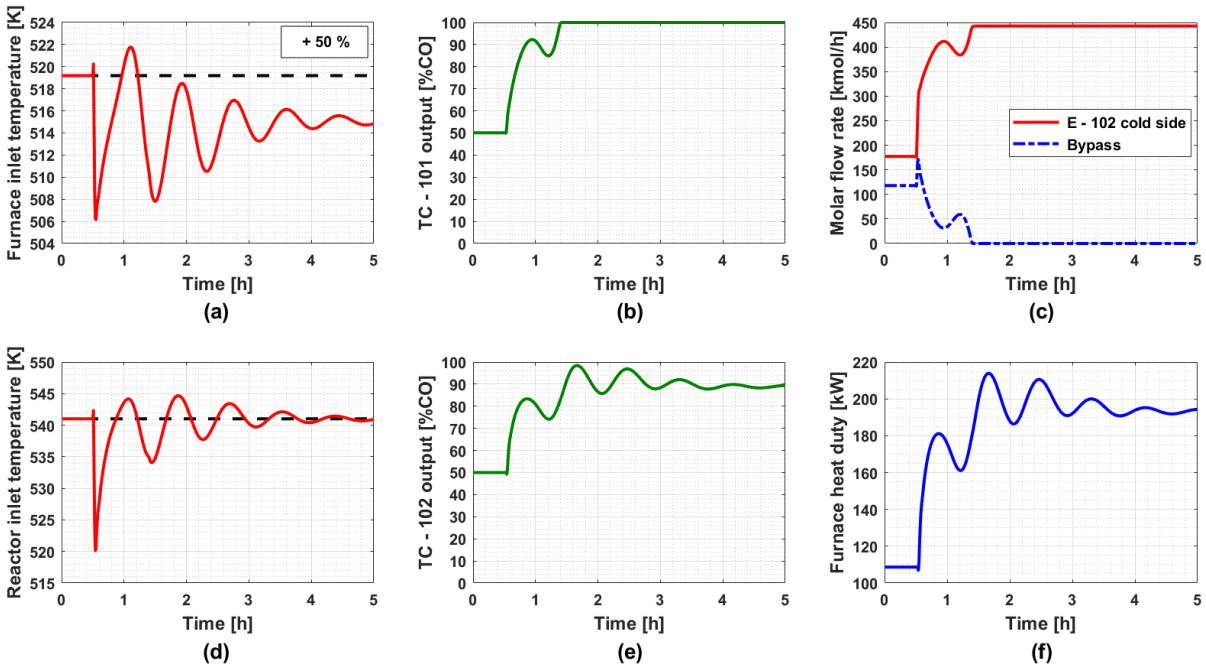

Figure 3.5. *Scenario with a + 50 % feed flow rate disturbance at 0.5 h:* (a) *furnace inlet temperature,* (b) *controller TC - 101 output,* (c) *molar flow rates for both the bypass stream and the cold side of E - 102,* (d) *reactor inlet temperature,* (e) *controller TC - 102 output, and* (f) *furnace heat duty.*

Under this perturbation, the furnace inlet temperature, shown in Figure 3.5(a), does not return to the set point. The controller TC - 101 saturates its output, as shown in Figure 3.5(b), resulting in the full opening of valve TCV - 102 and the complete closing of valve TCV - 102. Consequentely, the bypass fraction drops to zero, and all the vapor is directed through the heat

exchanger E - 102, as shown in Figure 3.5(c). However, E - 102 under these conditions results to be undersized, with insufficient heat exchange area to recover the required heat duty from the reactor effluent and preheat this large flow rate to the nominal furnace inlet temperature of 519 K. This issue also arises with the 40 % disturbance, though in that case, the furnace inlet temperature offset was only about 1 K. In this scenario, the offset is approximately 4 K.

Although the furnace inlet temperature is not restored to the desired value, the reactor inlet temperature, illustrated in Figure 3.5(f), remains effectively controlled, with the disturbance effects nearly completely mitigated within approximately 3 h. However, the furnace heat duty, presented in Figure 3.5(f), is increased by about 86 kW (+ 79 %), leading to a significant rise in fuel consumption and, consequently, higher operational costs for the furnace.

Figure 3.6 presents a comparison between the reactor inlet temperature dynamic responses following the 50 % step increase in the FC - 101 set point for the standard design and the previous design without furnace, which is discussed in §2.2.

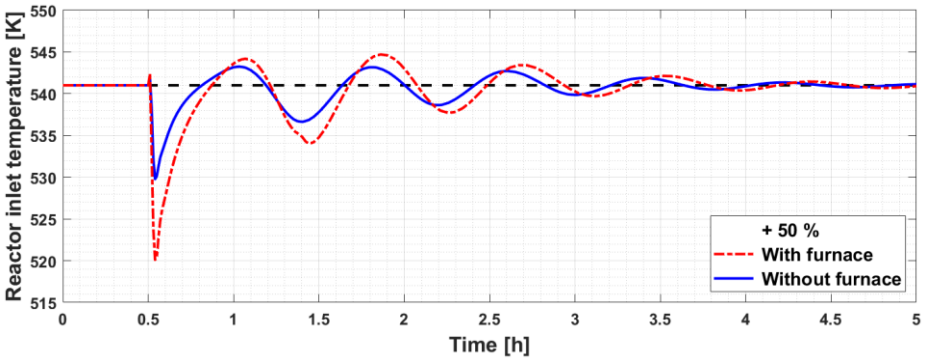

Figure 3.6. *Reactor inlet temperature following a + 50 % feed flow rate disturbance at 0.5 h in the 40 % bypass configuration with and without furnace.*

In this scenario, the combined delayed actions of the two temperature control loops in the design with furnace result in less effective control of the reactor inlet temperature. The larger preheating required by the increased reactor feed is not provided until the controllers, TC - 101 and TC - 102, respectively reduce the bypass fraction and increase the furnace duty.

Consequently, during the initial undershoot, the temperature drops 10 K lower than in the design without furnace, where the only temperature controller acted on the bypass fraction. Additionally, the subsequent oscillations are dampened slightly more slowly in this new design, although still effectively, due to the more severe undershoot.

Subsequently, the performance of the two temperature controllers is analyzed following the introduction of negative step changes in the FC - 101 set point. First, the - 20 % disturbance is considered, and the results of this analysis are summarized in Figure 3.7, as was done for the previous scenarios.

As illustrated in Figures 3.7(a) and 3.7(d), both the furnace inlet temperature and the reactor inlet temperature are efficiently restored to their nominal values within approximately 2 h after

the disturbance is introduced. It is observed that, under the new steady-state conditions, the furnace continues to provide approximately 87 kW of heat (- 20 %), despite the reduced feed flow conditions. Although the heat exchange area of E - 102 is sufficiently large to meet the reduced preheating demand, it is not utilized efficiently. The final steady-state bypass fraction is around 51 %, whereas from a steady-state perspective, with a bypass fraction of about 15 %, the furnace would no longer be required, and all the heat would be recovered by the preheater.

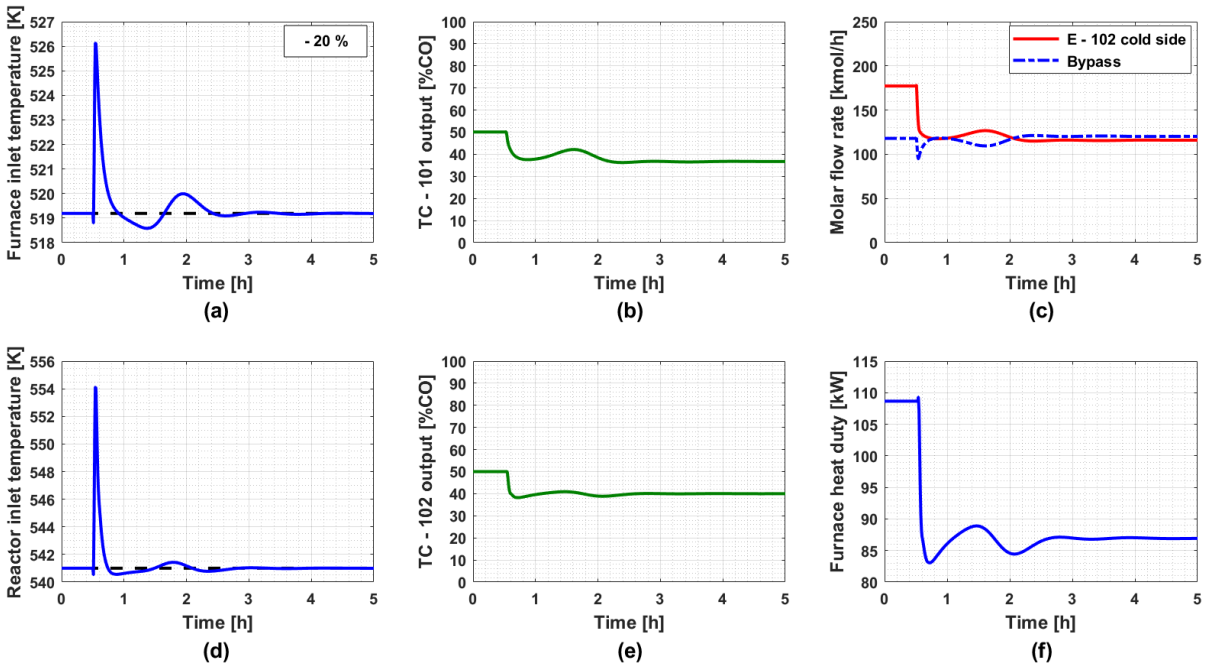

Figure 3.7. *Scenario with a - 20 % feed flow rate disturbance at 0.5 h:* (a) *furnace inlet temperature,* (b) *controller TC - 101 output,* (c) *molar flow rates for both the bypass stream and the cold side of E - 102,* (d) *reactor inlet temperature,* (e) *controller TC - 102 output, and* (f) *furnace heat duty.*

Additionally, as shown in Figure 3.7(c), the bypass molar flow is almost unaffected by the temperature controller TC - 101 action following the feed flow disturbance, which instead primarily impacts the heat exchanger cold side flow. Specifically, the 20 % feed flow decrease, corresponding to a reduction of 59 kmol/h, results in a comparable decrease of 61.4 kmol/h in the heat exchanger cold side flow, along with a slight increase of 2.4 kmol/h in the bypass flow. Figure 3.8 presents the same comparison between the standard configuration and the design without furnace as discussed for the other scenarios. As shown, the initial overshoot in reactor inlet temperature observed in the standard design is significantly more severe, reaching 554 K compared to the 546 K in the design without furnace. In the standard configuration, the lower feed flow rate is excessively preheated due to the delayed actions of both controllers. As the disturbance propagates through the system, the feed flow is overly preheated because the cold side flow rate in the preheater E - 102 decreases earlier than the hot side flow. Additionally, the furnace provides unnecessary heat to this stream, and this excess heat is further recycled into the FEHE/reactor system until the controllers begin to respond.

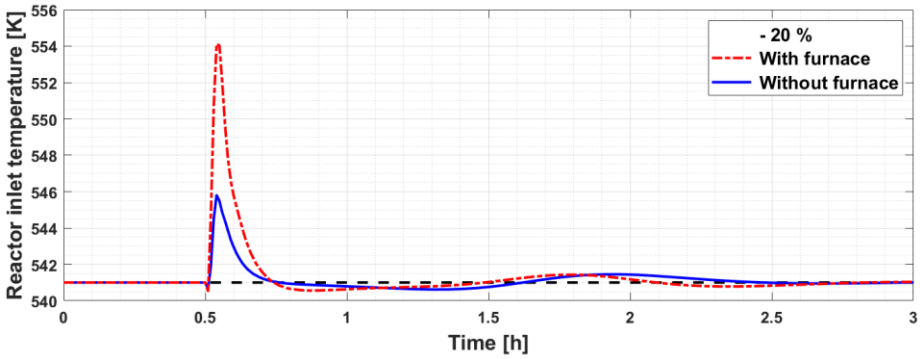

Figure 3.8. *Reactor inlet temperature following a - 20 % feed flow rate disturbance at 0.5 h in the 40 % bypass configuration with and without furnace.*

Following the 20 % step decrease in the FC - 101 set point, more severe disturbances are studied. In this instance, it is decided to present the results for the most critical disturbance, the - 50 % step change, given the similarities in the results of the intermediate scenarios, despite differences in the magnitude of both the furnace inlet and reactor inlet temperature variations. The dynamic responses following the - 50 % disturbance scenario are illustrated in Figure 3.9.

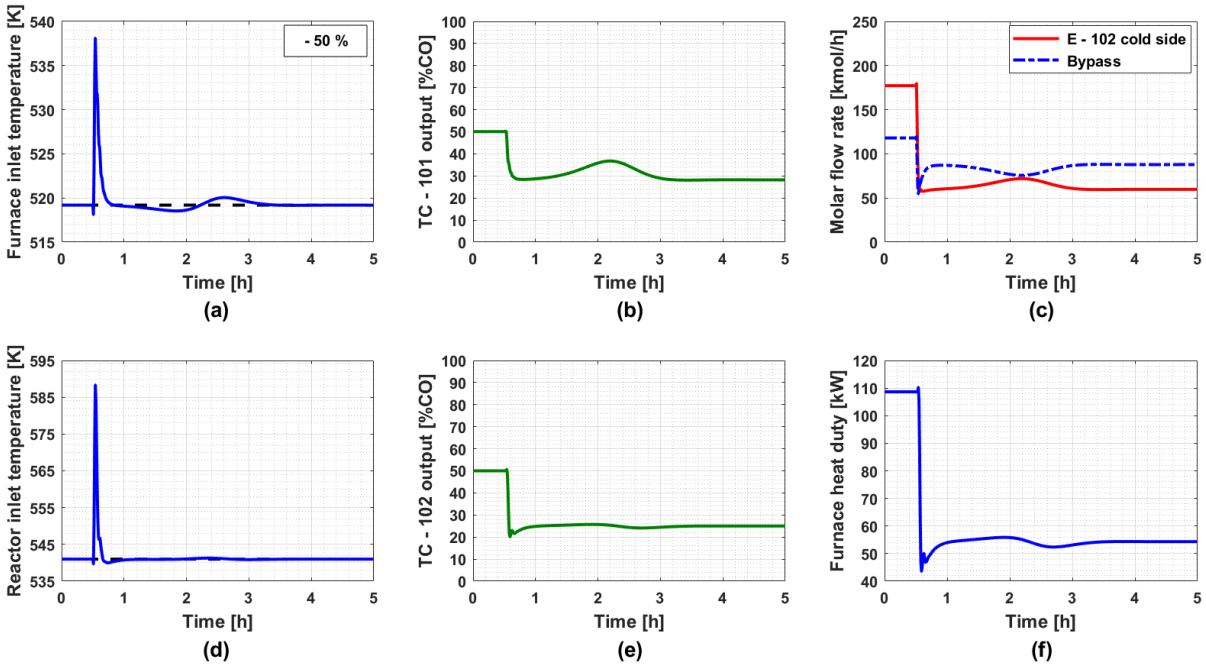

Figure 3.9. *Scenario with a - 50 % feed flow rate disturbance at 0.5 h:* (a) *furnace inlet temperature,* (b) *controller TC - 101 output,* (c) *molar flow rates for both the bypass stream and the cold side of E - 102,* (d) *reactor inlet temperature,* (e) *controller TC - 102 output, and* (f) *furnace heat duty.*

In this scenario, both controllers, TC - 101 and TC - 102, restore the furnace and reactor inlet temperatures to their set points within approximately 1 h after the disturbance is introduced. However, as in the - 20 % scenario, the new steady-state reached still results in the furnace providing unnecessary heat to the feed stream, around 54 kW (- 50 %). Under these reduced feed flows, the preheater E - 102 is not operated efficiently, as it has ample heat exchange area

to preheat the reactor feed without requiring additional furnace heat duty. Specifically, from a steady-state perspective, with a bypass fraction of approximately 33 %, the furnace heat provision could be stopped, making the process autothermal under these feed conditions.

Next, in Figure 3.9(e), following the system perturbation, the TC - 102 output shows a few low-frequency oscillations after the initial rapid decrease from 50 % to about 20 %. These oscillations do not stem from the process dynamics but are instead a consequence of the aggressive action of TC - 102 and the large step decrease in feed flow. Additionally, these oscillations are more noticeable in Figure 3.9(f) in the resulting furnace heat duty. However, the amplitude of these oscillations is negligible, and they disappear within a few minutes. Similar issues are also reported by Luyben (2012) under these conditions.

Figure 3.10 presents a comparison of the reactor inlet temperature results obtained with the standard configuration and the 40 % bypass design without furnace.

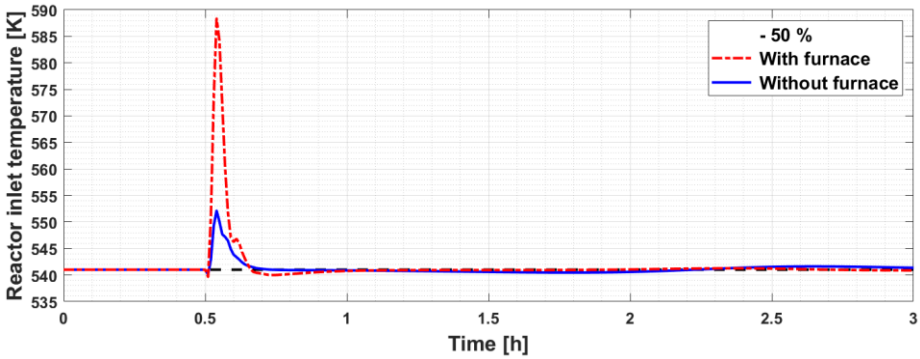

Figure 3.10. *Reactor inlet temperature following a - 50 % feed flow rate disturbance at 0.5 h in the 40 % bypass configuration with and without furnace.*

As depicted in Figure 3.10, with the - 50 % step change in the FC - 101 set point, the effects of this significant feed flow decrease are much more pronounced in the reactor inlet temperature for this new design using two temperature controller compared to the previous design without furnace, which uses only one temperature controller. Specifically, the reactor inlet temperature exhibits an initial overshoot reaching nearly 590 K, in contrast to the approximately 552 K in the previous design. Therefore, under these flow conditions, the aforementioned delayed actions of both the two controllers result in a much more critical situation, leading to a severe temperature overshoot with a magnitude of 50 K.

In conclusion, this section has presented the standard design and evaluated the performance of its associated control strategy in controlling the reactor inlet temperature. In al the scenarios examined, this temperature is not controlled as efficiently as in the design with 40 % bypass and without furnace. This inefficiency arises not only from the adoption of a more complex control strategy involving two controllers, but also the reduced heat exchange area of preheater E - 102. Specifically, the combined delayed actions of the two temperature controllers have been identified as detrimental to precise control of the reactor inlet temperature. Moreover, due

to the interactions between the two controllers, their actions cannot be overly aggressive, as this would render the system prone to instability, especially following feed flow step decreases. Additionally, this section highlights the inefficiencies of the current control strategy in utilizing the preheater E - 102, which results in the unnecessary use of furnace heat duty, particularly under low throughput conditions. This limitation, resulting in increased operational costs due to excess fuel consumption, will be addressed in §3.2. There, an alternative design and control scheme aimed at reducing furnace duty consumption will be discussed.

3.2 Alternative design configuration

Following the discussion on the standard design and the associated reactor inlet temperature control strategy, as presented in §3.1, this section considers a new alternative design and control strategy proposed by Luyben (2012), which aims to reduce furnace heat consumption.

3.2.1 Steady-state design and Aspen Plus simulation

The new alternative design presented in this section is developed using the same equipment designs and process feed conditions as the previous standard configuration. However, in this design, the bypass stream does not mix with the preheater cold side outlet stream before entering the furnace. Instead, it mixes directly with the hot furnace outlet stream just before entering the reactor. The new alternative design configuration is depicted in Figure 3.11. The relevant stream table, Table E.1, and equipment table, Table E.2, are provided in Appendix E.

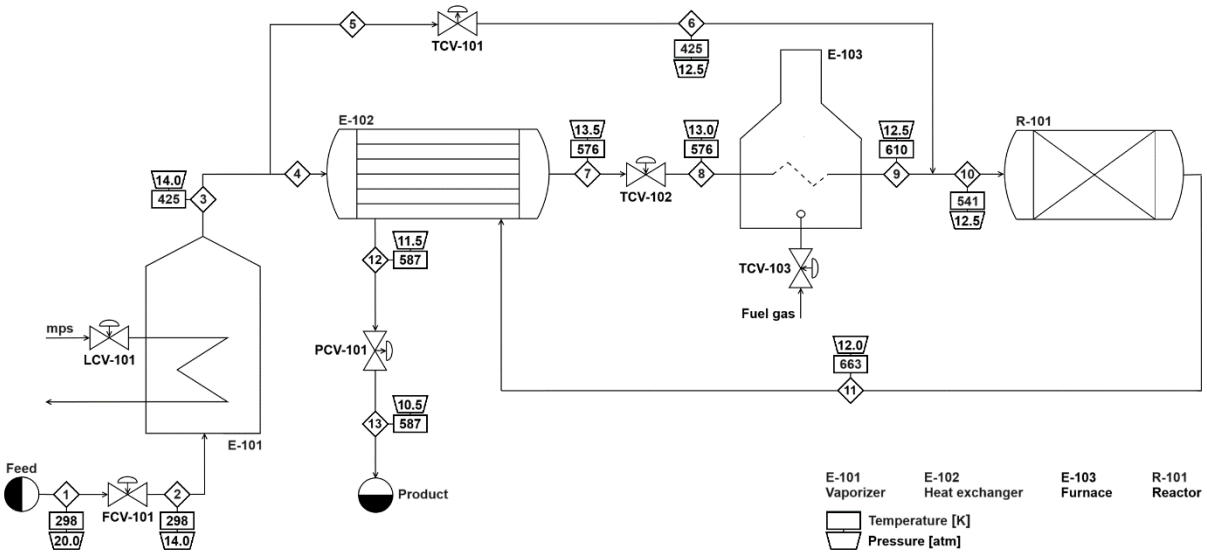

Figure 3.11. *Process flow diagram of the new alternative design, illustrating all equipment schematics and the temperatures and pressures of all streams.*

This design is conceived to enhance process controllability, particularly regarding the reactor inlet temperature. The key idea behind this design configuration is to develop a control system

which manipulates the bypass fraction, directly influencing the mixing between the cold vapor bypass stream with the preheated stream from both the preheater and the furnace. Since the mixing process has significantly faster dynamics compared to the furnace duty regulation, this approach is expected to improve the overall effectiveness of the temperature control action. The new control strategy will be explained in §3.2.2, where the dynamic simulation is developed.
Considering the furnace steady-state operation, since the mixing point is moved to after the furnace E - 103 and before the reactor R - 101, the temperature of the furnace inlet stream is increased from 519 K in the standard design to 576 K, which is the temperature of the cold side outlet stream of the preheater E - 102. This increased temperature is due to the reduced flow rate through the furnace, as only the fraction of the vapor exiting the vaporizer E -101 that is not bypassed flows through the furnace, even though the furnace design heat duty remains at 0.1087 MW. Consequently, the temperature of this stream is raised to 610 K in the furnace before mixing with the bypass stream, compared to 541 K in the previous design.
A drawback of these higher temperatures in the furnace is the potential need for a higher-temperature heat source, which could ultimately lead to increased furnace operating costs.
As a result of the new mixing point location, the pressure drop across valve TCV - 101 increases from 1 atm in the previous design to 1.5 atm, to ensure that the pressure drop in the bypass stream matches the overall pressure drop across the preheater E - 102, valve TCV - 102, and the fired heater E - 103 under the design steady-state condition
In conclusion, following the discussion in this section on the steady-state design of this new alternative configuration, the next section will present the associated control scheme and focus on the dynamic simulation of this process.

3.2.2 Aspen Plus Dynamics simulation

In this section, the Aspen Plus simulation is prepared to be exported into Aspen Plus Dynamics. The vaporizer and the reactor retain the same features implemented in §1.3, while the preheater and furnace are implemented as described in §3.1.2, as their designs remain unchanged.
Once Aspen Plus Dynamics is initiated, the vaporizer liquid level issue is resolved as detailed in §1.3, and the valves are appropriately sized to eliminate the flow rates mismatches observed in the dynamic simulation compared to the steady-state simulation developed in Aspen Plus. Specifically, valves FCV - 101, PCV - 101, and TCV - 102 are implemented and sized as outlined in §3.1.2, as their operation and nominal steady-state conditions remain unchanged. Additionally, valves LCV - 101 and TCV - 103 retain the same features detailed in §1.3 and §3.1.2, respectively, although they are not implemented in Aspen Plus Dynamics because the utility streams used in the vaporizer and the furnace are not modelled by the simulator.
Regarding valve TCV - 101, it requires to be resized compared to the standard design, due to the increased nominal pressure drop from 1 atm to 1.5 atm, as discussed in §3.2.1, which results

in a lower valve flow coefficient (K_v).

Finally, Table 3.4 summarizes the nominal conditions and main characteristics of all the valves implemented in Aspen Plus Dynamics, highlighting the updated features of valve TCV - 101.

Table 3.4. *Summary of all valves FCV - 101, PCV - 101, TCV - 101, and TCV - 102 design parameters.*

Valve	*q* [m^3/h]	ΔP_v [atm]	*Valve opening* [%OP]	K_v [$m^3 \cdot h^{-1} \cdot bar^{-0.5}$]	*Valve action*	*Valve characteristic*
FCV - 101	11.6	6	50	23.5	Air-to-open	Equal-percentage
PCV - 101	1236.6	1	50	229.3	Air-to-close	Linear
TCV - 101	293.9	1.5	50	58.6	Air-to-close	Linear
TCV - 102	620.6	0.5	50	170.3	Air-to-open	Linear

All the valves are also in this simulation configured with default first-order dynamics, with a time constant of 0.1 s and a valve gain of 1 %OP/%CO.

With the dynamics simulation properly configured, the control loops are implemented as illustrated in Figure 3.12. The relevant stream table, Table E.1, and equipment table, Table E.2, are provided in Appendix E.

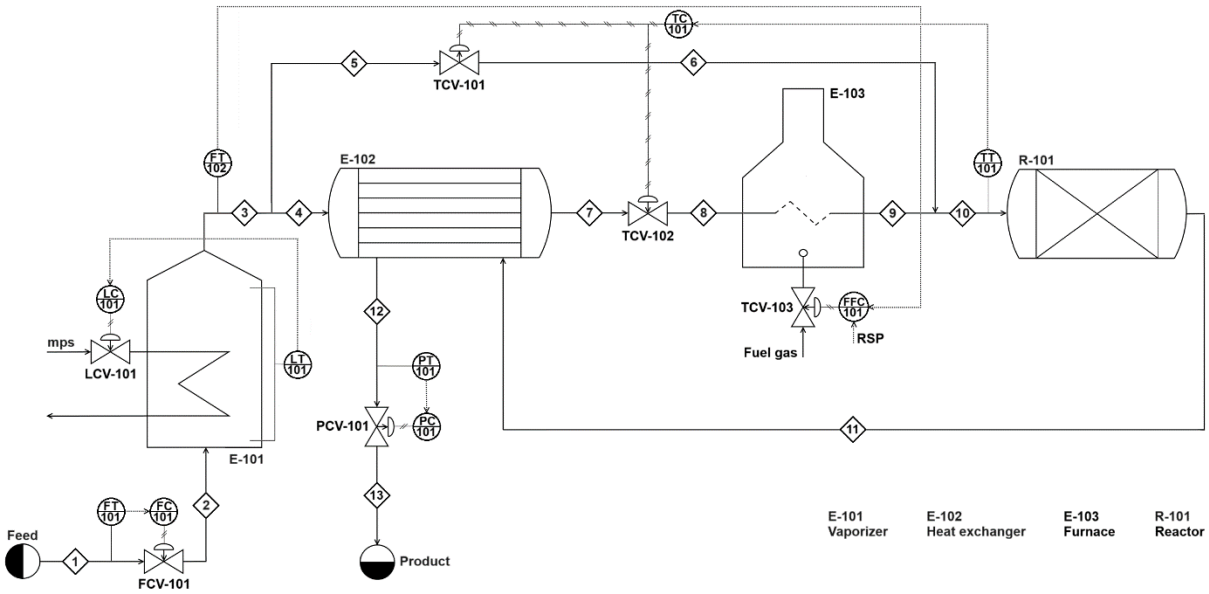

Figure 3.12. *Process flow diagram of the new alternative design and all the control loops, illustrating all equipment schematics.*

The control scheme includes the same flow controller FC - 101, level controller LC - 101, and pressure controller PC - 101 as in the previous designs. However, differently from the control strategy of the standard design detailed in §3.1.2, which employs *two* temperature controllers, this design uses *only one* reactor inlet temperature controller, TC - 101, and introduces a feedforward element, FFC - 101.

The feedforward controller is introduced to anticipate control actions during anomalous process

feed flow conditions by directly adjusting the furnace heat duty based on the measured vapor molar flow rate exiting the vaporizer E - 101. In Aspen Dynamics, this controller directly manipulates the furnace duty even if from a real industrial perspective, it would adjust the opening of the valve in the furnace fuel stream line.

Before implementing this feedforward element in Aspen Dynamics, a relationship between the vapor flow rate exiting the vaporizer and the furnace heat duty must be derived. This relationship is obtained following the approach outlined by Luyben (2012). Specifically, the process is simulated at steady-state in Aspen Plus at various throughputs to determine the furnace duty required to preheat the feed to the desired reactor inlet temperature of 541 K while keeping the bypass valve somewhat open. This ensures that the control action of TC - 101 can be maintained under these throughputs during the dynamic simulation.

Three scenarios are considered: - 40 %, + 40 %, and the design process feed flow rate. For the first two scenarios, the steady-state simulator is run at various bypass fractions to determine the corresponding furnace heat duties. The results of this analysis, summarized in Figure 3.13, are used to determine the optimal furnace duty based on the flow conditions. These findings are essential for fitting the parameters needed to define the relationship between these two variables.

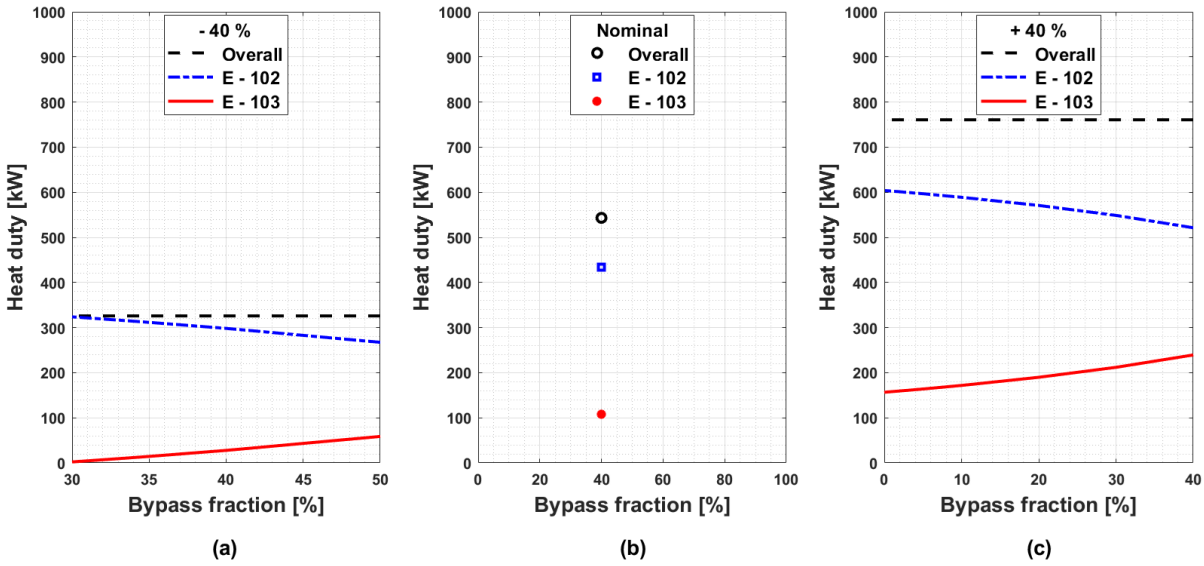

Figure 3.13. (a) *Overall heat duty required to preheat the reactor feed including the duties of heat exchanger E - 102 and furnace E - 103, calculated at various bypass fractions under steady-state conditions with a - 40 % increase in feed flow;* (b) *corresponding nominal conditions; and* (c) *at + 40 % feed flow.*

In Figure 3.13, it is evident that as the feed flow increases, the heat duty required to preheat the vapor flow exiting the vaporizer also increases, and consequently also the duties of the heat exchanger and the furnace. However, as depicted in Figure 3.13(a) and Figure 3.13(c), which correspond to the - 40 % and + 40 % feed flow scenarios, respectively, the distribution of the overall heat duty between the heat exchanger and the furnace is assigned by the selected bypass

fraction. Specifically, a lower bypass fraction results in a higher heat duty being supplied by the preheater, which recovers more heat from the hot reactor effluent, thereby reducing the furnace heat duty required.

For the - 40 % feed flow scenario, a furnace duty of approximately 2.2 kW is selected, corresponding to a 30 % bypass fraction. This value is chosen to avoid completely shutting down the furnace under these abnormal conditions, even though furnace heat supply is not necessary since the preheater can provide all the required heat to preheat the reactor feed.

In the + 40 % feed flow scenario, a furnace duty of 171.7 kW is selected, which is calculated with a 10 % bypass fraction. This choice ensures that the bypass valve is not fully closed, allowing for the maintenance of system controllability during dynamic simulation, specifically by enabling adjustment of the bypass fraction to control the reactor inlet temperature at + 40 % feed flow conditions.

The selected furnace heat duties (Q_F) corresponding to each of the considered vaporizer outlet molar flows (F) are shown in Table 3.5.

Table 3.5. *Vaporizer outlet molar flows and corresponding furnace duties selected from the steady-state analysis, used to define the relationship between these two variables, which will be implemented in the feedforward controller.*

F	**[kmol/h]**	177.1	295.2	413.3
$\boldsymbol{Q_F}$	**[kW]**	2.2	108.7	171.7

Given the non-linear relationship between these two variables, the initial approach was to apply the functional form proposed by Luyben (2012), defined as:

$$Q_F = 10^3 \cdot \exp\left(\alpha_L + \frac{\beta_L}{F}\right), \tag{3.1}$$

where the fitting parameters α_L and β_L are - 0.15 and - 653.5 kmol/h, respectively. Note that Q_F and F are expressed in units of [kW] and [kmol/h], respectively.

However, the resulting curve, labelled as ‘‘Luyben’’ in Figure 3.14, is not applicable. Specifically, under nominal feed flow conditions, the system operates with a furnace heat duty significantly lower than the design value, compromising process performance.

To address this issue, an alternative relationship is proposed to ensure proper system operation under nominal design conditions:

$$Q_F = \frac{\alpha_N}{1 + \exp[-\beta_N \cdot (F - \gamma_N)]}, \tag{3.2}$$

In this model, the parameters α_N, β_N, and γ_N are set to 172.5 kW, 0.04 h/kmol, and 282.4 kmol/h,

respectively. As before, Q_F and F must be expressed in [kW] and [kmol/h], respectively. The two fitting curves corresponding to these relationships are depicted in Figure 3.14.

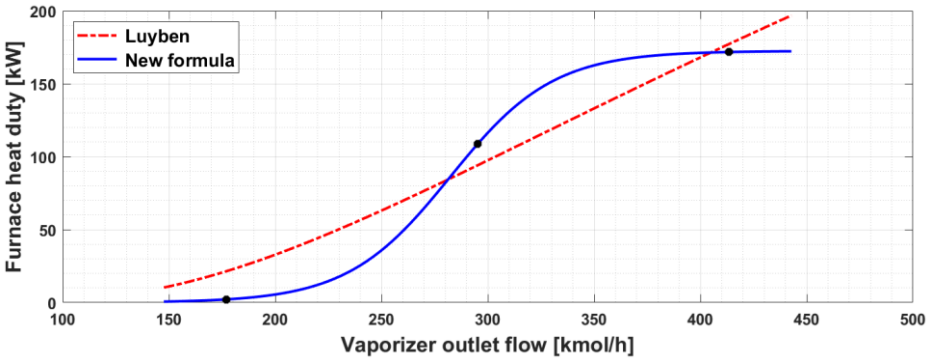

Figure 3.14. *Fitting curves obtained with the two relationships, one obtained with the function provided by Luyben (2012) and one retrieved in this Thesis, relating the furnace duty to the vaporizer outlet flow*

The new sigmoidal curve provides a consistently better fit to the data presented in Table 3.5. Additionally, this new formula resolves the discrepancy encountered with the previous formula, which calculated a furnace duty lower than the design value at the nominal flow conditions.
However, a limitation of this new model is that it fails to adequately increase the furnace duty at feed flow rates above 40 % of the nominal value. Consequently, the furnace duty remains insufficient for preheating at higher flow rates. Although these higher flow rates are of limited interest, it is decided to seek a new relationship that can calculate a sufficient furnace duty even at flow rates 50 % above the nominal value. This will also allow for a comparison with previous dynamic analyses of other designs when this design is studied under such flow conditions.
To derive this new relationship, the + 40 % feed flow scenario presented in Table 3.5 is replaced with a + 50 % scenario. The selected furnace heat duty of 199.5 kW corresponds to a bypass fraction of 0 %. However, during the dynamic simulation of the standard design, when a 50 % step increase in feed flow rate is implemented by the controller FC - 101, the valve FCV - 101 opening is increased from the nominal 50 %, leading to a reduction in the pressure drop across the valve. Consequently, the vaporizer pressure decreases, resulting in an increased saturation temperature of the liquid mixture. While this temperature rise has minimal impact at lower feed flow rate increases, at the + 50 % flow condition, the saturation temperature rises to approximately 435 K, compared to the previous 425 K, corresponding to the vaporizer pressure of about 18.2 atm instead of 14 atm. Additionally, the vessel pressure and the saturation temperature can vary depending on how the all the controllers interact during the transient period after the perturbation of the system.
Due to the higher temperature of the vaporizer outlet flow rate, the heat duty required to preheat this feed to the desired reactor inlet temperature is lower than expected from a steady-state perspective. This reduced furnace heat duty can be retrieved from the dynamic simulation of the standard design, as reported in Figure 3.5. Specifically, after the system stabilizes at the new

steady-state, the bypass fraction set to 0 % and the furnace duty adjusts to 193.9 kW, compared to the 199.5 kW predicted by the steady-state analysis.
In conclusion, it is decided to select this lower furnace duty corresponding to the + 50 % vaporizer outlet flow. The updated dataset used to derive the new relationship is provided in Table 3.6.

Table 3.6. *Vaporizer outlet molar flow and corresponding furnace duty, used to define the relationship between these two variables which will be implemented in the feedforward controller.*

F	**[kmol/h]**	177.1	295.2	442.8
Q_F	**[kW]**	2.2	108.7	193.9

The same relationship expressed in equation 3.2 is used, and the new fitting parameters are summarized in Table 3.7.

Table 3.7. *Fitting parameters utilized with the relationship in equation 3.2.*

α_N	**[kW]**	194.3
β_N	**[h/kmol]**	0.04
γ_N	**[kmol/h]**	289.2

With the relationship between furnace heat duty and vaporizer outlet flow derived, the resulting fitting curve is presented in Figure 3.15, labelled as ‘‘New design’’. In the same plot, another curve labelled ‘‘Standard design’’ is also illustrated, representing the final steady-state values obtained during the dynamic simulation of the standard design after introducing the various feed flow disturbances discussed in §3.1.2.

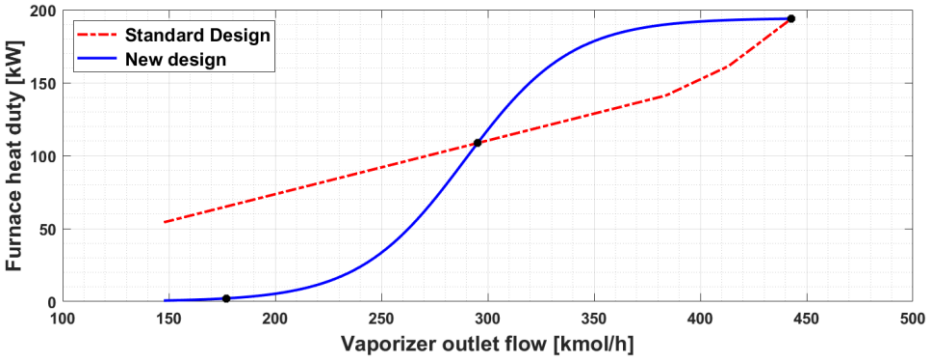

Figure 3.15. *Fitting curves relating the furnace duty to the vaporizer outlet flow utilized in the new design and final steady-state values obtained in the dynamic simulation of the standard design under the various feed flow disturbances considered in §3.1.2.*

As depicted in Figure 3.15, the new alternative design and control strategy is expected to reduce unnecessary furnace heat duty at feed flow rates lower than the design value. However, for flow

rates exceeding the nominal value, the furnace duty will be higher than that required at the new steady-state conditions achieved following the feed perturbations in the standard design. This can be considered a limitation of this new control strategy.

The feedforward control loop is now integrated. This loop utilizes the measures of the vapor flows exiting the vaporizer provided by the sensor-transmitter FT - 102, whose dynamics is neglected. The feedforward controller FFC - 101 then adjusts the furnace duty based on the relationship just derived, corresponding to the measured flow rate. Within the loop, a deadtime is introduced to approximate the furnace dynamics, similar to the approach used in the standard design. However, in this case, the deadtime is reduced to 1 min, compared to the 2 min used in the standard design, since the temperature controller employed in the previous design is not utilized in this new control loop.

With the feedforward control loop implemented, the reactor inlet temperature control loop is now studied. This loop operates similarly to the temperature control loop described in §3.1.2. A sensor-transmitter unit, TT - 102, with a range of 273 - 809 K, is employed, and its dynamics is approximated by introducing a 1 min deadtime in the control loop. The reactor inlet temperature measurement is used by the controller to adjusts the opening of valves TCV - 101 and TCV - 102, as detailed in Table 2.3.

The controller, TC - 101, is configured with a reverse action considering the action of the two valves. Additionally, it employs a PI control strategy, and its parameters are initially determined by performing an ATV test to find the ultimate period and controller gain, which are approximately 2.6 min and 8.8 %CO/%TO, respectively. By applying the Tyreus-Luyben tuning rules, an integral time constant of 5.8 min and a controller gain of 2.8 %CO/%TO are obtained. After further testing the controller performance, these parameters are fine-tuned to 1.2 min and 1.4 %CO/%TO, respectively.

All key features of controller TC - 101 are summarized in Table 3.8.

Table 3.8. *Tuning parameters of controller TC - 101.*

Controller	***Span***	$\mathbf{K_C}$ **[%CO/%TO]**	$\boldsymbol{\tau_I}$ **[min]**	***Action***
TC - 101	536 K	1.4	1.2	Reverse

With all control loops implemented into Aspen Plus Dynamics, the new alternative design and control strategy is dynamically studied. This analysis considers the same feed flow disturbances introduced as step changes in the set point of the flow controller FC - 101, as used in the previous studies and illustrated in Figure 2.14.

Firstly, the + 20 % disturbance is analyzed, and Figure 3.16 illustrates the results of the dynamic simulation. Specifically, in Figure 3.16(a), the reactor inlet temperature profile is depicted. As expected, due to the delayed responses of both the two controllers FFC - 101 and TC - 101, the

reactor feed initially is insufficiently preheated, and its temperature rapidly drops, showing a similar behaviour observed in the previous dynamic studies of the other designs analyzed. However, following the initial undershoot, the temperature rapidly grows due to the action of FFC - 101 which increases the furnace heat duty. Consequently, with the controller TC - 101 action, regulating the bypass fraction the temperature is efficiently restored to the set point.

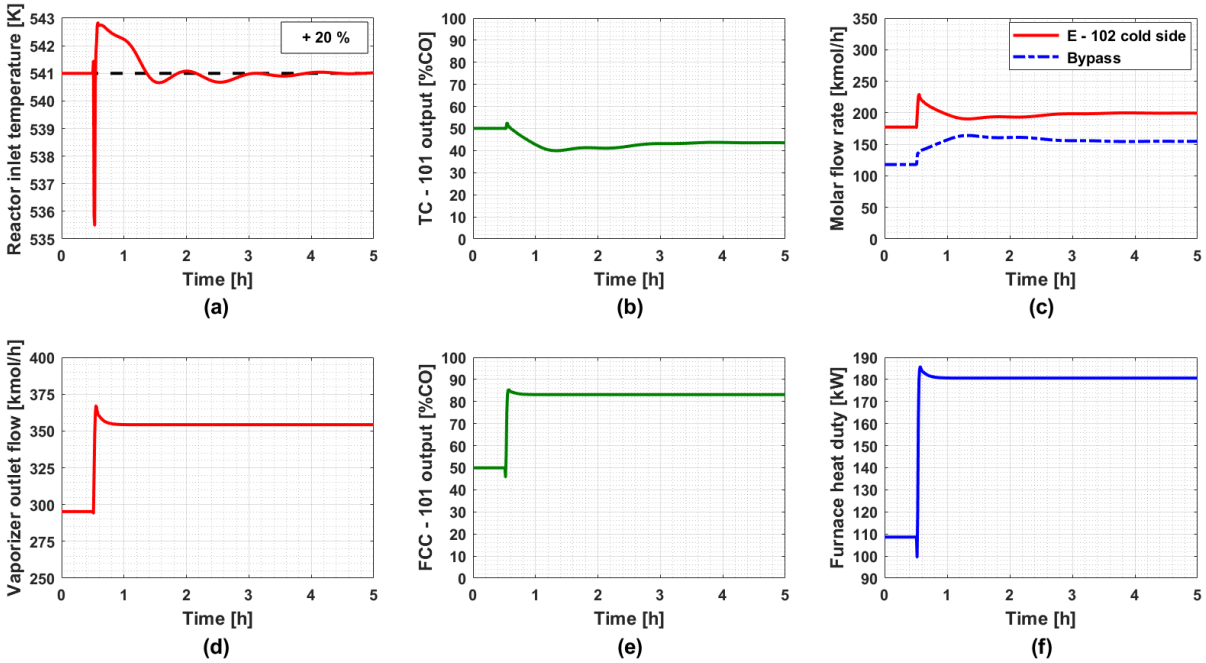

Figure 3.16. *Scenario with a + 20 % feed flow rate disturbance at 0.5 h:* (a) *reactor inlet temperature,* (b) *controller TC - 101 output,* (c) *molar flow rates for both the bypass stream and the cold side of E - 102,* (d) *vaporizer outlet flow,* (e) *controller FCC - 101 output, and* (f) *furnace heat duty.*

As shown in Figure 3.16(d), the vaporizer outlet flow profile closely resembles a step change that aligns with the behaviour of the feed flow controller FF - 101 set point. However, some deviations from an ideal step change are noticeable in the plot, including a slight initial decrease in flow rate and a rapid increase that briefly exceeds the expected + 20 % flow corresponding to the + 20 % feed flow. This higher flow is rapidly adjusted, and the expected + 20 % flow is reached at new steady-state condition. These deviations are attributable to the system dynamics, especially the vaporizer dynamics, and the control scheme response to restore proper process operation, even under this anomalous flow condition.

The outlet vapor flow is represented because the furnace duty is adjusted accordingly using the previously discussed relationship. Indeed, the furnace heat duty response, as illustrated in Figure 3.16(f), exhibits an even more pronounced initial decrease before following a similar dynamic pattern to the vaporizer outlet flow. This behaviour is attributed to the non-linear relationship used to adjust the furnace duty.

The performance of this new control strategy under the + 20 % feed flow disturbance is then compared to the results obtained with the standard design, as shown in Figure 3.17.

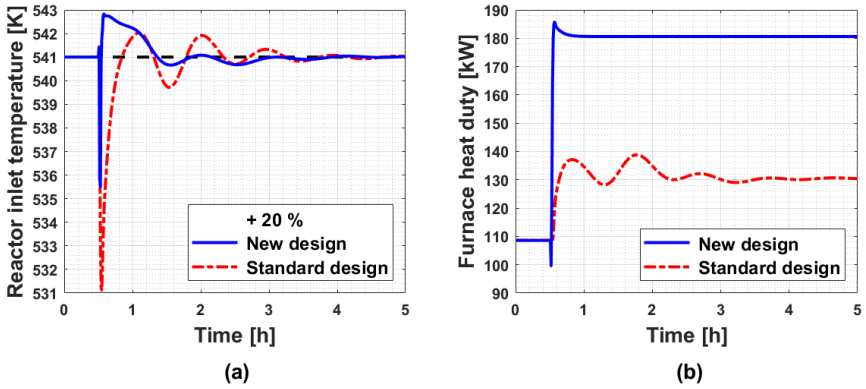

Figure 3.17. (a) *Reactor inlet temperature and* (b) *furnace duty following a + 20 % feed flow disturbance at 0.5 h in the standard design and in the new design.*

The reactor inlet temperature dynamics is improved in the new alternative design, as the initial undershoot is reduced by about 5 K compared to the standard design. Additionally, the subsequent oscillations are more effectively dampened, although the reactor inlet temperature increases slightly above the set point as the furnace heat duty is incremented, more so than in the standard design.

Regarding the furnace heat duty shown in Figure 3.17(b), the new design requires approximately 50 kW more at the final steady-state compared to the standard design, as also indicated in Figure 3.15. Therefore, while this new control strategy enhances temperature control, it does so at the cost of increased furnace heat duty compared to the standard design.

As with the standard design, the + 50 % step change scenario is directly presented. The intermediate scenarios are not detailed, as similar considerations apply, differing only in the magnitude of the effects of the various disturbances. The results obtained under the + 50 % disturbance condition are depicted in Figure 3.18.

As illustrated in Figure 3.18(a), the reactor inlet temperature is effectively controlled despite the significant perturbation to the system. The undershoot is limited to approximately 13 K, and the resulting oscillations are damped within roughly 3 h following the system disturbance.

Unexpectedly, the final steady-state value of the bypass fraction, shown in Figure 3.18(c), is approximately 6 %, rather than 0 % as observed in the standard design, even though the corresponding steady-state value of the furnace duty remains unchanged. This difference can be attributed to the system settling into a distinct steady-state condition due to slight variations in the interactions between the controllers and the system dynamics. Specifically, at this new steady-state, the temperature of the vaporizer outlet vapor flow is 1.5 K higher than in the standard design, which is a consequence of an increase in vaporizer pressure by about 0.5 atm. This higher pressure in the vaporizer is due to reduced pressure drop in valve FCV - 101, whose opening is regulated by the flow controller FC - 101 to introduce the 50 % increase in feed flow. Reaching the higher temperature in the vaporizer outlet vapor flow requires an increased heat duty in the vaporizer of about 10 kW, which is + 0.2 % of the vaporizer duty reached at the final

steady-state in the standard design, thus necessitating higher steam consumption. As a result, not all the heat provided by the furnace is required, and the bypass fraction stabilizes above zero to offset the additional vaporizer heat duty by reducing the preheater E - 102 heat duty.

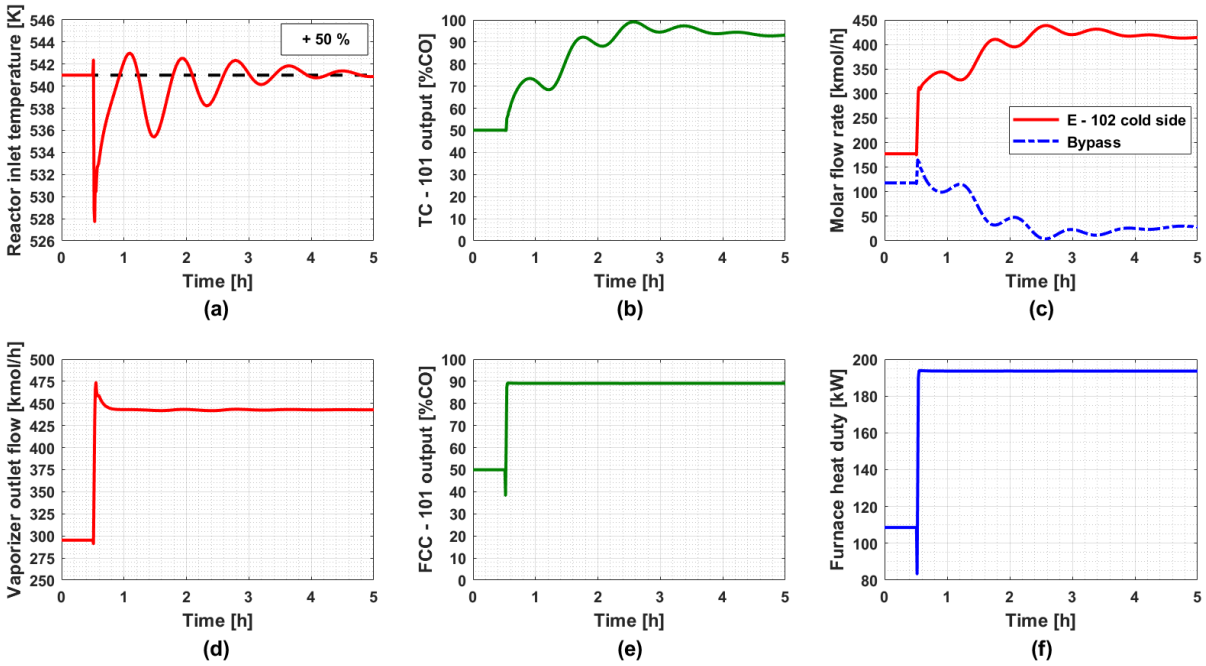

Figure 3.18. *Scenario with a + 50 % feed flow rate disturbance at 0.5 h:* (a) *reactor inlet temperature,* (b) *controller TC - 101 output,* (c) *molar flow rates for both the bypass stream and the cold side of E - 102,* (d) *vaporizer outlet flow,* (e) *controller FCC - 101 output, and* (f) *furnace heat duty.*

In Figure 3.19, the performance of the new alternative design in controlling the reactor inlet temperature is compared to that of the standard design.

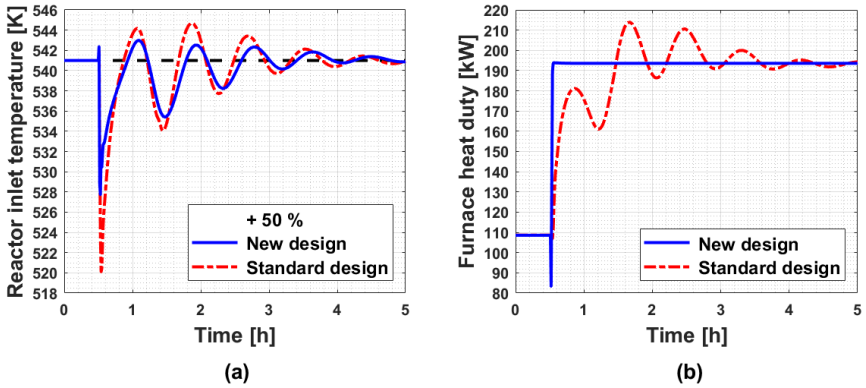

Figure 3.19. (a) *Reactor inlet temperature and* (b) *furnace duty following a + 50 % feed flow disturbance at 0.5 h in the standard design and in the new design.*

In this scenario, the reactor inlet temperature is controlled more efficiently in the new design, with the undershoot reduced by approximately 8 K and the subsequent oscillations damped slightly faster. The furnace duty is unchanged at the new steady-state. Notably, the transient oscillatory behaviour observed in the furnace for the standard design is absent in the new design.

Subsequently, the responses to negative step disturbances are analyzed. In this instance, only the 20 % and 50 % feed flow reductions are discussed, as the intermediate cases yield responses similar to these two scenarios. The - 20 % step disturbance is illustrated first in Figure 3.20.

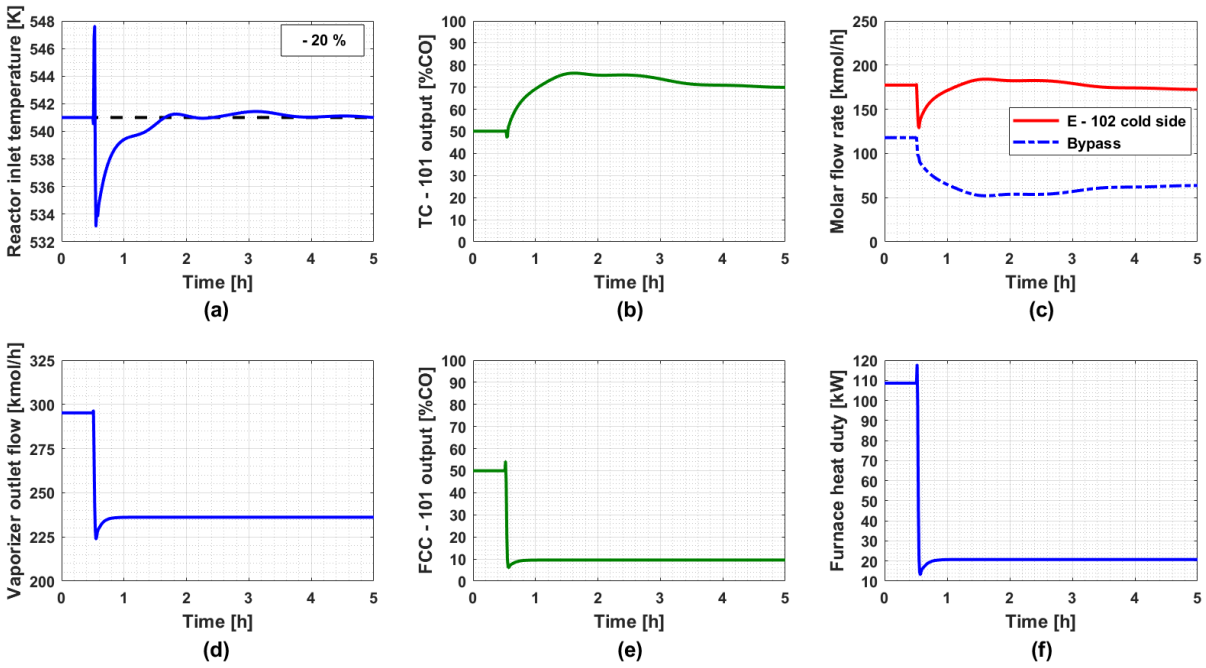

Figure 3.20. *Scenario with a - 20 % feed flow rate disturbance at 0.5 h:* (a) *reactor inlet temperature,* (b) *controller TC - 101 output,* (c) *molar flow rates for both the bypass stream and the cold side of E - 102,* (d) *vaporizer outlet flow,* (e) *controller FCC - 101 output, and* (f) *furnace heat duty.*

The reactor inlet temperature, shown in Figure 3.20(a), exhibits an initial overshoot of approximately 7 K, similar to the behaviour observed with previous designs, before quickly falling below the controller TC - 101 set point by about 8 K. This rapid decline is associated with a swift reduction in furnace heat duty, as illustrated in Figure 3.20(f). This reduction is enforced by controller FFC - 101 as soon as the vaporizer outlet flow experiences a nearly instantaneous 20 % decrease from its nominal value, as depicted in Figure 3.20(d).

The vaporizer outlet flow slightly increases before the sudden drop, reaching flow rates that are slightly lower than the final steady-state value. It then rapidly stabilizes at this final value, which corresponds to the decreased process feed flow. This behaviour, which differs slightly from a simple step decrease, results from the system dynamics, particularly the vaporizer dynamics, as well as the level controller action in conjunction with the operations of the other controllers. This pattern is similar to what was observed in the + 20 % disturbance scenario and is also evident in other scenarios, albeit with variations relative to the specific disturbance being examined.

The behaviour of the vaporizer outlet flow also leads to a corresponding change in the furnace heat duty due to the feedforward controller action and the previously discussed non-linear relationship. Consequently, the initial peak in furnace heat duty is more marked than the much

smaller peak observed in the vaporizer outlet flow. This discrepancy highlights the impact of the non-linear relationship between these two variables, which amplifies the magnitude of the peak in furnace heat duty relative to that of the vaporizer outlet flow.

As shown in Figure 3.20(c), the heat exchanger cold side flow is minimally impacted by the temperature controller TC - 101 action in response to the feed flow disturbance. Instead, the control action affects significantly only the bypass molar flow, exhibiting an opposite behaviour to that observed in the standard configuration. Specifically, the 20 % decrease in feed flow, corresponding to a reduction of 59 kmol/h, results in a comparable decrease of 54.2 kmol/h in the bypass flow, along with a slight decrease of 4.8 kmol/h in the heat exchanger cold side flow.

In Figure 3.21, the dynamic responses of the reactor inlet temperature and furnace duty in the new design under the - 20 % feed flow disturbance are compared to those of the standard design.

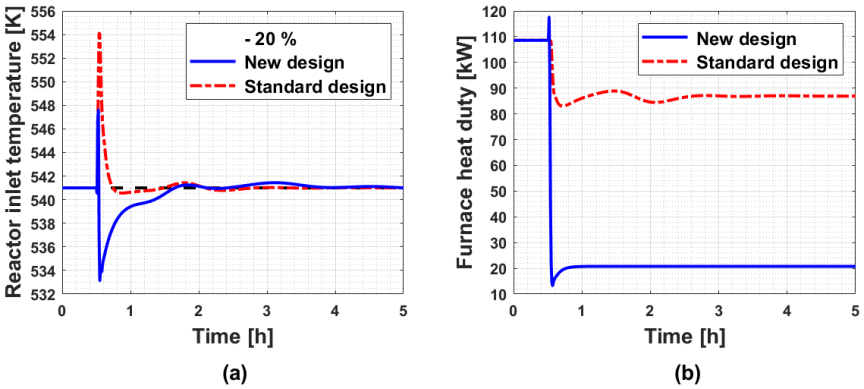

Figure 3.21. (a) *Reactor inlet temperature and* (b) *furnace duty following a - 20 % feed flow disturbance at 0.5 h in the standard design and in the new design.*

As shown in Figure 3.21(a), the reactor inlet temperature initial overshoot is reduced of 8 K in the new design, although the subsequent dynamics are somewhat deteriorated. In the new design, the reactor inlet temperature experiences an undershoot due to the sudden reduction in furnace duty imposed by controller FFC - 101. Additionally, unlike the standard design, the subsequent transient oscillations are slightly more pronounced, though still negligible.

Regarding furnace duty, the new design effectively reduces the furnace heat, avoiding the unnecessary preheating observed in the standard design. At the new steady-state, the overall furnace heat savings compared to the standard design are approximately 66 kW (- 76 %).

Finally, Figure 3.22 depicts the results of the dynamic simulation under the - 50 % feed flow disturbance. The reactor inlet temperature, shown in Figure 3.22(a), exhibits a response similar to that observed in the - 20 % scenario, although the magnitude of the initial overshoot is more pronounced, with an increase of approximately 22 K. Following this overshoot, a few high-frequency oscillations occur due to the sudden reduction in furnace duty by the feedforward controller FFC - 101 and the aggressive controller TC - 101 action. Afterward, a couple of low-frequency oscillations, attributed to the process dynamics, are observed before the reactor inlet

temperature is efficiently restored to the desired 541 K.

Regarding the vaporizer outlet flow and furnace duty, similar dynamics to those discussed for the - 20 % feed flow disturbance scenario are observed, though with more pronounced variations due to the more significant disturbance. The furnace heat duty is reduced to nearly zero, as the preheater E - 102 exchange area is sufficiently large to recover all the heat required to preheat the reactor feed from the hot reactor effluent, allowing the system to achieve the desired reactor inlet temperature.

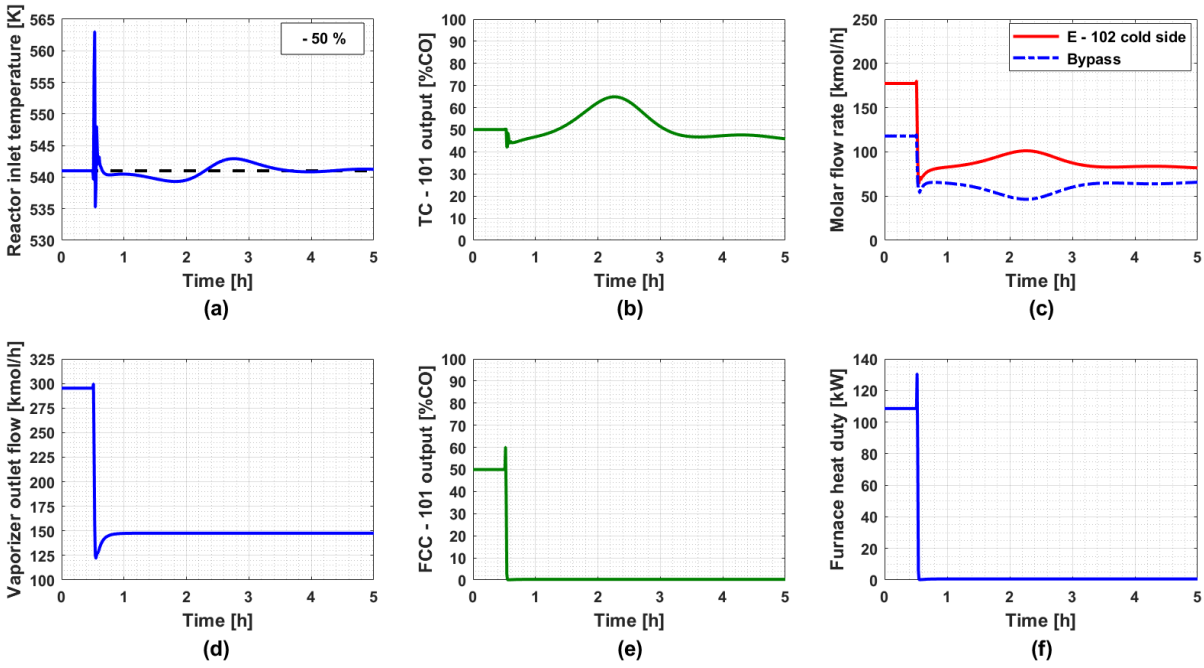

Figure 3.22. *Scenario with a - 50 % feed flow rate disturbance at 0.5 h:* (a) *reactor inlet temperature,* (b) *controller TC - 101 output,* (c) *molar flow rates for both the bypass stream and the cold side of E - 102,* (d) *vaporizer outlet flow,* (e) *controller FCC - 101 output, and* (f) *furnace heat duty.*

In Figure 3.23, the reactor inlet temperature and furnace heat duty of this new alternative design under the - 50 % feed flow disturbance are compared to the results obtained with the standard design configuration. As illustrated in Figure 3.23(a), the reactor inlet temperature is controlled much more efficiently in the new design, with the initial overshoot significantly reduced by approximately 25 K. This improvement is due to the faster reduction of unnecessary furnace heat achieved by the feedforward controller action, although in the standard design the temperature is restored to the set point more quickly after the overshoot, while the new alternative design exhibits few high-frequency oscillations due to the aggressive temperature controller TC - 101 action before stabilizing at the set point approximately 3 h after the disturbance is introduced.

Considering the furnace heat duty, as illustrated in Figure 3.23(b), the new design achieves a reduction of approximately 54 kW (- 99 %) at the new steady-state compared to the standard design.

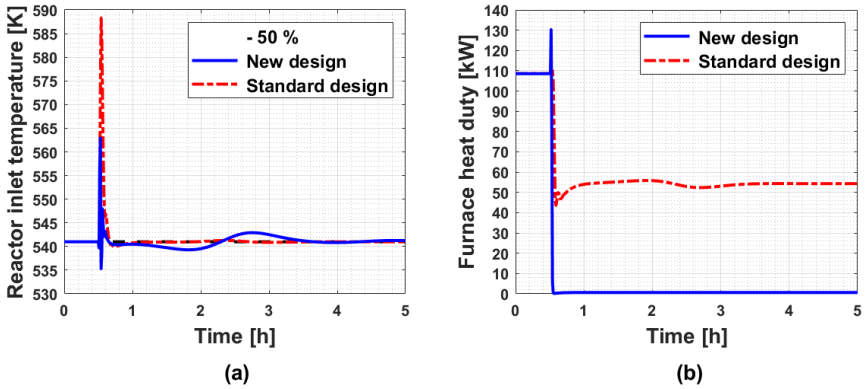

Figure 3.23. (a) *Reactor inlet temperature and* (b) *furnace duty following a - 50 % feed flow disturbance at 0.5 h in the standard design and in the new design.*

In conclusion, this Chapter has presented the new alternative design and compared its performance under various anomalous throughput conditions to that of the standard design. Overall, the new design has shown an improvement in controlling the reactor inlet temperature, particularly under severe step reductions in feed flow and for all step increases. This enhancement is notably reflected in the reduction of relative undershoots and overshoots, thanks to the anticipatory feedforward controller action that adjusts the furnace duty based on the measured vaporizer outlet vapor flow.

Regarding furnace heat duty, the new design significantly reduces it under negative step disturbances, although it increases during positive step disturbances.

Conclusions

The aim of this Thesis was to dynamically study various process designs with a FEHE/reactor system to evaluate the performance of the relative process control structures under throughput disturbances.

Chapter 1 has introduced a base process design, which included a vaporizer and an adiabatic packed tubular reactor with a FEHE, used in the production of dimethyl ether from methanol. The reactor was analyzed in isolation to highlight the importance of the inlet temperature for the steady-state and dynamic reactor performance. The dynamic analysis revealed the typical inverse response in the outlet temperature following a step disturbance in the inlet temperature, which is a characteristic behaviour of this type of reactor. The base process design was then dynamically simulated with disturbances in the feed flow, demonstrating the non-linearity and the critical dynamics of this FEHE/reactor system.

Based on the base design analysis, Chapter 2 presented a modified design incorporating a bypass around the preheater to control the reactor inlet temperature. Two designs, with 20 % and 40 % nominal bypass, were evaluated both from a steady-state and a dynamic perspectives. In the 20 % bypass design, the temperature control loop managed to restore the reactor inlet temperature to the set point following all the negative step decreases in the feed flow analyzed, including reductions of up to 50 %. However, when step increases were considered, the controller struggled to restore the set point with even a 20 % increase in feed flow. This issue was not related to controller tuning, but rather to the process design. As demonstrated in the steady-state analysis, the heat exchanger area was not sufficiently large to ensure the required heat transfer rate to recover the heat from the reactor effluent and preheat the reactor feed.

In the 40 % bypass design, due to greater bypass fraction selected, the larger exchange area of the heat exchanger enabled better temperature control, allowing the system to handle disturbances in the feed flow of up to both + 50 % and - 50 % of the nominal value, improving upon the limitation of the previous design. Thus, this has demonstrated that increasing the design bypass fraction significantly enhances process controllability, though it comes with a slight increase in plant capital investment due to the larger heat exchanger.

However, in real industrial applications, the start-up of these designs is not feasible without a furnace to provide an external heat source for preheating the reactor feed. Chapter 3 addressed this limitation by introducing a new design incorporating a furnace, developed from the 40 % bypass configuration. In this design, the furnace was positioned before the reactor, after the mixing point between the cold bypass stream and the preheated stream exiting the heat exchanger. The furnace fuel flow has been introduced as a new manipulated variable. Due to limitations in Aspen Plus Dynamics, the furnace dynamics was approximated, and the fuel flow

was not explicitly modelled. Instead, the furnace heat duty has been used as the manipulated variable to control the reactor inlet temperature, while the bypass was adjusted to control the furnace inlet temperature.

This new control strategy resulted in degraded performance compared to the 40 % bypass design without furnace, mainly due to the interaction between the two temperature controllers and the slower dynamics of the furnace heat duty regulation in controlling the reactor inlet temperature relative to the faster mixing dynamics of the hot and cold streams in the design without furnace. Specifically, when the same disturbances in the feed flow were introduced, as studied in the 40 % bypass design without furnace, the magnitudes of the initial reactor inlet temperature overshoots and undershoots in this design with furnace were much more pronounced, as well as the subsequent oscillations. Ultimately, the temperature was restored to the set point in all cases, but more slowly. Additionally, at low throughputs, the heat exchanger was not efficiently utilized, and unnecessary furnace heat was consumed despite sufficient heat exchange area to preheat lower feed flows.

To address these inefficiencies, a new alternative design and control structure from Luyben (2012) has been examined. In this design, the furnace was moved before the mixing point, allowing the reactor inlet temperature controller to manipulate the bypass fraction, benefiting from the faster mixing dynamics between the hot and cold streams. Additionally, a non-linear feedforward control element was introduced to regulate the furnace duty based on the measured reactor feed flow, using a relationship between these two variables derived from both steady-state and dynamic considerations on the system. This element was designed to anticipate control actions in response to feed flow disturbances, improving overall control performance.

This new strategy improved control performance, particularly at low feed flows, where the furnace duty was significantly reduced, addressing the inefficiency of the previous design. Specifically, considering - 20 % and - 50 % feed flow disturbances, once the control scheme restored the new steady-state, the furnace duty was significantly reduced by 76 % and 99 %, respectively, compared to the furnace duty consumed in the standard design under these throughputs. However, following feed flow step increases, although the temperature control performance also improved, furnace heat duty rose significantly. This occurred because the feedforward controller adjusted the furnace duty according to the vaporizer outlet flow, based on the proposed relationship between these two variables. At throughputs up to 50 % higher than nominal conditions, this relationship calculated a higher furnace heat duty than the one consumed in the standard configuration at the new steady-state following similar disturbances. As a result, for + 20 % and + 50 % feed flow disturbances, the furnace duty increased by 38 % and remained unchanged, respectively, compared to the furnace duty in the standard design reached at the new steady-state under these flow conditions. Therefore, at high throughputs, the furnace duty is not efficiently adjusted, and this remains a limitation of this alternative design and control strategy.

In conclusion, this Thesis demonstrated that the design bypass fraction in an FEHE/reactor system plays a crucial role in process controllability. Specifically, selecting a greater bypass fraction leads to a heat exchanger design with a larger exchange area, which can efficiently preheat a broader range of reactor feeds using the reactor effluent. This, in turn, improves temperature control performance.

Furthermore, the Thesis explored an alternative design developed by integrating considerations of both steady-state efficiency and dynamic controllability. By relocating the furnace before the mixing point, this new design allows for more direct manipulation of both the cold bypass stream and the hot stream exiting the furnace. This relocation leverages the fast mixing dynamics between these streams, resulting in more effective reactor inlet temperature control compared to the standard design that relied on furnace duty regulation.

The introduction of a feedforward controller, informed by a comprehensive analysis of both steady-state efficiency and system dynamics, further refined this approach. This controller replaces the need for two separate temperature controllers, whose interactions had proven detrimental in maintaining reactor inlet temperature control. The new control strategy anticipates control actions more effectively and improves overall thermal efficiency, by significantly reducing furnace heat consumption, especially at low throughputs.

Finally, as argued by Luyben (2012), further improvements to this alternative design could be achieved by reducing the nominal furnace duty through resizing the preheater with a larger heat exchange area. This adjustment would result in lower fuel consumption, under nominal operating conditions, enhancing the overall efficiency of the system and reducing the plant operative costs.

Appendices

Appendix A - Base design configuration

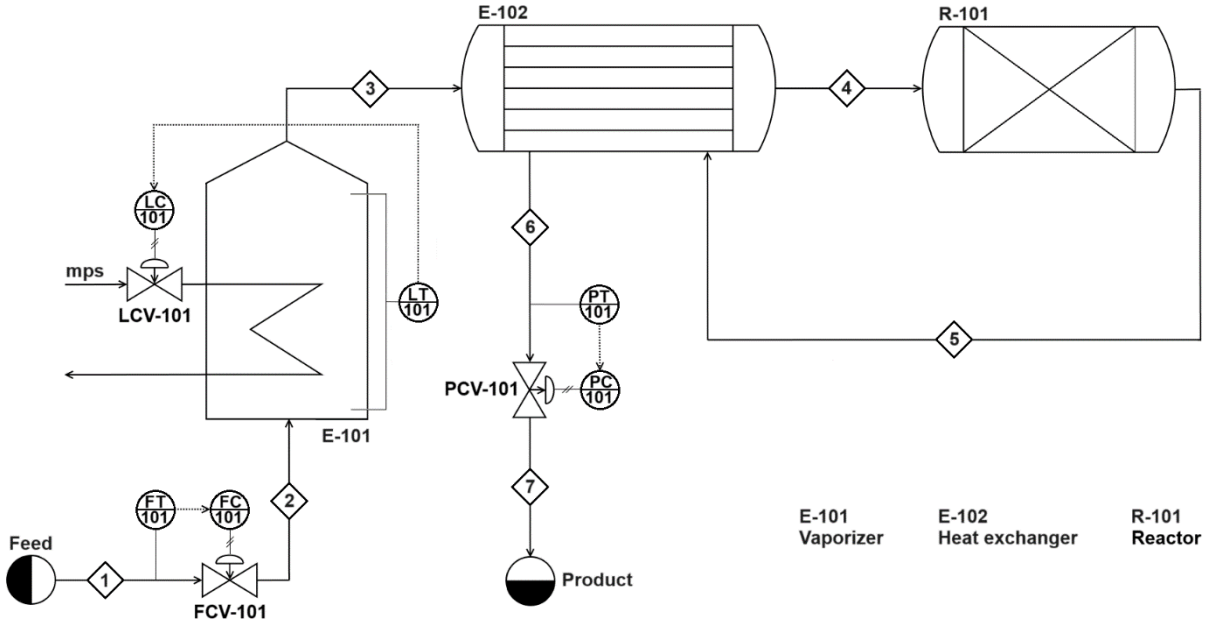

Figure A.1. *Process flow diagram of the base design configuration.*

Table A.1. *Stream table of the base design configuration*.

Stream number	*T* [K]	*P* [atm]	*Vapor fraction* [%]	*Mass density* [kg/m^3]	*Molar flow* [kmol/h]	x_{CH_3OH} [%]	x_{H_2O} [%]	$x_{CH_3OCH_3}$ [%]
1	298	20.0	0	796.60	295.2	95.0	5.0	0.0
2	298	14.0	0	796.60	295.2	95.0	5.0	0.0
3	425	14.0	100	12.57	295.2	95.0	5.0	0.0
4	541	12.5	100	8.82	295.2	95.0	5.0	0.0
5	663	12.0	100	6.92	295.2	17.6	43.7	38.7
6	568	11.5	100	7.74	295.2	17.6	43.7	38.7
7	568	10.5	100	7.07	295.2	17.6	43.7	38.7

Table A.2. *Equipment table of the base design configuration*.

Vaporizer E - 101	***Heat exchanger E - 102***	***Reactor R - 101***
Horizontal cylindrical vessel, flat head type d_v = 1.02 m h_v = 3.05 m Medium pressure steam (mps) Vaporizer heat duty = 3.6091 MW Steam mass flow = 6398.7 kg/h	Shell-and-tube design, 1-2 configuration $\dot{Q}$ = 0.5433 MW U = 170 W·m^{-2}·K^{-1} $F_{T1\text{-}2}$ = 0.88 A = 27.5 m^2 V_{sec} = 0.06 m^3 m_{sec} = 97 kg	Adiabatic packed tubular reactor L = 12 m d = 1.2 m ε = 0.28 Acid zeolite catalyst, spherical particles, uniform particle size distribution ρ_{cat} = 1700 kg/m^3 d_p = 0.01 m $c_{P,cat}$ = 1280 J·kg^{-1}·K^{-1}
Valve FCV - 101	***Valve LCV - 101***	***Valve PCV - 101***
Flow control valve Equal-percentage characteristic Air-to-open K_v = 23.5 m^3·h^{-1}·bar$^{-0.5}$ q = 11.6 m^3/h $\triangle P_v$ = 6 atm	Level control valve Air-to-open	Pressure control valve Linear characteristic Air-to-close K_v = 225.3 m^3·h^{-1}·bar$^{-0.5}$ q = 1195.0 m^3/h $\triangle P_v$ = 1 atm

Appendix B - Design case with 20 % bypass

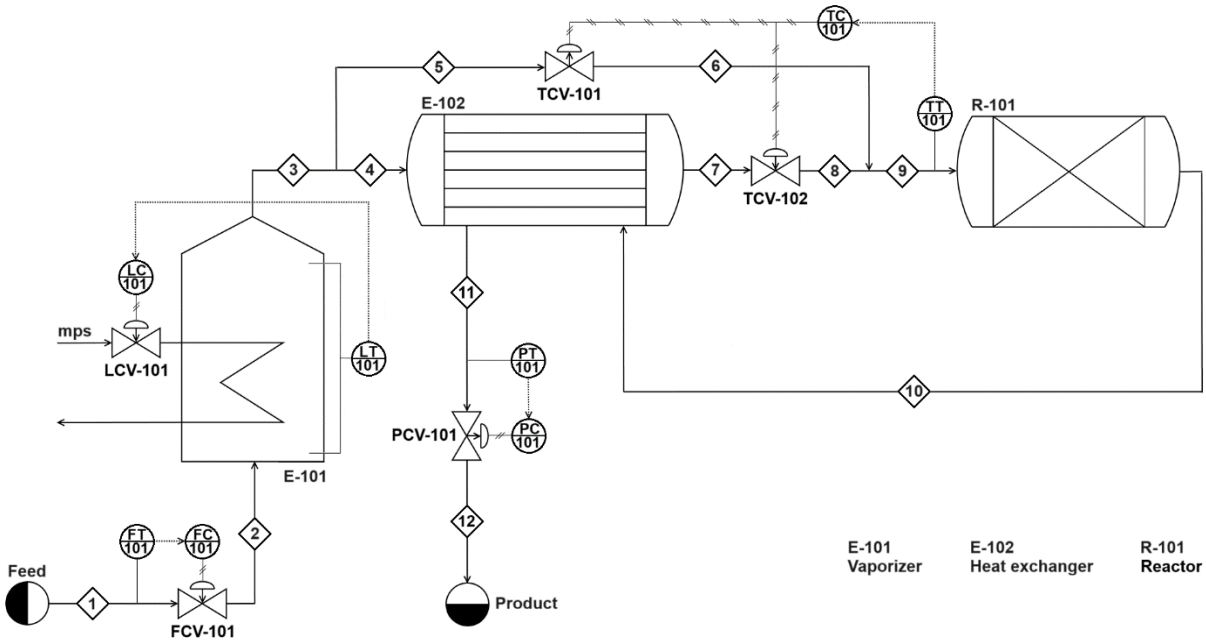

Figure B.1. *Process flow diagram of the 20 % bypass design configuration.*

Table B.1. *Stream table of the 20 % bypass design configuration*.

Stream number	*T* [K]	*P* [atm]	*Vapor fraction* [%]	*Mass density* [kg/m^3]	*Molar flow* [kmol/h]	x_{CH_3OH} [%]	x_{H_2O} [%]	$x_{CH_3OCH_3}$ [%]
1	298	20.0	0	796.60	295.2	95.0	5.0	0.0
2	298	14.0	0	796.60	295.2	95.0	5.0	0.0
3	425	14.0	100	12.57	295.2	95.0	5.0	0.0
4	425	14.0	100	12.57	236.2	95.0	5.0	0.0
5	425	14.0	100	12.57	59.0	95.0	5.0	0.0
6	425	12.5	100	11.23	59.0	95.0	5.0	0.0
7	568	13.0	100	9.09	236.2	95.0	5.0	0.0
8	568	12.5	100	8.41	236.2	95.0	5.0	0.0
9	541	12.5	100	8.82	295.2	95.0	5.0	0.0
10	663	12.0	100	6.92	295.2	17.6	43.7	38.7
11	568	11.5	100	7.74	295.2	17.6	43.7	38.7
12	568	10.5	100	7.07	295.2	17.6	43.7	38.7

Table B.2. *Equipment table of the 20 % bypass design configuration*.

Vaporizer E - 101	***Heat exchanger E - 102***	***Reactor R - 101***
Horizontal cylindrical vessel,	Shell-and-tube design,	Adiabatic packed tubular reactor
flat head type	1-2 configuration	L = 12 m
d_v = 1.02 m	$\dot{Q}$ = 0.5433 MW	d = 1.2 m
h_v = 3.05 m	U = 170 W·m^{-2}·K^{-1}	ε = 0.28
Medium pressure steam (mps)	$F_{T1\text{-}2}$ = 0.80	Acid zeolite catalyst, spherical
Vaporizer heat duty = 3.6091 MW	A = 34.0 m^2	particles, uniform size distribution
Steam mass flow = 6398.7 kg/h	V_{sec} = 0.08 m^3	ρ_{cat} = 1700 kg/m^3
	m_{sec} = 122 kg	d_p = 0.01 m
		$c_{P,cat}$ = 1280 J·kg^{-1}·K^{-1}
Valve FCV - 101	***Valve LCV - 101***	***Valve PCV - 101***
Flow control valve	Level control valve	Pressure control valve
Equal-percentage characteristic	Air-to-open	Linear characteristic
Air-to-open		Air-to-close
K_v = 23.5 m^3·h^{-1}·bar$^{-0.5}$		K_v = 225.3 m^3·h^{-1}·bar$^{-0.5}$
q = 11.6 m^3/h		q = 1195.0 m^3/h
$\triangle P_v$ = 6 atm		$\triangle P_v$ = 1 atm
Valve TCV - 101	***Valve TCV - 102***	
Temperature control valve	Temperature control valve	
Linear characteristic	Linear characteristic	
Air-to-close	Air-to-open	
K_v = 29.3 m^3·h^{-1}·bar$^{-0.5}$	K_v = 164.5 m^3·h^{-1}·bar$^{-0.5}$	
q = 146.5 m^3/h	q = 815.5 m^3/h	
$\triangle P_v$ = 1.5 atm	$\triangle P_v$ = 0.5 atm	

Appendix C - Design case with 40 % bypass

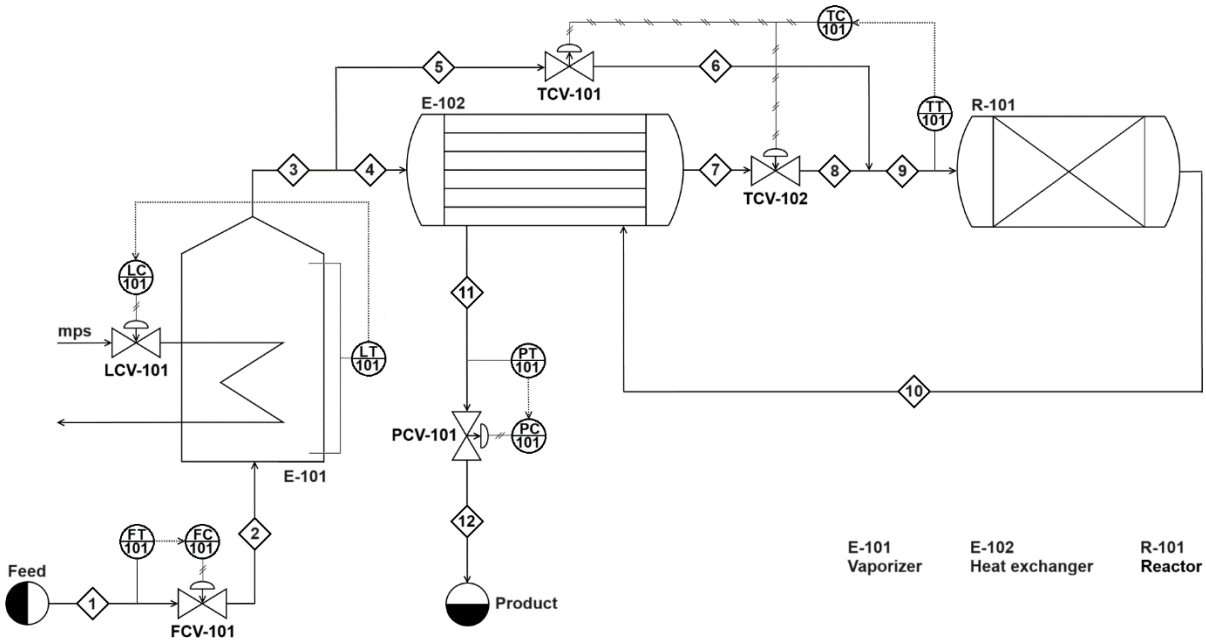

Figure C.1. *Process flow diagram of the 40 % bypass design configuration.*

Table C.1. *Stream table of the 40 % bypass design configuration.*

Stream number	*T* [K]	*P* [atm]	*Vapor fraction* [%]	*Mass density* [kg/m^3]	*Molar flow* [kmol/h]	x_{CH_3OH} [%]	x_{H_2O} [%]	$x_{CH_3OCH_3}$ [%]
1	298	20.0	0	796.60	295.2	95.0	5.0	0.0
2	298	14.0	0	796.60	295.2	95.0	5.0	0.0
3	425	14.0	100	12.57	295.2	95.0	5.0	0.0
4	425	14.0	100	12.57	236.2	95.0	5.0	0.0
5	425	14.0	100	12.57	118.1	95.0	5.0	0.0
6	425	12.5	100	11.23	118.1	95.0	5.0	0.0
7	610	13.0	100	8.14	177.1	95.0	5.0	0.0
8	610	12.5	100	7.83	177.1	95.0	5.0	0.0
9	541	12.5	100	8.82	295.2	95.0	5.0	0.0
10	663	12.0	100	6.92	295.2	17.6	43.7	38.7
11	568	11.5	100	7.74	295.2	17.6	43.7	38.7
12	568	10.5	100	7.07	295.2	17.6	43.7	38.7

Table C.2. *Equipment table of the 40 % bypass design configuration*.

Vaporizer E - 101	***Heat exchanger E - 102***	***Reactor R - 101***
Horizontal cylindrical vessel,	Shell-and-tube design,	Adiabatic packed tubular reactor
flat head type	2-4 configuration	L = 12 m
d_v = 1.02 m	$\dot{Q}$ = 0.5433 MW	d = 1.2 m
h_v = 3.05 m	U = 170 W·m^{-2}·K^{-1}	ε = 0.28
Medium pressure steam (mps)	$F_{T2\text{-}4}$ = 0.90	Acid zeolite catalyst, spherical
Vaporizer heat duty = 3.6091 MW	A = 39.4 m^2	particles, uniform size distribution
Steam mass flow = 6398.7 kg/h	V_{sec} = 0.09 m^3	ρ_{cat} = 1700 kg/m^3
	m_{sec} = 139 kg	d_p = 0.01 m
		$c_{P,cat}$ = 1280 J·kg^{-1}·K^{-1}
Valve FCV - 101	***Valve LCV - 101***	***Valve PCV - 101***
Flow control valve	Level control valve	Pressure control valve
Equal-percentage characteristic	Air-to-open	Linear characteristic
Air-to-open		Air-to-close
K_v = 23.5 m^3·h^{-1}·bar$^{-0.5}$		K_v = 225.3 m^3·h^{-1}·bar$^{-0.5}$
q = 11.6 m^3/h		q = 1195.0 m^3/h
$\triangle P_v$ = 6 atm		$\triangle P_v$ = 1 atm
Valve TCV - 101	***Valve TCV - 102***	
Temperature control valve	Temperature control valve	
Linear characteristic	Linear characteristic	
Air-to-close	Air-to-open	
K_v = 58.5 m^3·h^{-1}·bar$^{-0.5}$	K_v = 179.0 m^3·h^{-1}·bar$^{-0.5}$	
q = 294.0 m^3/h	q = 610.0 m^3/h	
$\triangle P_v$ = 1.5 atm	$\triangle P_v$ = 0.5 atm	

Appendix D - Standard design configuration

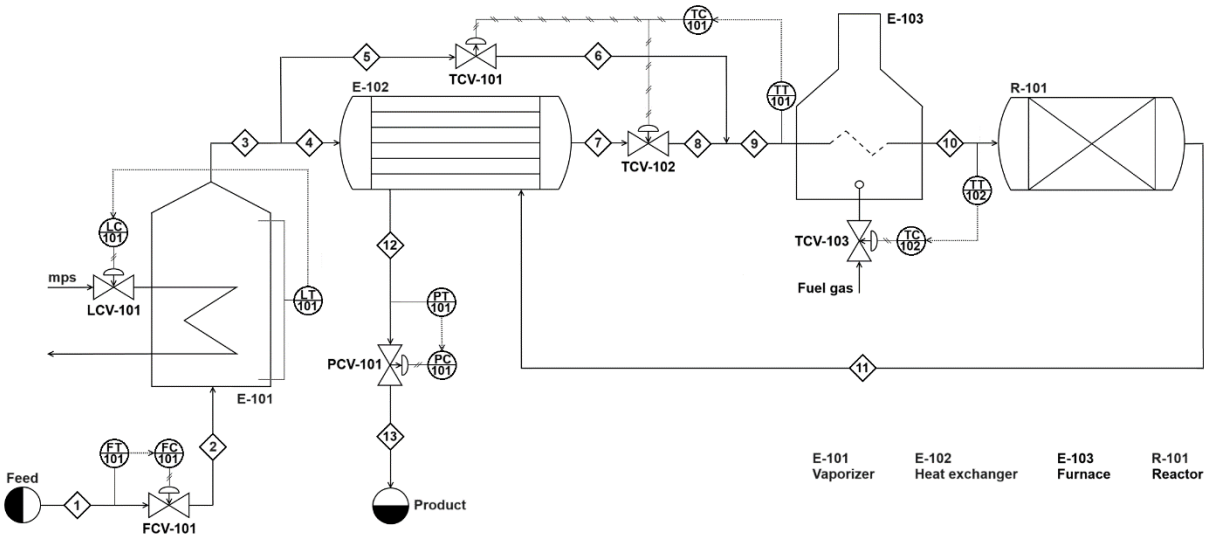

Figure D.1. *Process flow diagram of the standard design configuration.*

Table D.1. *Stream table of the standard design configuration*.

Stream number	*T* [K]	*P* [atm]	*Vapor fraction* [%]	*Mass density* [kg/m^3]	*Molar flow* [kmol/h]	x_{CH_3OH} [%]	x_{H_2O} [%]	$x_{CH_3OCH_3}$ [%]
1	298	20.0	0	796.60	295.2	95.0	5.0	0.0
2	298	14.0	0	796.60	295.2	95.0	5.0	0.0
3	425	14.0	100	12.57	295.2	95.0	5.0	0.0
4	425	14.0	100	12.57	236.2	95.0	5.0	0.0
5	425	14.0	100	12.57	118.1	95.0	5.0	0.0
6	425	13.0	100	11.68	118.1	95.0	5.0	0.0
7	576	13.5	100	8.95	177.1	95.0	5.0	0.0
8	576	13.0	100	8.62	177.1	95.0	5.0	0.0
9	519	13.0	100	9.56	295.2	95.0	5.0	0.0
10	541	12.5	100	8.82	295.2	95.0	5.0	0.0
11	663	12.0	100	6.92	295.2	17.6	43.7	38.7
12	587	11.5	100	7.48	295.2	17.6	43.7	38.7
13	587	10.5	100	6.83	295.2	17.6	43.7	38.7

Table D.2. *Equipment table of the standard design configuration.*

Vaporizer E - 101	***Heat exchanger E - 102***	***Furnace E - 103***
Horizontal cylindrical vessel, flat head type d_v = 1.02 m h_v = 3.05 m Medium pressure steam (mps) Vaporizer heat duty = 3.6091 MW Steam mass flow = 6398.7 kg/h	Shell-and-tube design, 1-2 configuration $\dot{Q}$ = 0.4346 MW U = 170 W·m^{-2}·K^{-1} $F_{T1\text{-}2}$ = 0.85 A = 25.1 m^2 V_{sec} = 0.06 m^3 m_{sec} = 89 kg	Fuel gas Furnace heat duty = 0.1087 MW Fuel mass flow = 651.9 kg/h
Reactor R - 101		
Adiabatic packed tubular reactor L = 12 m d = 1.2 m ε = 0.28 Acid zeolite catalyst, spherical particles, uniform size distribution ρ_{cat} = 1700 kg/m^3 d_p = 0.01 m $c_{P,cat}$ = 1280 J·kg^{-1}·K^{-1}		
Valve FCV - 101	***Valve LCV - 101***	***Valve PCV - 101***
Flow control valve Equal-percentage characteristic Air-to-open K_v = 23.5 m^3·h^{-1}·bar$^{-0.5}$ q = 11.6 m^3/h $\triangle P_v$ = 6 atm	Level control valve Air-to-open	Pressure control valve Linear characteristic Air-to-close K_v = 229.3 m^3·h^{-1}·bar$^{-0.5}$ q = 1236.6 m^3/h $\triangle P_v$ = 1 atm
Valve TCV - 101	***Valve TCV - 102***	***Valve TCV - 103***
Temperature control valve Linear characteristic Air-to-close K_v = 69.6 m^3·h^{-1}·bar$^{-0.5}$ q = 293.9 m^3/h $\triangle P_v$ = 1.0 atm	Temperature control valve Linear characteristic Air-to-open K_v = 170.3 m^3·h^{-1}·bar$^{-0.5}$ q = 620.6 m^3/h $\triangle P_v$ = 0.5 atm	Temperature control valve Air-to-open

Appendix E - Alternative configuration

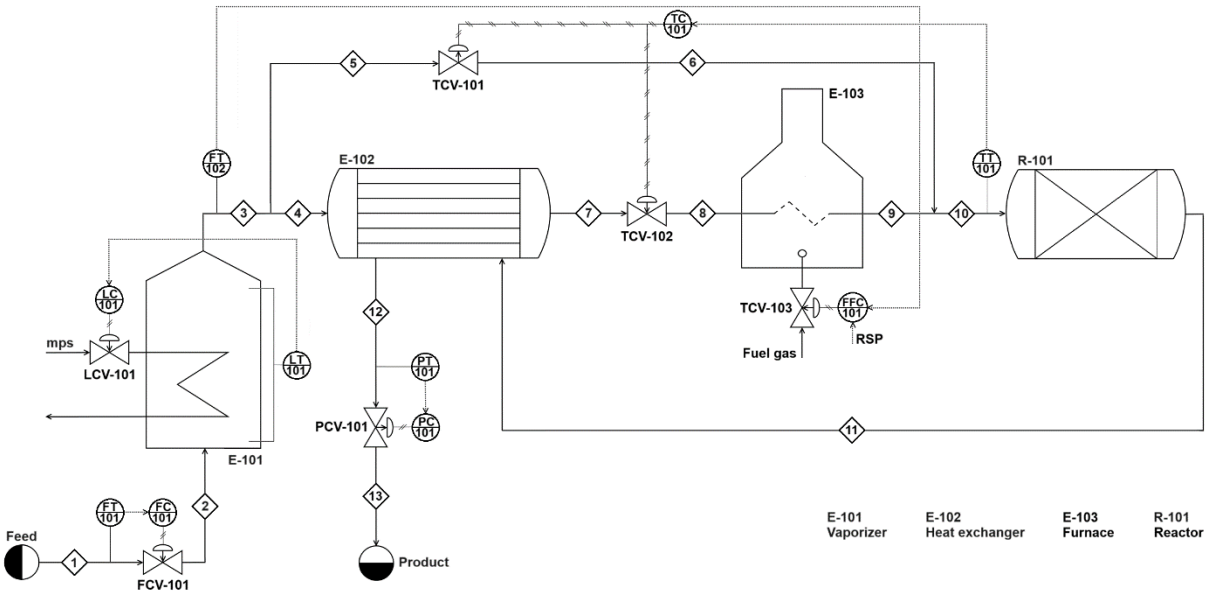

Figure E.1. *Process flow diagram of the alternative configuration.*

Table E.1. *Stream table of the alternative configuration*.

Stream number	*T* [K]	*P* [atm]	*Vapor fraction* [%]	*Mass density* [kg/m^3]	*Molar flow* [kmol/h]	x_{CH_3OH} [%]	x_{H_2O} [%]	$x_{CH_3OCH_3}$ [%]
1	298	20.0	0	796.60	295.2	95.0	5.0	0.0
2	298	14.0	0	796.60	295.2	95.0	5.0	0.0
3	425	14.0	100	12.57	295.2	95.0	5.0	0.0
4	425	14.0	100	12.57	236.2	95.0	5.0	0.0
5	425	14.0	100	12.57	118.1	95.0	5.0	0.0
6	425	12.5	100	11.23	118.1	95.0	5.0	0.0
7	576	13.5	100	8.95	177.1	95.0	5.0	0.0
8	576	13.0	100	8.62	177.1	95.0	5.0	0.0
9	610	12.5	100	7.83	177.1	95.0	5.0	0.0
10	541	12.5	100	8.82	295.2	95.0	5.0	0.0
11	663	12.0	100	6.92	295.2	17.6	43.7	38.7
12	587	11.5	100	7.48	295.2	17.6	43.7	38.7
13	587	10.5	100	6.83	295.2	17.6	43.7	38.7

Table E.2. *Equipment table of the alternative configuration*.

Vaporizer E - 101	***Heat exchanger E - 102***	***Furnace E - 103***
Horizontal cylindrical vessel, flat head type d_v = 1.02 m h_v = 3.05 m Medium pressure steam (mps) Vaporizer heat duty = 3.6091 MW Steam mass flow = 6398.7 kg/h	Shell-and-tube design, 1-2 configuration $\dot{Q}$ = 0.4346 MW U = 170 W·m^{-2}·K^{-1} $F_{T1\text{-}2}$ = 0.85 A = 25.1 m^2 V_{sec} = 0.06 m^3 m_{sec} = 89 kg	Fuel gas Furnace heat duty = 0.1087 MW Fuel mass flow = 651.9 kg/h
Reactor R - 101		
Adiabatic packed tubular reactor L = 12 m d = 1.2 m ε = 0.28 Acid zeolite catalyst, spherical particles, uniform size distribution ρ_{cat} = 1700 kg/m^3 d_p = 0.01 m $c_{P,cat}$ = 1280 J·kg^{-1}·K^{-1}		
Valve FCV - 101	***Valve LCV - 101***	***Valve PCV - 101***
Flow control valve Equal-percentage characteristic Air-to-open K_v = 23.5 m^3·h^{-1}·bar$^{-0.5}$ q = 11.6 m^3/h $\triangle P_v$ = 6 atm	Level control valve Air-to-open	Pressure control valve Linear characteristic Air-to-close K_v = 229.3 m^3·h^{-1}·bar$^{-0.5}$ q = 1236.6 m^3/h $\triangle P_v$ = 1 atm
Valve TCV - 101	***Valve TCV - 102***	***Valve TCV - 103***
Temperature control valve Linear characteristic Air-to-close K_v = 58.6 m^3·h^{-1}·bar$^{-0.5}$ q = 293.9 m^3/h $\triangle P_v$ = 1.5 atm	Temperature control valve Linear characteristic Air-to-open K_v = 170.3 m^3·h^{-1}·bar$^{-0.5}$ q = 620.6 m^3/h $\triangle P_v$ = 0.5 atm	Temperature control valve Air-to-open

List of symbols

A	=	heat exchanger exchange area [m^2]
b	=	bypass fraction [-]
$c_{P,cat}$	=	catalyst heat capacity [$J \cdot kg^{-1} \cdot K^{-1}$]
$c_{P,cold}$	=	heat exchanger cold side molar heat capacity at constant pressure [$J \cdot mol^{-1} \cdot K^{-1}$]
$\bar{c}_{P,cold}$	=	average value of $c_{P,cold}$ [$J \cdot mol^{-1} \cdot K^{-1}$]
$c_{P,hot}$	=	heat exchanger hot side molar heat capacity at constant pressure [$J \cdot mol^{-1} \cdot K^{-1}$]
$c_{P,i}$	=	molar heat capacity at constant pressure of the specie i [$J \cdot mol^{-1} \cdot K^{-1}$]
d	=	reactor diameter [m]
d_p	=	catalyst particle diameter [m]
$d_{t,ext}$	=	heat exchanger tube external diameter [m]
d_v	=	vaporizer vessel diameter [m]
E_d	=	direct activation energy [J/mol]
E_r	=	reverse activation energy [J/mol]
f	=	valve inherent flow characteristic [-]
F	=	vaporizer outlet molar flow [kmol/h]
$F_{T1\text{-}2}$	=	temperature correction factor for the 1-2 heat exchanger design [-]
$F_{T2\text{-}4}$	=	temperature correction factor for the 2-4 heat exchanger design [-]
h_v	=	vaporizer vessel height [m]
K_C	=	controller gain [%CO/%TO]
K_v	=	valve flow coefficient [$m^3 \cdot h^{-1} \cdot bar^{-0.5}$]
l	=	valve stem position [-]
L	=	reactor length [m]
L_t	=	heat exchanger tube length [m]
m	=	heat exchanger mass [kg]
m_{sec}	=	heat exchanger section mass [kg]
$\dot{n}_{by}$	=	bypass stream molar flow [mol/s]
$\dot{n}_{cold}$	=	heat exchanger cold side molar flow [mol/s]
N_{cold}	=	dimensionless heat exchanger cold side molar flow [-]
$\dot{n}_{hot}$	=	heat exchanger hot side molar flow [mol/s]
$\dot{n}_i$	=	molar flow rate of the component i [mol/s]
$\dot{n}_{mix}$	=	mixed stream molar flow [mol/s]
$\dot{n}_{tot}$	=	total vapor molar flow exiting the vaporizer [mol/s]
N_t	=	heat exchanger number of tubes [-]
P	=	pressure [atm]

p_i = partial pressure of component *i* [Pa]
q = volumetric flow rate [m^3/h]
$\dot{Q}$ = heat exchanger heat transfer rate [MW]
Q_d = dimensionless heat exchanger heat duty [-]
Q_F = furnace heat duty [kW]
$\dot{Q}_{max}$ = maximum heat exchanger heat duty [MW]
$\dot{Q}_R$ = volumetric heat transfer rate of reaction [W/m^3]
R = dimensionless parameter for the temperature correction factor calculation [-]
R_G = universal gas constant [$J \cdot mol^{-1} \cdot K^{-1}$]
R_d = direct reaction rate [$mol \cdot m^{-3} \cdot s^{-1}$]
R_r = reverse reaction rate [$mol \cdot m^{-3} \cdot s^{-1}$]
S = dimensionless parameter for the temperature correction factor calculation [-]
s_t = heat exchanger tube thickness [m]
T = temperature [K]
T_0 = reference temperature at which the standard enthalpies are defined [K]
$T_{C,in}$ = heat exchanger cold side inlet temperature [K]
$T_{C,out}$ = heat exchanger cold side inlet temperature [K]
$T_{H,in}$ = heat exchanger hot side inlet temperature [K]
$T_{H,out}$ = heat exchanger hot side outlet temperature [K]
T_{mix} = temperature of the mixed stream entering the reactor [K]
U = overall heat transfer coefficient [$W \cdot m^{-2} \cdot K^{-1}$]
V_R = reactor volume [m^3]
V_{sec} = heat exchanger section volume [m^3]
V_t = heat exchanger volume inside the tubes [m^3]
x = reactor axial coordinate [m]
x_i = molar fraction of the specie *i* [-]

Greek letters

α_L = utilized in equation 3.1 [-]
α_N = fitting parameter utilized in equation 3.2 [kW]
β_L = fitting parameter utilized in equation 3.1 [kmol/h]
β_N = fitting parameter utilized in equation 3.2 [h/kmol]
γ_N = fitting parameter utilized in equation 3.2 [kmol/h]
$\triangle H_{by}$ = molar enthalpies of the bypass stream [kJ/mol]
$\triangle H_{cold}$ = molar enthalpies of the heat exchanger cold side outlet stream [kJ/mol]
$\triangle H^{\circ}_{F,i}$ = standard molar enthalpy of formation of the component *i* [kJ/mol]
$\triangle H_{mix}$ = molar enthalpy of the mixed stream entering the reactor [kJ/mol]

$\triangle H_R^{\circ}$ = standard molar enthalpy of reaction [kJ/mol]
$\triangle P_v$ = valve pressure drop [atm]
ε = reactor bed voidage [-]
ν_i = stoichiometric coefficient of the component *i* [-]
ρ_{cat} = catalyst solid density [kg/m^3]
τ_I = integral time constant [min]

Acronyms

ATV = auto-tune variation
CO = controller output
DAE = algebraic differential equation
DME = dimethyl ether
FC = flow controller
FCV = flow control valve
FEHE = feed-effluent heat exchanger
FFC = feedforward controller
FT = flow sensor-transmitter
LC = level controller
LCV = level control valve
LMTD = log-mean temperature difference
LT = level sensor-transmitter
mps = medium pressure steam
ODE = ordinary differential equation
OP = valve opening position
PC = pressure controller
PCV = pressure control valve
PDAE = partial differential and algebraic equation
PI = proportional-integral
PT = pressure sensor-transmitter
RSP = remote set point
TC = temperature controller
TCV = temperature control valve
TO = transmitter output
TT = temperature sensor-transmitter

References

Aspen Technology, Inc. (2022a). Aspen Plus®, *Aspen Plus Help* (V14).

Aspen Technology, Inc. (2022b). Aspen Plus®, *Aspen Plus Dynamics Help* (V14).

Douglas, J. M., J. C. Orcutt, P. W. Berthiaume (1962). Design and control of feed-effluent, exchanger-reactor systems. *Ind. Eng. Chem. Fundamen.* **4**, 253-257.

Kern, D. Q., (1997). *Process Heat Transfer*. McGraw Hill, New York (N.Y.).

Kuphaldt, T. R. (2019). *Lessons In Industrial Instrumentation* (2a ed.). Open source available at: `https://control.com`.

International Society of Automation (2007). *Control Valve Standards*. ISA-75.01.01-2007.

Luyben, W. L., B. D. Tyreus and M. L. Luyben (1999). *Plantwide Process Control* (1st ed.). McGraw-Hill, New York (N.Y.).

Luyben, W. L. (2002). *Plantwide Dynamic Simulators in Chemical Processing and Control* (1st ed.). Marcel Dekker, New York (N.Y.).

Luyben, W. L. (2007). *Chemical Reactor Design and Control.* Wiley, Hoboken (N.J.).

Luyben, W. L. (2011). Heat-exchanger bypass control. *Ind. Eng. Chem. Res*. **50**, 965-973.

Luyben, W. L. (2012). New control structure for feed-effluent heat exchanger/reactor systems. *Ind. Eng. Chem. Res*. **51**, 25, 8566-8574.

Poling, B. E., J. M. Prausnitz, and J. P. O'Connell (2001). *The Properties of Gases and Liquids* (5th ed.). McGraw-Hill, New York (N.Y.).

Sierra, I., J. Ereña, A. T. Aguayo, A. Ateka, J. Bilbao (2013). Kinetic modelling for the dehydration of methanol to dimethyl ether over γ-Al_2O_3. *Chem. Eng. Trans*. **32**, 613-618.

Soave, N., M. Barolo (2021). On the effectiveness of heat-exchanger bypass control. *Processes.* **9(2)**, 244.

Turton, R., J. A. Shaeiwitz, D. Bhattacharyya and W. B. Whitin (2018). *Analysis, Synthesis, and Design of Chemical Processes* (5th ed.). Pearson, Upper Saddle River (N.J.), Appendix B.1.

Web sites

NIST Chemistry WebBook (2024), URL: `https://webbook.nist.gov/cgi/fluid.cgi?PLOw=1&PHigh=10&PInc=1&Digits=5&ID=C7732185&Action=Load&Type=SatT&TUnit=K&PUnit=bar&DUnit=kg%2Fm3&HUnit=kJ%2Fkg&WUnit=m%2Fs&VisUnit=Pa*s&STUnit=N%2Fm&RefState=DEF`, visited on 22/07/2024.